ApJS, accepted

Intrinsic Absorption in Radio-Selected QSOs[1]

Gordon T. Richards[2,3]

University of Chicago

Department of Astronomy and Astrophysics, 5640 S. Ellis Avenue, Chicago, IL 60637

richards@oddjob.uchicago.edu

ABSTRACT

Moderate resolution spectra have been recorded for a sample of radio-selected QSOs ($z \sim 2.5$) discovered in the "Faint Images of the Radio Sky at Twenty centimeters" (FIRST) VLA survey. This work is motivated by the study of a heterogeneous set of QSO absorption line spectra that showed that as many as 36% of the absorbers normally thought to be intergalactic are correlated with physical properties of the background QSO, including the radio source spectral index. Spectra were taken for 24 newly discovered quasars in order to test this finding on a more homogeneous data set. The spectra have been searched for the most frequently observed absorption lines. The absorption line properties are compared to the radio properties of the quasars. The primary results are summarized as follows: 1) an excess of C IV absorbers in flat-spectrum quasars as compared to steep-spectrum quasars is confirmed (based on a total sample of 165 systems), 2) a small excess of high-velocity C IV absorbers is seen in radio-quiet QSOs as compared to radio-loud quasars, and 3) the Sloan Digital Sky Survey QSO spectra will allow for the detection of a high-velocity, narrow, intrinsic population of absorbers that is as small as 7% of the C IV absorber population in QSOs at $z \sim 2.5$.

Subject headings: quasars: absorption lines — quasars: general — radio continuum: galaxies

---

[1]Based on observations obtained with the Apache Point Observatory 3.5-meter telescope, which is owned and operated by the Astrophysical Research Consortium.

[2]Presented as part of a dissertation to the Department of Astronomy and Astrophysics, The University of Chicago, in partial fulfillment of the requirements for the Ph.D. degree.

[3]Current address: Department of Astronomy and Astrophysics, The Pennsylvania State University, University Park, PA 16802

1. Introduction

The physical location of the narrow absorption features found in the spectra of QSOs has been of considerable interest since their discovery over 30 years ago (Stockton & Lynds 1966; Burbidge et al. 1966). There is a considerable body of evidence that QSO absorption lines are, in general, the result of a galaxy along the line of sight to the QSO, where the galaxy is blocking some of the QSO light (Young et al. 1982; Sargent et al. 1988; Steidel 1990; Steidel et al. 1997). Whether the material causing the absorption is caused by extended galactic halos (Bahcall & Spitzer 1969), or by dwarf galaxies in the vicinity of a larger galaxy (York et al. 1986), is still a matter of debate.

Despite the fact that intervening galaxies are clearly *a* cause of absorption lines seen in the spectra of background QSOs, it is also well-known that QSOs are also subject to self-absorption. The broad troughs that are characteristic of so-called Broad Absorption Line QSOs (BALQSOs) are clearly material that is associated with the QSOs (**?**, e.g.,)]tur88,wey97. There is also an excess of narrow C IV absorption lines seen in the spectra of steep-spectrum radio QSOs, within $5000\,\mathrm{km\,s^{-1}}$ of the emission redshift of the QSO. This excess is also thought to be associated with the QSO in some way (Foltz et al. 1986; Anderson et al. 1987; Foltz et al. 1988).

These facts come together to form the commonly accepted picture that heavy-element QSO absorption lines are caused by intervening galaxies, unless: 1) the lines are broad (typically $2000\,\mathrm{km\,s^{-1}}$ or wider), or 2) narrow, with a relative velocity with respect to the QSO rest frame of less than $5000\,\mathrm{km\,s^{-1}}$. For these two cases the lines are either "intrinsic" to the QSO (directly related to the QSO) or "associated" with the QSO (either directly related to the QSO or influenced by the radiation field of the QSO).

There is a growing body of evidence that some QSO absorption line systems do not fit into any of the above categories. These are lines that display characteristics of intrinsic or associated lines, but have relative velocities that are greater than $5000\,\mathrm{km\,s^{-1}}$ (blueward of the QSO emission redshift)[4] and are not broad enough to satisfy the BAL classification scheme set forth by Weymann et al. (1991). Examples of such systems can be found in Hamann et al. (1997) and Jannuzi et al. (1996).

This study attempts to determine if there is any evidence for a population of narrow, high-velocity intrinsic/associated absorbers that have been masquerading as intervening galaxies. In particular, this work is motivated by a desire to use the absorption line data from the catalog of York et al. (1991), an updated version of which is in preparation (Vanden Berk et al. 2001), as probes of galaxies at high redshift. For example, Quashnock et al. (1996) have used the data in the catalog to explore the clustering of absorbers out to scales of hundreds of Mpc. In another paper based on this catalog, Vanden Berk et al. (1996) found that bright QSOs tend to have more C IV systems along their line of sight than faint QSOs. A statistical weak lensing effect was suggested as

[4] $v = \beta c = \frac{R^2-1}{R^2+1}$, where $R = \frac{1+z_{em}}{1+z_{abs}}$, such that positive velocities are blueshifted with respect to the QSO redshift.

the origin of this effect; however, it was acknowledged that a population of high velocity intrinsic absorbers might yield similar observational consequences.

Studies like these use heavy-metal QSO absorption line systems as powerful cosmological probes that allow astronomers to study structures at redshifts higher than would otherwise be observable. Thus, it is important to understand the nature of QSO absorption lines and to what extent they actually do represent galaxies along the line of sight to QSOs. If the heavy-metal QSO absorption line population is heavily contaminated by intrinsic QSO material, it may not be possible to use QSO absorption lines as probes of high-z galaxies unless it is possible to identify intrinsic systems on a case-by-case basis.

In a recent paper (Richards et al. 1999, hereafter Paper I), the existing evidence for a population of high-velocity, but narrow intrinsic/associated absorption lines was summarized and new evidence that supports the reality of said population was presented. The primary result of Paper I was the discovery that there is an excess of narrow C IV absorption with $v > 5000\,\mathrm{km\,s^{-1}}$ in flat-spectrum quasars as compared to steep-spectrum quasars. Since some radio properties of quasars are thought to be correlated with the line-of-sight angle of inclination of quasars (Rowan-Robinson 1977; Orr & Browne 1982; Padovani & Urry 1992), it was postulated that this excess may be the result of an orientation-dependent population of intrinsic/associated absorbers. This excess can be accounted for by a 36% contamination of the intervening C IV absorption line sample by intrinsic absorbers that are preferentially found in flat-spectrum quasars.

While statistical tests by Richards et al. (1999) apparently removed various biases from the inhomogeneous catalog of absorbers (York et al. 1991), there is no way to prove that all biases were removed. In particular, there was concern that variability in the radio data (compromising the derivation of the radio spectral index from multi-band observations that were not coincident in time) and the varying quality of the optical spectra (and thus the equivalent width detection limit) might affect the conclusions of Paper I. **?**)hereafter Paper III]rlb00, addresses the inhomogeneity of the radio data. Confirming that the results from Paper I hold in light of more homogeneous optical spectra is left to be examined herein. The primary goals of this work are to 1) confirm that the excess of C IV absorbers in flat-spectrum quasars observed in Paper I persists for a sample of more homogeneous data, and 2) test whether the observed excess may instead be due to evolution of the absorber population as a function of redshift.

This paper is laid out as follows: §2 presents the target list and the details of the observations. An indepth account of the data reduction is given in §3. In §4, detailed notes on the individual objects are given. §5 presents an analysis and discussion of the science, including the impact that the Sloan Digital Sky Survey will have on this and other QSO absorption line studies. Finally, §6 presents the conclusions.

2. Observations

The primary goal of this work is to determine if the results of Paper I hold for a more homogeneous set of absorption line data. Since that work depended on knowing the radio properties of the QSOs, it was necessary to select radio-detected QSOs for observation. It was decided to select targets from those quasars discovered (or recovered) as part of the FIRST Bright Quasar Survey (FBQS; Gregg et al. 1996) as of January 1998. All FBQS quasars with $2.27 < z_{em} < 4.0$ were included as potential targets. The redshift range was chosen such that any C IV absorption lines with velocities relative to z_{em} between $-5000\,\mathrm{km\,s^{-1}}$ and $75000\,\mathrm{km\,s^{-1}}$ would fall between the wavelength limits of the spectra (3965.2 – 8235.0 Å). The redshift range was further restricted to $z_{em} \leq 2.8$ shortly after the start of the project when it became clear that the red spectra would not be suitable for finding C IV absorption lines.

Not all of the objects in the initial target list were observed as a result of time constraints on the telescope. Targets were observed without prior knowledge of absorption line properties. Brighter objects close to the meridian were chosen over fainter objects and those at higher airmass.

The final analysis includes some of the data from Paper I in order to form a sample that is large enough for statistical analysis of the correlation of absorption with radio spectral index. Included are all QSOs from the revised York catalog (York et al. 1991; Vanden Berk et al. 2001) that meet the following requirements: 1) $z_{em} \geq 2.2$, 2) $z_{em} \leq 2.8$, 3) spectral resolution between $35\,\mathrm{km\,s^{-1}}$ and $450\,\mathrm{km\,s^{-1}}$, 4) not known or suspected gravitational lenses, and 5) not known or suspected Broad Absorption Line QSOs (BALQSOs). Furthermore, Q0237-233 was removed since this object has an unusually high number of C IV absorbers in a small redshift range.

The entire target list is given in Table 1. In Table 1, the columns are the IAU name for the object, the redshift, the right ascension and declination in J2000 coordinates, the E magnitude, the O-E color, the peak (i.e. core) flux density (mJy) from the FIRST maps, the integrated FIRST flux density (mJy), and the signal-to-noise of both the blue and red spectra. The optical magnitudes and radio flux densities are taken from Gregg et al. (1996). The "blue" signal-to-noise is the average from the region between Lyman-α and C IV emission; the "red" signal-to-noise is taken at 6000 Å. The redshifts in Table 1 are flux weighted redshifts measured from the C IV emission lines.

The signal-to-noise threshold was set so as to yield equivalent width limits similar to or better than previously achieved for C IV absorption: the goal was to obtain a 5σ rest equivalent width limit of 0.1 Å for C IV doublets at $z = 2$. Given a resolution of $3.2\,\text{Å pixel}^{-1}$ and a two-pixel resolution element, the required signal-to-noise is 75. For the spectra that are only signal-to-noise of 50, the 5σ rest equivalent width limit is 0.15 Å.

The observations were carried out with the Double Imaging Spectrograph (DIS)[5] on the ARC

[5]The Double Imaging Spectrograph (DIS) was built at Princeton University by Jim Gunn, Michael Carr, Brian Elms, Ricardo Lucinio, Robert Lupton, and George Pauls. See http://www.apo.nmsu.edu/Instruments/DIS/dis.html

3.5m telescope at Apache Point Observatory (APO). The DIS detectors are a thinned, uv-coated SITe 512x512 CCD with 27 micron pixels (blue camera), and a thinned 800x800 TI CCD with 15 micron pixels (red camera). The platescale at the detectors is $1.086''\,\mathrm{pixel}^{-1}$ in the blue and $0.610''\,\mathrm{pixel}^{-1}$ in the red. The gratings used for these observations have 600 lines mm^{-1}, giving a dispersion of about $3.2\,\text{Å}\,\mathrm{pixel}^{-1}$ (blue camera) and 300 lines mm^{-1} with a dispersion of about $3.5\,\text{Å}\,\mathrm{pixel}^{-1}$ (red camera). Throughout the course of the observations, a $2''$ wide steel slit (which is about $6'$ long) was used. All observations were made at the parallactic angle (Filippenko 1982).

Though DIS is only a medium resolution spectrograph, it is ideal for the study at hand. DIS is able to obtain complete spectral coverage from 3965.2 to 8235.0 Å at a resolution sufficient to split (two pixels between minima) the C IV doublet at $z \geq 1.488$. Though the resolution is good enough to split C IV, it is not always good enough to formally resolve it. This apparent detriment is more than made up for by the wavelength coverage, which allows for the discovery of other lines in the system. The presence of other lines in the system thus confirm the reality of C IV even though it may not be properly resolved.

DIS performed quite well throughout the course of this project; however, there are a few problems worth noting. The first is that the red CCD is not nearly as sensitive as the blue CCD and suffers from some noise problems. Second, there is, inevitably, flexure in the spectrograph when the spectrograph rotates during long exposures. Therefore, one must be careful to obtain wavelength calibration exposures on a frequent basis. Finally, when attempting to observe at the parallactic angle, it was sometimes difficult to place the target directly on the boresight (the point around which the field rotates). As a result, there may be some light loses that affect the absolute spectrophotometry of the spectra. Accurate guiding negates this problem, but it was difficult at times to keep the object fully in the slit as a result of long time delays between guiding exposures for faint targets.

Table 2 gives a log of all of the observations. The first column gives a truncated name of the QSOs. The next two columns give the UT date and time of the observations. The exposure times were typically 1800 seconds (30 minutes): exposure times different from 1800 seconds are indicated by notes to the table. No exposures that resulted in signal-to-noise less than 10 per pixel were used. At least 4 exposures were taken of each target to allow for proper detection (and removal) of cosmic rays.

---

for details.

3. Data Reduction

The data were reduced with the Image Reduction and Analysis Facility (IRAF)[6] using a package called DISTOOLS, which was written by the author. The DISTOOLS package was written to facilitate the reduction of data from the Double Imaging Spectrograph (DIS) at the Apache Point Observatory (APO). This package is largely a series of "wrappers" to existing IRAF routines (version 2.11.x)[7], with parameters that are optimized for the camera used for this project.

3.1. Converting 2-D Images into 1-D Spectra

The conversion of the 2-D images into 1-D spectra proceeded in the usual manner, following the optimal extraction process of Horne (1986). Wavelength calibration was accomplished through the observation of helium, neon, argon (HeNeAr) comparison lamps, which were taken before and after each standard star and object spectrum. The wavelengths are all vacuum heliocentric.

Typically the blue spectra required a third order Chebyshev polynomial, giving an average root-mean-square (RMS) residual of 0.30Å, while the red spectra were best fit by a third order cubic spline with an average RMS residual of 0.14Å. The RMS residuals of the dispersion solution fits are quite good; however, they should be interpreted with caution: there are always additional contributions to both the statistical and systematic errors in the wavelength that can be as large as, or larger than the RMS values. For this particular project, the wavelength errors are vastly more accurate than what is required.

Next, the spectra are extinction corrected and flux calibrated. The standard Kitt Peak National Observatory (KPNO) extinction spectrum was used despite the fact that these observations were taken at APO. Tests showed that the use of the KPNO extinction vector was better than not applying a correction at all.

After extinction correction and flux calibration, the red spectra were also corrected for telluric absorption. A template correction spectrum was made by taking a very high signal-to-noise spectrum of Feige 110 at an airmass of approximately 1.5 on the night of 9 July 1999. Each separate red spectrum of every object was corrected for telluric absorption using the TELLURIC task (new to IRAF V2.11.1) with the above telluric correction template; the same template was used to correct every individual spectrum.

All the spectra for each object are variance coadded to produce the final 1-D spectrum. Before variance coaddition, each spectrum has bad pixels masked out and is scaled to the the individual

---

[6]IRAF is distributed by the National Optical Astronomy Observatories, which are operated by the Association of Universities for Research in Astronomy, Inc., under cooperative agreement with the National Science Foundation.

[7]See the IRAF "Help Pages" (http://iraf.noao.edu/iraf/web/iraf-help.html) for detailed explanations of any IRAF tasks describe herein.

spectrum with the largest flux. Bad pixels (cosmic rays, etc.) are masked out under the premise that one should reject bad data, not attempt to fix it. After bad pixels have been masked, all the spectra of each object are scaled. It is assumed that the spectrum with the highest mean flux is that which is closest to the intrinsic spectrum. Failure to normalize the spectra can cause spectra with equal signal-to-noise but lower absolute fluxes (as a result of flux calibration errors, slit losses, etc.) to be weighted improperly. Upon completion of the scaling process, the spectra are then variance coadded. The final weighted error spectrum is the square root of the variance spectrum.

3.2. Continuum Fitting

A continuum vector was fit to and removed from each composite spectrum before searching for absorption lines. Each composite spectrum was first split into segments at the peaks of strong emission lines. Then each segment was fit with a cubic spline polynomial using the CONTINUUM procedure in IRAF. The order, high- and low-rejection thresholds were adjusted until the fit reproduced the continuum plus emission spectrum suitably. These pieces were then merged together and the entire continuum spectrum was examined again.

That this method produced reasonable continuum spectra can be confirmed by looking at the distribution of residuals (spectrum - continuum). If the continuum was well fit, then the residual distribution should be nearly Gaussian (centered at zero with a width of one over the signal-to-noise of the spectrum) with a tail of positive-going points corresponding to absorption line features. For each object, the distribution of residuals was examined in order to make sure that the continuum residuals indeed were reasonable.

3.3. Redshift Determination

Generally, for each QSO emission line the redshift is determined by fitting a Gaussian (or Gaussians), using the peak flux, or taking a flux weighted average. For the sake of this project a simple determination of the redshift will suffice. The redshifts were calculated as a flux weighted average of the signal in pixels with more than 50% of the peak flux in each C IV emission line. Pixels for which the actual flux deviated from the fitted continuum value by more than 10% were weighted according to the continuum flux and not the raw flux of the spectrum, since to do otherwise would allow for strong absorption lines to affect the determination of the redshift.

The use of a flux weighted average of the peak of the C IV emission line only should be more than adequate for this work. The measurement error should typically be much less than the resolution of the spectrum ($\Delta v = 350\,\mathrm{km\,s^{-1}}$ or $\Delta z = 0.004$). Other methods may change the redshift by as much as $\Delta z = 0.01$ ($\Delta v = 850\,\mathrm{km\,s^{-1}}$) or more, but such a shift will have negligible impact on this study. For asymmetric lines with steeper red wings, the flux weighted method will yield slightly lower redshifts than using the peak. A more proper determination of the redshift

would use not only the C IV emission line, but also all of the other observed lines. Low-ionization lines are closer to the systemic redshift, which is typically larger than that measured by higher ionization lines such as C IV (Tytler & Fan 1992).

3.4. Finding Absorption Lines

The identification of significant absorption lines in the composite QSO spectra largely follows the algorithm of Schneider et al. (1993). The process consists of normalizing the spectrum, finding local minima, subtracting a Gaussian profile from significant lines, and looking for secondary lines. The blue and red spectra were treated separately.

A number of quantities are determined for each significant absorption line as per Schneider et al. (1993). These include the observed equivalent width (EW), given by

$$\mathrm{EW} = D \sum_j P_j \left(F_j - 1\right) / \sum_j P_j^2, \tag{1}$$

where P_j is the gaussian weighting function of the slit spread function (SSF) whose width is given by $\sigma_{\mathrm{SSF}} = \mathrm{FWHM}/2.354$, F is the observed (normalized) flux at a given pixel, and D is the dispersion. At the edges of the spectrum, no attempt is made to buffer the spectrum and the SSF is modified accordingly.

The corresponding observed equivalent width error is then given by

$$\sigma(\mathrm{EW}) = D \left(\sum_j P_j^2 E_j^2 \right)^{1/2} / \sum_j P_j^2, \tag{2}$$

where E is the normalized flux error. The so-called "interpolated" equivalent width error spectrum is the same except for the use of the interpolated flux error in place of the raw (normalized) flux error. The interpolated flux error is determined by interpolating the error spectrum across strong absorption lines and is a better estimate of the signal-to-noise when determining the significance of a line. However, the usual flux error is still used to calculate the error in the equivalent width measurement after a line has been deemed significant. Lines with significance limits ($SL = |W|/\overline{\sigma}_W$) less than 3 are rejected. The SL is simply the signal-to-noise (S/N) except that the equivalent width error is replaced by the interpolated equivalent width error.

Some additional quantities are also determined. The wavelength error for a particular line is

$$\sigma(\lambda) = \sqrt{2} D \sigma_{SSF} \left| \frac{\sigma_W}{W} \right|. \tag{3}$$

An alternative measure of the equivalent width is also calculated using:

$$W = D \sum_j (1 - F_j), \tag{4}$$

where the sum over j is carried out over the range of pixels that are less than unity in the vicinity of the absorption feature. These equivalent width values can be compared to those computed for single, isolated lines to test how well the input FWHM reproduces the SSF.

Finally, the observed FWHM is determined by

$$FWHM = D(\lambda_{\rm hi} - \lambda_{\rm lo}), \tag{5}$$

where $\lambda_{\rm hi(lo)}$ is the wavelength where $F = 1/2(1 - F_{\rm min})$, $\lambda_{\rm hi(lo)}$ is larger(smaller) than the central wavelength, and $F_{\rm min}$ is the flux at the minimum of the absorption trough. This observed FWHM can be compared to the input FWHM (for single lines) to test the appropriateness of the input FWHM for a given spectrum. In addition, this measure allows one to identify blended and resolved lines, since this measure of the FWHM will be significantly larger than the input FWHM for such lines.

3.5. Identification of Absorption Line Systems

The identification of absorption line *systems* from the list of individual absorption lines is a difficult task. The code used for this step in the data analysis was adapted from that used by Daniel Vanden Berk in his 1997 University of Chicago Ph.D. Thesis (Vanden Berk 1997; Vanden Berk et al. 1999). The code is based on the ZSEARCH algorithm developed by the *HST* Quasar Absorption Line Key Project Team (**?**, e.g.,)]bbb+93,jbb+98 and was modified to fit the needs of this project.

Identification of the absorption lines begins by comparing the observed lines to those that are typically found in the spectra of QSOs. The template lines used to identify systems are taken from Morton, York, & Jenkins (1988). The lines that were searched for are given in Table 3. The first column is the ion, the second column is the vacuum wavelength of the particular transition, the third column is the strength of the line, and the fourth column is the ionization potential for the ion given. Ionization potentials are taken from Moore (1971). In this table, lines with $\lambda > 1036\,$Å are sorted in increasing wavelength order of the the largest f value from each ion. Then, within each ion, the lines are sorted in order of decreasing f.

The first step in the system identification procedure is to try to match each input line with the line transitions listed in Table 3. A redshift is calculated for each observed-line/template-line pairing. These redshifts are used as the basis set for the system identification process. The rest of the process involves rejecting unlikely identifications. That is, 1) are other lines from the same atom/ion observable and are their strengths consistent with the first line, and 2) are there other lines from different ions at the same redshift that are also consistent? All C IV and Mg II doublets that are stronger than the 5σ equivalent width limit should be properly identified. In some cases, these systems consist only of the doublet, in which case the identification should be considered as possible, but not definite.

Table 4 lists all of the lines identified in the spectra presented herein. All lines with significance limit greater than 3σ are marked in the spectra, but only lines stronger than 5σ are listed in the tables for the sake of brevity. The numbering scheme includes the 3σ lines, since those are marked in the spectra. Lines weaker than 5σ may be included in the table if they are identified as part of an identified system. The first column gives the number of the line. Column 2 is the observed wavelength of the line center, and column 3 is the error in the wavelength. Columns 4 and 5 are the observed equivalent width and its error in Angstroms. The FWHM is given in column 6. The significance limit is in column 7. If the line was identified with a given system, then the line identification and the system redshift are given in columns 8 and 9 respectively. The alphabetic notes to columns 2 and 8 are as follows: a — line in Lyman α forest, b — possibly a continuum fitting artifact, c — questionable identification, d — possibly a telluric residual, e — possible night sky artifact. These designations were made without knowledge of the identification of the lines (if any).

The number of significant lines in the red spectra ($\lambda > 5500\,\text{Å}$) is somewhat larger than would be expected for the signal-to-noise of the spectra. This excess is probably caused by difficulty in properly measuring the errors in the red spectra. The noise characteristics of the red CCD are not as stable as one might like and the distribution of bias values is noticeably non-Gaussian. This means that the read noise measured for the red CCD is not a true measure of the error. This effect causes the equivalent width errors in the red spectra to be underestimated and, as a result, there are more significant lines in the red spectra than there should be. However, nearly all of the C IV systems are in the blue spectra and only 5σ (or stronger) lines have been used for analysis, so this problem is of little significance to the work at hand.

4. Notes on Individual Objects

Figures 1 through 24 present spectra of 24 quasars. With the exception of FBQS1625+2646 (also known as KP 76), none of these quasars has been previously analyzed for absorption. For each of these objects the blue spectra ($\lambda < 5000\,\text{Å}$) are typically quite good. Lines identified within these blue spectra should generally be real. The quality of the red spectra is somewhat worse: all lines stronger than 3σ are marked, but many are likely to be artifacts. Lines that are thought to be artifacts are noted as such in Table 4.

An important facet of the analysis of individual absorption lines is the knowledge of not only what lines are actually observed, but also of what lines could have been observed. Since the spectra all have exactly the same wavelength coverage and are comparable in signal-to-noise, it suffices to give the redshift ranges for interesting combinations. Of most interest is whether or not Mg II is observed in C IV systems. For the spectra presented herein any reasonably strong ($W_{obs} \geq 0.6\,\text{Å}$) Mg II system will be detected to 3σ or better for $z \leq 1.937$. Similarly, at least three of the five strongest lines of Fe II could be detected up to $z = 2.456$.

4.1. FBQS0047-0156 ($z = 2.479$)

This is a Broad Absorption Line QSO (BALQSO) with a strong, complex BAL trough near the C IV line ($\sim$5325 Å) and two smaller troughs at larger velocities ($\sim$5050 Å and $\sim$5200 Å). The lower velocity trough looks as though it might break up at higher resolution. There is no Si IV trough, but the N V BAL is prominent ($\sim$4275 Å). Of particular interest is the partially resolved Si IV emission line ($\sim$4875 Å).

There are 42 absorption lines with significance greater than 5σ redward of Lyman-α emission; however this number includes the narrow lines that were fit to the BAL profiles. Removing the narrow line fits to the BAL profiles, there are only 14 strong, narrow lines, six of which remain unidentified (#34,45,69,72,76,81). All but one of the unidentified lines are broad features, noted as possible artifacts of the continuum definition, or longward of 5500 Å, where the noise characteristics are suspect.

$z_{\rm abs} = 1.8103$. — Other than the BALs, this is the only readily identifiable system in this spectrum. With 10 lines including C IV $\lambda\lambda$1548,1550 (#28,29), Mg II $\lambda\lambda$2796,2803 (#89,90), five lines of Fe II (#33,78,79,83,84) and Al II λ1670 (#35) this system is certain.

4.2. FBQS0210-0152 ($z = 2.372$)

This object shows very strong N V emission and rather weak Si IV emission. It is rich in absorption lines, having 46 lines stronger than 5σ. These lines define six systems of which four are certain, one is probable and one is possible. Redward of Lyman-α emission there are 34 strong lines: five remain unidentified (#43,55,58,59,61). All but one of the unidentified lines are in the lower quality, red spectrum.

$z_{\rm abs} = 0.9962$. — Only the Mg II doublet (#45,46) is observed in this questionable system, which is coincident with a strong night sky feature.

$z_{\rm abs} = 1.3097$. — This system is defined by ten lines including Mg II $\lambda\lambda$2796,2803 (#53,54), Mg I λ2852 (#56), Al III $\lambda\lambda$1854,1862 (#19,20), and five lines of Fe II (#40,41,42,49,50).

$z_{\rm abs} = 2.1474$. — Seven lines define this mixed ionization system. Al II λ1670 (#39), C II λ1334 (#18), and Si II λ1526 (#30) are observed in addition to C IV $\lambda\lambda$1548,1550 (#31,32) and Si IV $\lambda\lambda$1393,1402 (#24,25). The Si IV doublet is quite strong as is C IV.

$z_{\rm abs} = 2.3216$. — This redshift is suggested by a relatively weak C IV doublet (#33,34), a possible detection of N V $\lambda\lambda$1238,1242 (#13,14) and Lyman-α (#6). If the system is real, then the N V λ1242 is blended with N V λ1238 from the $z_{\rm abs} = 2.3342$ system.

$z_{\rm abs} = 2.3342$. — This is a strong, high-ionization C IV system with Ly-α (#8) and very strong N V (#14,15), but no Si IV. The C IV absorption (#35,36) is in the blue wing of the C IV

emission line and is $\sim 3400\,\mathrm{km\,s^{-1}}$ from the emission redshift of the quasar. The presence of strong N V coupled with the location of the system make it a nearly certain associated system. The N V λ1238 line may be blended with N V λ1242 from the $z_{\rm abs} = 2.3216$ system.

$z_{\rm abs} = 2.3709$. — In this system the C IV doublet (#37,38) is found at essentially the same redshift as the quasar itself. The Lyman-α line (#12) is quite strong. Si IV $\lambda\lambda$1393,1402 (#28,29) are readily apparent and N V $\lambda\lambda$1238,1242 (#16,17) may be detected; however they are shifted redward relative to C IV.

4.3. FBQS0256-0119 ($z = 2.491$)

This is another BALQSO. There are two C IV troughs; the higher velocity trough has two minima. The lower velocity trough has an obvious N V counterpart and there is evidence for a weaker Si IV trough. There are no unambiguous narrow line systems in this QSO; however we list all of the lines, including the narrow line fits to the BAL profiles. There are seven unidentified lines at 5σ significance (#30,32,33,34,36,68,69).

4.4. FBQS0725+2819 ($z = 2.662$)

This QSO has relatively weak broad emission lines. There are 33 significant absorption lines longward of Lyman-α emission. Twenty-eight of these lines are identified with four absorption line systems. Of the remaining five unidentified lines (#49,53,62,63,79), none are marked as possible blemishes.

$z_{\rm abs} = 1.4968$. — This is an unusual system in that Cr II $\lambda\lambda\lambda$2056,2062,2066 (#54,55,56) and Mn II $\lambda\lambda\lambda$2576,2594,2606 (#71,73,75) are observed. In addition to these uncommon lines, the more common lines of Mg II $\lambda\lambda$2796,2803 (#83,84), Mg I λ2852 (#85) and Al III $\lambda\lambda$1854,1862 (#44,45) are observed. Finally, there is evidence for Si II λ1808 (blended with C IV λ1550 from $z_{\rm abs} = 1.9095$), Zn II $\lambda\lambda$2026,2062 and Mg I λ2026.

$z_{\rm abs} = 1.9095$. — Eleven lines make this system unambiguous. Six lines of Fe II (# 46,77,81,82,86,87) are observed in the company of Mg II $\lambda\lambda$2796,2803 (#89,90), Al II λ1670 (possible) and Si II λ1526 (possible). It is also quite probable that the C IV doublet is seen (#40,41); however the red line is corrupted and may be blended with Si II λ1526 from $z_{\rm abs} = 1.4968$.

$z_{\rm abs} = 2.2674$. — Only the C IV $\lambda\lambda$1548,1550 doublet (#50,51) is observed in this system. However, this identification is considered very unlikely since both lines can be accounted for by other systems.

$z_{\rm abs} = 2.2735$. — A strong Lyman-α line (#1) and a weak C IV doublet (#51,52) make this a probable system. The Si IV $\lambda\lambda$1393,1402 doublet (#42,43) may also be seen, though at lower

significance.

4.5. FBQS0729+2524 ($z = 2.300$)

In this object there are 24 lines stronger than 5σ, 18 of which are identified in three likely systems and one possible system. Included in the unidentified lines (#3,4,7,24,31,32) are three lines that may be part of the $z_{\rm abs} = 2.2871$ system, but are not deblended.

$z_{\rm abs} = 0.5114$. — Only the two lines of the Mg II doublet (#10,11) are observed in this system; however the only other observable line would be Mg I λ2852, so this system is considered possible. If real, the Mg II λ2803 line is partially blended with C IV λ1548 from $z_{\rm abs} = 1.7422$.

$z_{\rm abs} = 1.7422$. — This systems contains C IV $\lambda\lambda$1548,1550 (#12,13), Si II λ1526 (#9), Al II λ1670 (#18, which may be blended with Si IV λ1393 from $z_{\rm abs} = 2.2871$), the Mg II doublet (#40,41) and possibly Mg I λ2852. There is also a hint of the Al III doublet, but it is blended with C IV from $z_{\rm abs} = 2.2871$.

$z_{\rm abs} = 2.2295$. — Both the C IV (#22,23) and Si IV doublets (#16,17) are observed in this probable system.

$z_{\rm abs} = 2.2871$. — The identification of this very high ionization system is certain and may be classified as an associated system. Lyman-α (#2) is observed and is very strong. Both the C IV (#25,26) and N V doublets (#5,6) are observed and are very strong compared to the Si IV doublet (#18,19). In fact, the Si IV doublet may be an artifact, since the proposed Si IV λ1393 line is blended with Al II λ1670 from $z_{\rm abs} = 1.7422$ and Si IV λ1402 coincides with the trough between the two (partially resolved?) lines of Si IV seen in emission. The line fitting code required extra lines to fit both the N V and C IV doublets. This may indicate blending with other systems or that these lines would be resolved at higher resolution.

4.6. FBQS0804+2516 ($z = 2.290$)

The emission spectrum of this QSO is unusual. The C IV emission line is somewhat asymmetric. Emission lines of Lyman-α, N V, O I, C II and Si IV are also seen, but they are all shifted to the red as compared to C IV. In addition, there are two "extra" bumps ($\sim 4150\,$Å) of emission just redward of N V emission, which straddle the predicted location of Si II λ1260. The redder of the two is probably Si II λ1260, since the redshift as measured from C IV is smaller than that measured from other lines. The bluer of the bumps may be S II.

In contrast with the emission spectrum, the absorption spectrum is rather bare. There are only 21 relatively strong lines (many of which are noted as possible artifacts) that can be grouped into two systems, one of which is uncertain. There also appears to be a pair of weak lines sitting

on top of the C IV emission line, but these lines remain unidentified.

$z_{\rm abs} = 0.7096$. — This system contains Mg II $\lambda\lambda$2796,2803 (#15,16) in addition to two iron lines, Fe II λ2382 (#5) and possibly Fe II λ2600 (#9).

$z_{\rm abs} = 1.6408$. — This system is quite uncertain. It only has a relatively weak Mg II doublet (#34,35) and a possible detection of Fe II λ2382 (#27) that is coincident with a strong night sky feature.

4.7. FBQS0821+3107 ($z = 2.604$)

This QSO spectrum may harbor a damped Lyman-α absorption system. It also has strong N V emission and partially resolved Si IV emission. There is a wealth of absorption lines blueward of Lyman-α emission, and 23 strong lines redward of Lyman-α. Twenty-one lines are identified with five different systems.

$z_{\rm abs} = 0.7806$. — This is a low ionization system with Mg II $\lambda\lambda$2796,2803 (#57,58), Mg I λ2852 (#59) and Fe II λ2600 (#48). Other lines of Fe II may also be evident, but they are either in the forest or blended with other systems.

$z_{\rm abs} = 1.9440$. — Only the C IV doublet (#44,45) is observed in this system, which defines it as possible.

$z_{\rm abs} = 2.4445$. — Similar to the above system, this redshift is indicated by the C IV doublet (#60,61). However, Lyman-α (#17) is also observable at this redshift and is detected.

$z_{\rm abs} = 2.5152$. — Again C IV $\lambda\lambda$1548,1550 and Lyman-α are detected, though the significance of the red line of C IV is less than 3σ. There is also a possible detection of both Si IV λ1393 and Si IV λ1402, but the red line is obscured by Si IV λ1393 from $z_{\rm abs} = 2.5351$.

$z_{\rm abs} = 2.5351$. — At least 13 lines are found in this mixed-ionization system. Both the C IV (#64,65) and Si IV doublets (#54,56) are found. Also seen are Lyman-α (#29), Si II λ1260 (#40), C II λ1334 (#50), Si II λ1526 (#62), Fe II λ1608 (#67), Al II λ1670 (#68) and possibly S II. Furthermore O I λ1302 and Si II λ1304 are observed (#46,47); this pair is often mistaken for a C IV doublet.

4.8. FBQS0857+3313 ($z = 2.340$)

The emission lines of this QSO are fairly narrow. In fact, they are so narrow that the Si IV+O IV] emission line is clearly resolved into two components. In this spectrum there are four absorption line systems, which are drawn from the 33 5σ lines redder than Lyman-α.

$z_{\rm abs} = 1.3838$. — This system, which is defined by Mg II $\lambda\lambda$2796,2803 (#44,45) is unusual in

that it does not show any of the other lines normally seen with a Mg II doublet this strong, but it does show weak Al III $\lambda\lambda$1854,1862 (#16,17).

$z_{\rm abs} = 1.8888$. — At this redshift there is a strong C IV doublet (#18,19). Si IV (#7,9) may also be detected in absorption, but it is lost in the forest. There are no other significant lines identified with this system.

$z_{\rm abs} = 2.2691$. — Fifteen lines leave little doubt about the reality of this system. Strong lines are seen in both low and high ionization. Both the C IV (#26,27) and Si IV (#21,22) doublets are strong. Lyman-α (#2) is also strong. Also seen are four Fe II lines (#33,54,55,56), three Si II lines (#11,14,25), C II λ1334 (#15), O I λ1302 (#13) and Al II λ1670 (#34). The Si II λ1260 line may be blended with a weak N V λ1242 line from $z_{\rm abs} = 2.3167$. Mg II is beyond the range of the spectrum.

$z_{\rm abs} = 2.3167$. — Only C IV $\lambda\lambda$1548,1550 (#30,31) are unambiguous in this system. However, there is absorption at the expected position of Lyman-α and there is evidence for N V λ1238. N V λ1242 may also be present, but if so, it is blended with Si II λ1260 from $z_{\rm abs} = 2.2691$.

4.9. FBQS0910+2539 ($z = 2.744$)

This is the highest redshift QSO in the sample. The C IV emission line is shifted into the red spectrum. This significantly reduces the S/N near the emission line, which, in turn, makes it more difficult to detect C IV absorption lines near the redshift of the QSO. The Si IV emission line is resolved. There are six strong absorption lines past Lyman-α emission. Among these lines only two systems are found. There is evidence for absorption in the blue wing of C IV emission (#52,53), but a better spectrum is needed in order to identify it.

$z_{\rm abs} = 1.6060$ — The only lines seen at this redshift are Mg II $\lambda\lambda$2796,2803 (#61,62). However, the agreement between the lines is not very good – making this system uncertain.

$z_{\rm abs} = 2.0101$. — Only the C IV doublet (#47,48) is observed in this system. However, the lines are strong, so the system is probably real.

4.10. FBQS0934+3153 ($z = 2.420$)

This is an obvious BALQSO. No attempt has been made to search for narrow lines and this object is excluded from any analysis. The broad troughs near ~ 4400 Å and ~ 4875 Å are BALs where the continuum is incorrectly following the troughs.

4.11. FBQS0955+3335 ($z = 2.503$)

The spectrum for this object is very nice. There is a weak N V emission line that is well separated from Lyman-α emission. The C IV emission line is fairly symmetric. As for Si IV emission, it is not clear whether it is resolved, or if there is absorption at the peak of the line. This spectrum has 25 significant lines redward of Lyman-α emission that are part of six absorption line systems.

$z_{\rm abs} = 1.5364$. — Given that there are nine lines in this system, it can be considered as certain. The Mg II doublet (#61,62) is quite strong and five lines of Fe II are observed (#54,55,56,58,59). Al III $\lambda\lambda$1854,1862 (#31,33) and Al II λ1670 (#23) may also be detected; however, the Al II line is in the Lyman-α forest and the red Al III line may be blended with a possible detection of Si II λ1526 from $z_{\rm abs} = 2.0953$.

$z_{\rm abs} = 2.0953$. — There are many lines in this system, but all are relatively weak. C IV $\lambda\lambda$1548,1550 (#34,35) is clearly seen; there is also evidence for the Si IV doublet (#28,29). Other possible lines are Al II λ1670, Si II λ1526 (though, if real, it would be blended with Al III λ1862 from $z_{\rm abs} = 1.5364$) and possibly some weak Fe II lines.

$z_{\rm abs} = 2.2857, 2.2923$. — These C IV(#40,41,42)+Lyman-α(#3,4) systems are uncertain; however if one is real, then the other one is needed to explain the doublet ratio.

$z_{\rm abs} = 2.3188$. — This is another system with only C IV $\lambda\lambda$1548,1550 (#43,44) and Lyman-α (#7).

$z_{\rm abs} = 2.5087$. — The reality of this redshift is questionable. The proposed detection of C IV λ1548 (#45) is below the 5σ detection threshold; however there is a weak feature at the expected position of C IV λ1550 and there is a Lyman-α (#25) line to go with it.

4.12. FBQS1045+3440 ($z = 2.353$)

This QSO is extremely rich in absorption lines with 55 5σ lines redward of Lyman-α emission. This is another example of a QSO where it is not clear if Si IV emission is partially resolved or if the apparent separation is caused by an absorption feature. There are as many as 11 absorption line systems.

$z_{\rm abs} = 0.6232$. — This system is very uncertain; however, if it were real it would explain some of the residual features in the absorption spectrum that are not accounted for by the other systems. Possible lines are Mg II $\lambda\lambda$2796,2803 (#29,30) and Fe II λ2600 (#19). They are badly blended with lines from other systems.

$z_{\rm abs} = 0.8811$. — Only the Mg II doublet (#50,51) is seen at this redshift, making it "possible".

$z_{\rm abs} = 1.7157$. — The Mg II doublet (#74,76) is contaminated by residual telluric absorption;

however, with a dozen or more lines, this system is unambiguous. Also seen are six lines of Fe II (#23,57,59,60,67,68), Al III $\lambda\lambda$1854,1862 (#40,42), Al II λ1670 (#29) and possibly Si II λ1526 (#13) though it is blended with the N V absorption from the complex of "associated" systems. Finally, there is strong evidence for C IV $\lambda\lambda$1548,1550 (#15,16), though the doublet is not resolved — this could reflect the fact that the lines are broader than usual or that there is contamination from another system.

$z_{\rm abs} = 1.7270$. — This system has all the same lines as the previous system; however, none of them are unblended. As such the system is considered probable, but not definite.

$z_{\rm abs} = 1.9456$. — The lines in this system are all very strong. The C IV $\lambda\lambda$1548,1550 (#31,32) lines are stronger than 1 Å REW. Many Fe II lines (#36,65,66,67,76,78) are seen as are Al III $\lambda\lambda$1854,1862 (#52,53), Al II λ1670 (#39) and Si II λ1526 (#27). The blue line of the Si IV doublet (#9) is also strong; the red line is blended with N V from the associated absorption complex. The spectrum does not quite cover Mg II, but there is an indication of the Mg II λ2796.

$z_{\rm abs} = 2.0750$. — Only C IV $\lambda\lambda$1548,1550 (#37,38) and Si IV $\lambda\lambda$1393,1402 (#21,22) are found, but they are not blended with any other lines, so this redshift is fairly certain.

$z_{\rm abs} = 2.2525$. — This system is suggested by a likely detection of the C IV doublet (#40,41) and possible detection of the Si IV doublet (#29,32), though Si IV is badly blended.

$z_{\rm abs} = 2.3325, 2.3375, 2.3432, 2.3496$. — This is a set of four overlapping systems of C IV $\lambda\lambda$1548,1550 (#44,45,46,47,48), N V $\lambda\lambda$1238,1242 (#10,11,12,13,14) and Lyman-α (#5,6,7,8). It is unclear if all four systems are real; however, it is difficult to explain the line ratios with fewer systems.

4.13. FBQS1253+2905 ($z = 2.565$)

This object is the host of yet another example of a complex Si IV emission line. Either there is significant absorption at the redshift of the QSO, or the emission line doublet is partially resolved. N V emission is fairly strong and is well-separated from Lyman-α emission. There is a complex of associated absorption lines that are of particular interest. Twenty-four absorption lines with significance greater than 5σ are found to the red of the Lyman-α emission line. These lines constitute six different systems.

$z_{\rm abs} = 1.3186$. — Mg II $\lambda\lambda$2796,2803 (#66,67) and Fe II λ2382 (#57) are the only lines observed at this redshift: as such it is considered "possible".

$z_{\rm abs} = 1.9127$. — Only C IV $\lambda\lambda$1548,1550 (#38,39) is detected.

$z_{\rm abs} = 2.0654$. — The C IV doublet (#41,42), Si II λ1526 (#40) and Al II λ1670 (#49) define this mixed ionization system.

$z_{\rm abs} = 2.1083$. — C IV $\lambda\lambda$1548,1550 (#43,44) are observed and there is a possible detection of Si IV $\lambda\lambda$1393,1402 (#30,32).

$z_{\rm abs} = 2.5411, 2.5497$ — Both of these systems exhibit C IV $\lambda\lambda$1548,1550 (#52,53,54,55), N V $\lambda\lambda$1238,1242 (#33,34,35,36) and Lyman-α (#27,28,29). The $z_{\rm abs} = 2.5497$ system is quite strong and fairly unambiguous. The $z_{\rm abs} = 2.5411$ system is necessary to account for the unusual profile of the complex and is less certain.

4.14. FBQS1348+2840 ($z = 2.466$)

The C IV emission line of this QSO is somewhat asymmetric. Otherwise it is a fairly ordinary QSO emission spectrum. However, there is a noticeable lack of absorption.

$z_{\rm abs} = 1.0179$. — This redshift is suggested by a possible Mg II doublet (#38,39) and Fe II λ2382 (#27); however, it is equally likely that the Mg II absorption is a continuum fitting feature. As such this system is considered unlikely.

$z_{\rm abs} = 1.6610$. — There is little more than a possible detection of Al III $\lambda\lambda$1854,1862 (#31,32) to indicate this rather unlikely system.

4.15. FBQS1416+2649 ($z = 2.303$)

The signal-to-noise of this spectrum is lower than the goal as a result of inclement weather during observations at this right ascension. Many of the lines in the red spectrum are likely to be spurious. In the blue spectrum there are 15 significant lines to the red of Lyman-α emission. These lines are found in five systems.

$z_{\rm abs} = 1.6975$. — The C IV doublet (#8,9) in this system is somewhat suspect as as result of blending; however, with six or more other lines, the system itself is certain. Mg II $\lambda\lambda$2796,2803 (#56,57) are obvious even at the lower signal-to-noise of the red spectrum. Also found are two or more Fe II lines (#41,43,48) along with Si II λ1526 (#6) and Al II λ1670 (#14).

$z_{\rm abs} = 2.0162$. — Weak Si IV $\lambda\lambda$1393,1402 (#10,11) is seen in this C IV (#16,17) absorption line system. There is also a hint of Fe II λ2382 (#49), but this may be an artifact.

$z_{\rm abs} = 2.2044$. — Strong lines of C IV $\lambda\lambda$1548,1550 (#19,20) are the only lines found in this system. Si IV would be observable but is not detected.

$z_{\rm abs} = 2.2328$. — This is another C IV only system (#21,22).

$z_{\rm abs} = 2.2928$. — This system is defined by a very strong C IV doublet (#23,24) found very close to the emission redshift of the QSO. N V $\lambda\lambda$1238,1242 (#4,5) is also clearly seen. There is some evidence for Si IV (#15), but the red line is not detected. In addition, there is a feature near

the expected position of C II λ1334 (#13).

4.16. FBQS1457+2707 ($z = 2.531$)

This QSO is yet another example from this sample of QSOs where the Si IV emission line ($\sim$4950 Å) appears resolved. N V emission is also clearly seen in the wing of Lyman-α. Thirty lines stronger than 5σ are found to the red of Lyman-α emission. These lines constitute four systems. The two lowest redshift systems are particularly interesting. They are low ionization systems separated by approximately the doublet splitting of C IV. This splitting made the identification difficult, since the resulting features look like poorly resolved C IV doublets with ratios that are not quite correct. There is also evidence for Mn II absorption.

$z_{\rm abs} = 0.9854, 0.9888$. — This pair of low ionization systems wreaked some havoc with the line identification code as mentioned above. However, from visual inspection it is clear that it is a pair of systems with Mg II $\lambda\lambda$2796,2803 (#43,44), Fe II (#32,33,34,35,37,38,39,40) and probably Mn II. The higher redshift line is similar in strength to the blue line in Fe II, but is considerably weaker in Mg II.

$z_{\rm abs} = 1.5701$. — The only evidence for this redshift is a possible detection of the Mg II doublet (#60,61) that is near a telluric feature.

$z_{\rm abs} = 1.8346$. — C IV $\lambda\lambda$1548,1550 (#28,29) is clearly detected and there is evidence for many other lines. These include Mg II $\lambda\lambda$2796,2803 (#76,77), two lines of Fe II (#51,52), Si II λ1526 (#27) and possibly Al III λ1854 (#41). There is also a line at the locations of Al II λ1670 (#35); however, this line overlaps the Fe II λ2382 lines from the $z_{\rm abs} = 0.9854, 0.9888$ complex and may not be real.

4.17. FBQS1537+2716 ($z = 2.445$)

This QSO has a rather unusual emission spectrum; the emission lines are *very* weak. In particular, the C IV emission line merges smoothly with the continuum on the blue side and is discernible only by the red wing of the line. Redward of Lyman-α emission there are 9 strong absorption lines, of which half are identified. Many of the unidentified lines are in the red spectra and may be continuum fitting artifacts resulting from lower S/N in the red spectra.

$z_{\rm abs} = 0.8595$. — Only Mg II $\lambda\lambda$2796,2803 (#32,33) is found.

$z_{\rm abs} = 1.7341$. — The Mg II doublet (#53,54) and Fe II λ2382 (#44) lines are seen; however, they are all questionable identifications.

4.18. FBQS1540+4138 ($z = 2.512$)

The emission spectrum of this QSO has C IV much stronger than Si IV, and the N V line is clearly seen in the red wing of Lyman-α. Thirty-five significant lines are detected longward of Lyman-α emission. These lines are distributed among six systems.

$z_{\rm abs} = 0.8697$. — This system is identified by a saturated Mg II doublet (#50,51) and a weak Mg I λ2852 (#53) line. Fe II lines are also found at rest wavelengths of $\lambda 2344, 2382, 2586$ and 2600 (#30,31,38,39). The Fe II λ2586 line is blended with Si II λ1526 from $z_{\rm abs} = 2.1675$.

$z_{\rm abs} = 1.9219$. — The C IV $\lambda\lambda$1548,1550 doublet (#32,33) suggests the possibility of this redshift.

$z_{\rm abs} = 2.0265$. — At this redshift a nearly saturated C IV doublet (#36,37) is seen as are Si II λ1526 (#35) and Al II λ1670 (#46). Si IV $\lambda\lambda$1393,1402 and C II λ1334 may also be present, but they are in the forest.

$z_{\rm abs} = 2.1675$ — A strong C IV doublet (#41,42) is found in the midst of the Si IV emission line. Other lines include Si IV $\lambda\lambda$1393,1402 (#29,30), Al II λ1670 (#52) and Si II λ1526 (which is blended with Fe II from $z_{\rm abs} = 0.8697$). Other low ionization lines also may be detected, but are lost in the noise of the forest.

$z_{\rm abs} = 2.2291$ — A weak C IV doublet (#44,45) is the only thing observed at this redshift.

$z_{\rm abs} = 2.2791$ — Again only C IV $\lambda\lambda$1548,1550 (#47,48) is seen.

4.19. FBQS1625+2646 ($z = 2.507$)

This object, otherwise known as KP 76, was previously studied by Crotts (1989). The Lyman-α, Si IV and C III] emission lines are shifted significantly redward from the redshift indicated by C IV. There are 40 lines of significant strength not including those lines found in the Lyman-α forest. As many as 12 systems may be found in this spectrum, though most are questionable. There is one strong line on top of the C IV emission line that remains unidentified.

$z_{\rm abs} = 0.7503$ — It is possible that there might be absorption by Mg II $\lambda\lambda$2796,2803 (#35,37) at this redshift.

$z_{\rm abs} = 0.8873$ — A Mg II doublet (#42,43), Mg I λ2852 (#47) and three Fe II lines (#25,28,37) define this system. The blue line in the Mg II doublet is blended with one or more other lines.

$z_{\rm abs} = 1.0388$ — Mg II $\lambda\lambda$2796,2803 (#54,55) is evident. Fe II $\lambda 2382, \lambda 2344$ and λ2600 (#32,34,44) are also present.

$z_{\rm abs} = 1.1346$ — While it is unlikely, a doublet of Mg II (#58,59) may be detected at this redshift.

$z_{\rm abs} = 1.4240$ — There appears to be an absorption feature at the wavelength indicated by a Mg II doublet (#63,64) at this redshift. The reality of the identification is highly questionable.

$z_{\rm abs} = 1.4805$ — The feature near λ6940 may be a continuum fitting residual, but may also be Mg II $\lambda\lambda$2796,2803 (#66,67).

$z_{\rm abs} = 1.8799$ — A doublet of C IV (#26,27) may suffice to explain this absorption feature near λ4460.

$z_{\rm abs} = 2.0520$ — Strong C IV $\lambda\lambda$1548,1550 (#30,31) absorption defines this system. This redshift may be confirmed by possible identification of Si IV $\lambda\lambda$1393,1402 and C II λ1334; however those lines are all in the forest.

$z_{\rm abs} = 2.2453$ — A weak C IV doublet (#38,39) suggests this redshift.

$z_{\rm abs} = 2.4010$ — This may be a system with C IV $\lambda\lambda$1548,1550 (#41,42). If real the blue line is clearly observed, but the red line is blended with Mg II λ2796 from $z_{\rm abs} = 0.8873$. However, a strong line is seen at the expected position of Lyman-α (#11) so this system is considered probable.

$z_{\rm abs} = 2.4441$ — This is another Lyman-α+C IV system. The C IV doublet (#45,46) is weaker in this system than in the previous one.

$z_{\rm abs} = 2.5288$ — There is strong evidence for both Lyman-α (#23) and C IV λ1548 (#49) absorption at this redshift; however, C IV λ1550 is not detected. As such this system is questionable.

4.20. FBQS1634+3203 ($z = 2.336$)

The C IV emission line is very broad as is the Lyman-α+N V blend. Thirty-four significant lines are found in the six systems redward of Lyman-α emission.

$z_{\rm abs} = 0.7293$ — This system is defined by a weak Mg II doublet (#25,26).

$z_{\rm abs} = 1.2839$ — There is evidence for Mg II $\lambda\lambda$2796,2803 (#49,50) and some Fe II lines at this redshift; however they are all very likely to be spurious.

$z_{\rm abs} = 1.4942$ — The detection of eight lines leaves little doubt regarding the reality of this systems. Doublets of Mg II (#56,57) and Al III (#19,20) are found along with Al II λ1670 (#11). Three or more Fe II lines are also seen.

$z_{\rm abs} = 2.0921$ — This system is somewhat unusual: Al II λ1670 (#31), Si II λ1526 (#23) and C II λ1334 (#9) are the strongest lines in the system. The Fe II lines are somewhat weaker and the C IV and Si IV doublets are even weaker. In addition, there is absorption at the expected position of Ni II λ1709 (#35). Mg II is beyond the range of the spectrum.

$z_{\rm abs} = 2.2582$ — C IV $\lambda\lambda$1548,1550 (#29,30) are seen along with Si IV $\lambda\lambda$1393,1402 (#16,17) and possibly Si II λ1526 (#23); however, Al II λ1670 is not detected.

$z_{\rm abs} = 2.3504$ — This is clearly an "associated" system with a redshift slightly higher than that of the QSO. The C IV (#32,33), Si IV (#21,22) and N V (#10,11) doublets are all clearly detected. A very strong Lyman-α line (#7) is also observed.

4.21. FBQS1645+2244 ($z = 2.723$)

The redshift of this QSO pushes the C IV emission line into the red spectrum. Both C III] and Al III are also observed in emission in the red part of the spectrum. The blue spectrum shows a broad Lyman-α emission line along with relatively strong lines of C II ($\sim$4975 Å) and O I ($\sim$ 4850 Å), with weaker Si IV. There are 21 5σ lines longward of Lyman-α emission. Only three systems are identified with these lines.

$z_{\rm abs} = 1.9648$ — This is a C IV doublet (#49,50) of moderate strength. Si IV may also be detected, but it is in the forest.

$z_{\rm abs} = 2.3992$ — Both C IV $\lambda\lambda$1548,1550 (#59,60) and Si IV $\lambda\lambda$1393,1402 (#52,53) are fairly strong in this absorber. Lower ionization lines of Si II λ1526 (#58) and C II λ1334 (#46) may also be detected. In the forest, the Lyman-α line (#10) is strong and stands out from the forest. N V may also be present, but it is difficult to determine if the lines are real or simply Lyman-α forest lines.

$z_{\rm abs} = 2.5738$ — There is a possible detection of C IV (#62,63) at this redshift. The reality of this system is further supported by detections of Si IV (#54,55) and Lyman-α (#27).

4.22. FBQS1651+4002 ($z = 2.339$)

The emission lines in this QSO all have very nearly the same redshift. Redward of Lyman-α emission, there are 29 absorption lines with greater than 5σ significance. These lines constitute six systems.

$z_{\rm abs} = 0.4991$ — This is a very low redshift Mg II doublet (#10,11). The presence of Mg I λ2852 (#12) supports the reality of this redshift.

$z_{\rm abs} = 1.6380$ — A strong doublet of C IV (#7,8) in the red wing of Lyman-α emission defines this system. Mg II may also be detected, but it is uncertain.

$z_{\rm abs} = 1.7992$ — Only C IV $\lambda\lambda$1548,1550 (#14,15) serves to define this system.

$z_{\rm abs} = 1.8912$ — This system is certain; it has at least six strong lines with many more weaker lines. Both the C IV (#19,20) and Mg II (#67,68) doublets are found. Si II λ1526 (#16) and Al II λ1670 (#24) also are clearly detected and there is evidence for a few of the Fe II transitions as well.

$z_{\rm abs} = 1.9920$ — Weak C IV $\lambda\lambda$1548,1550 (#21,22) is seen in the blue wing of Si IV emission.

Lyman-α is not in the range of the spectrum.

$z_{\rm abs} = 2.1905$ — This is another C IV only system (#27,28). If real, it is very weak.

4.23. FBQS2216-0057 ($z = 2.392$)

This QSO has an asymmetric C IV emission line (~ 5250 Å) that is skewed towards the red. N V and O I are also clearly observable. Twenty-one lines that are significant are observed longward of Lyman-α emission. There are five absorption line systems.

$z_{\rm abs} = 0.5372$ — This redshift is suggested by weak Mg II $\lambda\lambda$2796,2803 (#17,18) absorption. It is considered questionable.

$z_{\rm abs} = 0.6791$ — Strong lines of Mg II (#23,24) and Mg I λ2852 (#27) are seen as are Fe II λ2586 and λ2600 (#19,20).

$z_{\rm abs} = 1.5724$ — This is another strong Mg II $\lambda\lambda$2796,2803 (#50,51) system. Mg I λ2852 is not detected but six Fe II lines are (#14,42,43,44,45,46). The Al III $\lambda\lambda$1854,1862 doublet (#25,27), Al II λ1670 (#17) and Si II λ1808 (#22) are also seen. C IV is lost in the forest.

$z_{\rm abs} = 2.1674$ — Only C IV (#29,30) serves to indicate this redshift. Lyman-α is out of range.

$z_{\rm abs} = 2.3927$ — Strong Lyman-α (#13) is seen in this relatively weak C IV system (#36,37). It is just blueward of the emission redshift.

4.24. FBQS2233-0838 ($z = 2.339$)

This QSO has a fairly innocuous emission spectrum. N V is seen in the red wing of Lyman-α. Longward of Lyman-α emission, there are 24 strong lines in nine systems. Six lines remain unidentified.

$z_{\rm abs} = 0.5860$ — Strong Mg II (#20,21) is detected at this redshift. Also seen are Mg I λ2852 (#22) and Fe II λ2600 (#11). Fe II λ2586 would also be observable, but it is blended with C IV from $z_{\rm abs} = 1.6465$.

$z_{\rm abs} = 1.0674$ — There is a hint of Mg II (#38,39) to suggest this redshift, which is very uncertain.

$z_{\rm abs} = 1.1123$ — Another uncertain Mg II $\lambda\lambda$2796,2803 system (#40,41).

$z_{\rm abs} = 1.5140$ — No match to the pair of lines on top of Si IV emission could be found other than the Al III doublet (#24,25). The agreement is not perfect, but there is absorption at the expected locations of Mg II (#52,53) and Al II λ1670 (#15). As such, this redshift is considered probable.

$z_{\rm abs} = 1.6465$ — Strong C IV $\lambda\lambda$1548,1550 (#9,10) is detected at this redshift. It is partially contaminated by Fe II λ2586 from $z_{\rm abs} = 0.6791$.

$z_{\rm abs} = 1.7527$ — This is a questionable C IV (#16,17) only system. Lyman-α is not observable.

$z_{\rm abs} = 1.7809$ — Same as for $z_{\rm abs} = 1.7527$ (#18,19).

$z_{\rm abs} = 2.3226$ — Weak C IV (#29,30) absorption is seen is the blue wing of C IV emission. A strong Lyman-α (#5) line bolsters the reality of this system.

$z_{\rm abs} = 2.3398$ — This is an associated absorption system that is at nearly the same redshift of the QSO. Lyman-α (#7) is seen along with N V (#12,13) and C IV (#31,32). Si IV is not detected.

5. Analysis and Discussion

Prior to discussing the evidence for and against high-velocity, intrinsic C IV absorption, it is necessary to have a basis for comparison. As such, the distribution of all C IV and Mg II absorbers both as a function of redshift and velocity are presented here. Some preliminary comments are necessary. When discussing the redshift distribution of absorbers, we make the assumption that *all* of the absorbers have redshifts that are indicative of their cosmological distribution and that there are no significant relativistic velocity components to their redshifts. Yet, it is well-known that there are absorbers that have large relativistic velocity components to their redshifts, for example, BALs and associated absorption lines. Fortunately, both of these species are easy to recognize and they can be removed from the sample when and if called for.

Similarly, when discussing the velocity distribution of absorbers, it is assumed that *all* the absorbers have cosmological redshifts that are very close to the redshift of the QSO and that any differences are due to relative velocities. However, many, if not most, QSO absorption lines are cosmological in origin, i.e. they are caused by material along the line of sight, but not physically associated with the QSO. Unlike the case described in the previous paragraph, there is almost no way to distinguish these systems a priori so that the intrinsic/associated systems can be studied by themselves.

This fundamental inability to separate the two classes of absorbers is the basis for this study. The ability to separate these populations is crucial to the science that comes from the analysis of QSO absorption lines systems. Should it be confirmed that there is indeed a significant population of apparently high-velocity absorbers that also have narrow profiles, it will have a strong impact on previous and future absorption lines studies. The ability to discern the differences in the classes of absorption lines systems using low resolution spectra, as opposed to more time consuming high resolution spectra as discussed by Barlow & Sargent (1997), would be of considerable value.

The primary diagnostics used throughout this work are plots of the number of absorbers per unit redshift ($dN/dz \equiv N(z)$) and the number of absorbers per unit velocity ($dN/d\beta \equiv N(\beta)$). Both

of these quantities are normalized by the number of times a given absorber of a given strength could have been observed in the other QSOs in the sample, and should be independent of the velocity and redshift distribution of the parent objects (unless there is a physical meaning to such correlations).

Table 5 gives the different samples that are studied herein. Sample S1 includes all objects from the York et al. (1991) absorption line catalog, plus some systems from the update to this catalog (Vanden Berk et al. 2001). Sample S3 includes only the absorbers discovered in the 24 spectra presented herein. Sample S2 includes all of Sample S3 in addition to absorbers from objects in Sample S1 that met the selection criteria of Sample S3. The other sample types restrict either the intrinsic QSO properties or the element studied. Each of these samples can be combined with a bitwise AND to create a new, more restricted sample. For example, Sample S1C4L contains only C IV systems from the radio-loud quasars in Sample S1.

5.1. Redshift distribution of absorbers

Presented here are the normalized redshift distributions for C IV and Mg II. The redshift distribution of absorbers as a function of atom/ion will be discussed in detail by Vanden Berk et al. (2001); however, a brief discussion is necessary here. Figure 25 shows the normalized redshift distribution of all the C IV absorbers from Sample S1C4. The solid line in the bottom half of the plot gives the number of absorbers found in a given redshift bin (left axis). The dashed line in the bottom plot gives the number of quasars searched (right axis). The top plot is essentially the ratio of the two bottom plots and gives the normalized redshift distribution after correcting for selection effects; error bars are Poisson. In the top plot, thick lines are for bins with more than ten absorbers and are considered significant. Bins delineated by thinner lines have fewer than ten absorbers in a bin; these bins should be treated with caution (or they could be combined together in a single, more significant bin). Lines within $5000\,\mathrm{km\,s^{-1}}$ of the QSO redshift have been removed.

For comparison, the new data taken specifically for this project (Sample S3), yield a value for the number of absorbers per unit redshift (at $z \sim 2$) of 2.54 ± 0.44 for C IV absorbers with rest equivalent widths stronger than $0.15\,\mathrm{\AA}$. Note that this value is somewhat higher than that of Sample S1 as shown in Figure 25. For absorbers stronger than $0.30\,\mathrm{\AA}$, dN/dz is 1.43 ± 0.32. Both values are consistent with those determined by Sargent, Steidel, & Boksenberg (1988).

Figure 26 is similar to Figure 25 except that here Mg II is plotted instead of C IV (i.e. Sample S1M2). The most obvious difference is that the Mg II absorption is found at much lower redshift, since Mg II is at longer wavelengths and moves out of the optical and into the IR sooner than C IV. Ideally, one would like to compare the two species as tracers of high- and low-ionization lines, but the redshift discrepancy makes such a comparison difficult. Of particular interest is the well-known fact that Mg II absorption is seen less than half as often as C IV. This is true even in the small redshift range where the samples overlap.

5.2. Velocity Distribution

As with the redshift distribution analysis, it is also possible to assume that all of the absorbers are associated with the QSO and observed wavelengths that represent outflow velocities (positive or negative) with respect to the QSO redshift. Figure 27 shows the velocity distribution of all of the C IV (and Mg II) absorbers in the entire sample. The 375 C IV absorbers with relative velocities in excess of $5000\,\mathrm{km\,s^{-1}}$ are the same absorbers as in Figure 25, which emphasizes the different assumptions made in each type of analysis. The flatness of the distribution at large velocities typically is taken as evidence for the intervening hypothesis (Sargent et al. 1988). That is, if the absorbers are *not* associated with the QSOs but rather with intervening galaxies, then the erroneous assumption that the absorbers are associated with the QSOs will yield a random velocity distribution. For these (and all of the following) graphs of $dN/d\beta$, the first bin includes all systems within $5000\,\mathrm{km\,s^{-1}}$ of the QSO redshift. That most of these systems (those within $5000\,\mathrm{km\,s^{-1}}$) are primarily associated with QSOs and not intervening galaxies is generally accepted. Discussion of data in this velocity range will be reserved for a future study. For C IV absorbers with $v > 5000\,\mathrm{km\,s^{-1}}$ in Sample S3, the C IV $dN/d\beta$ values are 7.84 ± 1.34 and 4.44 ± 0.99 at $z \sim 2$ for $W_{rest} > 0.15\,\text{Å}$ and $W_{rest} > 0.30\,\text{Å}$, respectively. These values are somewhat larger than the average value for Sample S1.

Figure 27 also shows the velocity distribution of Mg II. Since the Mg II emission line is at a much longer wavelength than the Lyman-α forest (as compared to C IV), Mg II absorption is detected at apparent velocities much higher than that of C IV. Note that the distribution is quite flat and that there is no peak at or near zero apparent velocity. These facts are consistent with Mg II absorption being purely cosmological. The distributions of C II, Si II and Fe II are similar.

5.3. Absorption Lines as a Function of Radio Properties

In this section the velocity distribution of QSO absorption lines is studied as a function of radio properties. In each case, two samples are examined. First, the entire data set from York et al. (1991) and Vanden Berk et al. (2001) as of this writing (Sample S1), and second, Sample S2, the sample that includes Sample S3 and that is supplemented with data of similar quality from Sample S1.

5.3.1. Radio-Loud versus Radio-Quiet

The initial premise of this work was the comparison of the distribution of absorption lines as a function of radio luminosity. The observed dichotomy of radio-detected quasars provides a natural starting point for such a comparison (Stocke et al. 1992). If radio-loud and radio-quiet quasars constitute separate species (whether as a result of actual physical differences, or apparent physical

differences due to the viewing angle) and if QSO absorption line systems are not associated with the parent QSOs, then the distribution of these absorbers should be the same for both radio-loud and radio-quiet sources. We test this hypothesis for both C IV and Mg II in Samples S1 and S2.

Figure 28 gives the velocity distribution of absorbers for both radio-loud and radio-quiet quasars from Sample S1. Plotted is the number of C IV absorbers per unit velocity interval versus velocity. The solid line represents C IV absorbers seen in radio-loud quasars, while the dashed line represents the lines seen in radio-quiet quasars. In each case the number of absorbers is given in the legend since that number cannot be derived from looking at the plot (because it is a *normalized* number per unit velocity and not simply the number in a velocity bin). The legend gives the number with $v > 5000\,\mathrm{km\,s^{-1}}$ and the expected number in the same velocity range as determined by the average level for the entire sample. This average level for the entire sample (and its 1σ error) for $5000\,\mathrm{km\,s^{-1}} < v < 55,000\,\mathrm{km\,s^{-1}}$ is represented by the dotted line.

Figure 29 gives the velocity distribution of absorbers for both radio-loud and radio-quiet quasars for Sample S2. What is interesting is that the radio-loud sample agrees well with the predicted $dN/d\beta$ from the entire sample, but the radio-quiet sample shows a small excess over the expected level. Though the excess doesn't appear all that significant, it is the way that these excess absorbers are distributed that are interesting. In particular, for the whole sample, as depicted in Figure 28, the excess is at low and high velocities and is not prevalent at all velocities. This effect could simply be statistical error, but it may also be indicative of interesting physical processes. For comparison, the new data (Sample S3), give $dN/d\beta$ as 6.96 ± 2.01 and 6.09 ± 2.72 for C IV absorbers at $z \sim 2$ with $W_{rest} > 0.15\,\text{Å}$ in radio-quiet and radio-loud quasars, respectively.

Similar to C IV, the velocity distribution of Mg II is plotted in Figure 30 for Samples S1M2L and S1M2Q. The first bin shows just those systems within $\pm 5000\,\mathrm{km\,s^{-1}}$ of the QSO redshift. The other bins are $50,000\,\mathrm{km\,s^{-1}}$ wide. A similar analysis using Sample S2 confirms that there is no significant difference in the velocity distribution of Mg II between radio-quiet and radio-loud quasars. This fact demonstrates that the intervening galaxy hypothesis for Mg II is probably correct. It is unclear why the last bin of Figure 30 shows a difference between the radio-loud and radio-quiet Mg II absorbers. One possibility is that this difference is caused by N V doublets being mistaken for Mg II doublets in BAL-like radio-quiet QSOs.

5.3.2. Steep-spectrum versus Flat-spectrum

Though difference in the distribution of C IV in QSOs as a function of radio luminosity is interesting, a comparison of the distribution of C IV between flat-spectrum and steep-spectrum sources is somewhat more intriguing. Using the spectral indices of the quasars might be expected to be a better way to discern if there is any evidence for a population of high velocity, intrinsic narrow absorption given that quasars are distinctly asymmetric and that spectral indices are thought to correlate with the viewing angle of quasars (Padovani & Urry 1992).

Figure 31 shows the velocity distribution of C IV in the steep- and flat-spectrum quasars from Sample S1. At least three things of interest can be discerned from this plot. First, there is a well-known excess of absorbers in steep-spectrum quasars at low velocity (Foltz et al. 1988). Second, a small "spike" in steep-spectrum absorbers is seen near $\beta \sim 0.2$, which also will be commented on later. Finally, there is the excess of absorbers in flat-spectrum quasars as compared to steep-spectrum quasars that was first reported in Paper I. (However, we note that Sample S1 is not independent of the sample as used in Paper I).

The primary goal of this work is to attempt to determine if this result from Paper I is real. It is important to determine if the use of relatively inhomogeneous optical spectra have biased the result. For example, if the steep-spectrum quasars were not searched for absorption as thoroughly as the flat-spectrum quasars, such an effect might be observed. Since the levels have been corrected for the number of times each line could have been observed in terms of the wavelength coverage *and* the equivalent width detection threshold, such an effect in unlikely. Nevertheless, it is worth investigating this result with a more homogeneous sample.

Sample S2 is just such a sample. The systems from Sample S2 are all either from Sample S3, or from those objects in Vanden Berk et al. (2001) that meet the criteria of Sample S3. As such, Sample S2 is intended to be a sample that is relatively unaffected by inhomogeneity in the quality of the optical spectra. Figure 32 presents the velocity distribution of C IV absorption in a sample of steep- and flat-spectrum quasars from Sample S2, which is more homogeneous in its optical spectra than Sample S1 and includes only QSOs with $z_{em} \sim 2.5$. As was first reported in Paper I and as can be seen in Figure 31, there is an excess of C IV absorption from 5000 to $55,000\,\mathrm{km\,s^{-1}}$ in the flat-spectrum sample as compared to the steep-spectrum sample. The dotted line is the expected distribution (shown with one standard deviation errors) from all of the data in Paper I.

The excess of C IV in flat-spectrum quasars in Sample S2, while not terribly significant, is consistent with Figure 31 and the result from Paper I. The persistence of this excess in the more homogeneous sample is interpreted as a confirmation of the excess of C IV in flat-spectrum quasars and therefore of an orientation dependent population of intrinsic absorbers. This new result suggests that the old result from Paper I is not an artifact of inhomogeneous optical spectra. In Paper I, we used the excess absorption in the flat-spectrum sources to postulate that there is contaminated at the 36% level of the C IV sample in flat-spectrum quasars by a population of intrinsic absorbers. The numbers are too small in this sample for a similar analysis, but they are not inconsistent with the value derived in Paper I. The observed value of $dN/d\beta$ for Sample S3 is 8.03 ± 2.15 C IV absorbers with $W_{rest} > 0.15\,\text{Å}$ in flat-spectrum quasars. This value is consistent with the claimed excess in the larger sample. Unfortunately, the number of steep-spectrum quasars in Sample S3 is too small to determine a similar value for steep-spectrum quasars.

It is also significant that Sample S2 includes only those QSOs with $z_{em} \sim 2.5$. The result from Paper I could also have been biased if there is strong evolution in the frequency of C IV absorption as a function of redshift and if the flat- and steep-spectrum QSOs sampled somewhat different

redshift ranges (which they do). Therefore, the continued excess, albeit small, suggests that the excess observed in Paper I (and as seen in Figure 31) is not an artifact of redshift evolution.

For comparison of Mg II with C IV, Figure 33 gives the distribution of Mg II absorption line systems towards both steep- and flat-spectrum quasars in Sample 1M2. This plot serves to demonstrate that this excess of absorbers in flat-spectrum quasars does not extend to lower ionization species such as Mg II. Sample S2M2 has too few Mg II absorption line systems to make a similar comparison.

In addition to suffering from the use of inhomogeneous absorption line data, Paper I also suffered from a lack of homogeneous radio data. As such, one must be concerned that the evidence that was found for an intrinsic population of narrow, high-velocity C IV absorption line systems was merely an artifact of the inhomogeneity of the data. We address the problem of inhomogeneous radio spectral indices in Paper III using new, simultaneous 3.5 and 20 cm images (from the VLA in the A configuration) of 144 of the quasars from Paper I.

Since the idea that narrow absorption lines are caused by intervening galaxies is so entrenched and is backed up by considerable evidence, it is worth discussing what might cause the observed effects that lead to the conclusion that intrinsic absorption is not the only possible explanation for the steep/flat dichotomy. One obvious way to produce an excess of absorbers in one sample over another is for there to be systematic differences in the quality of the spectra or in the search algorithms. For instance, if the equivalent width limits for the steep-spectrum quasars are worse than for the flat-spectrum quasars because most of the steep-spectrum quasars come from a single study, then this might explain the dearth of absorption in those objects. While such a problem would certainly produce the observed effect, it is unlikely simply because $N(\beta)$ and $N(z)$ have been normalized not only by the number of quasars that the lines could have been observed in, but also by the number of times that a line of that equivalent width could have been measured in those quasars. However, more absorption line data from bright, steep-spectrum quasars are needed to fully rule out selection effects.

5.4. The Sloan Digital Sky Survey (SDSS)

The amount of data used for this study is only just enough for any sort of reasonable statistical analysis. Even the larger, less homogeneous sample (Sample 1) from which the primary sample studied herein (Sample 2) is drawn from is not large enough for certain kinds of analysis. However, the Sloan Digital Sky Survey should resolve any problems caused by the lack of data, let alone the lack of homogeneous data. The SDSS will produce spectra for approximately 10^5 QSOs to a limiting magnitude of $i' \sim 19$. All stellar sources that are detected by FIRST will be selected as QSO candidates. These spectra will be of sufficient signal-to-noise and resolution that they will be very valuable for QSO absorption line studies (York et al. 1999).

With a spectral resolution ($R = \lambda/\Delta\lambda$) of 2000 and wavelength coverage from 3900 to 9000 Å,

the SDSS QSO spectra will be well suited for QSO absorption line studies. Between redshift 2 and 3 alone, the SDSS will find about 7700 QSOs to a magnitude limit of $i' = 18.5$ (D. P. Schneider 1999, private communication). Typical studies of C IV at moderate redshifts obtain a 5σ rest equivalent width limit of 0.15 Å (Sargent et al. 1988). For a C IV absorption line system, the signal-to-noise ratio needed to achieve a 5σ rest equivalent width limit in an $R = 2000$ spectrum is 25.8 — independent of redshift. If the average $i' = 17.5$ magnitude SDSS QSO reaches this signal-to-noise (which it should), then there will be approximately 1050 QSOs in the SDSS sample between redshift 2 and 3 with spectra suitable for measuring C IV absorption to a rest equivalent width limit of 0.15 Å. Furthermore, the 7700 ($2 < z < 3$) SDSS QSOs brighter than $i' = 18.5$ and will be more than suitable for studying C IV absorbers stronger than $W_{rest} > 0.30$ Å.

Sargent et al. (1988) found that at $z \sim 2$ there are about 2.57 C IV absorbers per unit redshift with $W_{\rm o} > 0.15$ Å; they found that lines stronger than $W_{\rm o} > 0.30$ Å are found at the rate of approximately 1.48 per unit redshift. Given this frequency of C IV, we can ask how small of an intrinsic absorption population the SDSS sample could measure. That is, if there really are narrow, intrinsic absorption lines in QSOs at large velocities, what fraction of C IV systems would need to be intrinsic for them to be detected statistically? If we assume that we can separate the parent population with 100% efficiency and that the extra absorbers are all in one type of QSO, then we can determine the minimum observable fraction. Here we assume that the observed value of $dN/d\beta$ is the average of all QSOs over a velocity range of $5000 < \Delta v/c < 70000\,{\rm km\,s^{-1}}$. Given these assumptions, 16% of the C IV absorption line systems must be intrinsic in order to have a statistically significant detection in the SDSS data. For absorption stronger than 0.30 Å, an intrinsic population as small as 7% could be detected, largely as a result of the greatly increased number of QSOs.

6. Conclusions

New spectra of 24 $z \sim 2.5$ radio-detected quasars are presented. These spectra were searched for the most commonly observed QSO absorption lines. The number of C IV absorbers per unit redshift was found to be 2.54 ± 0.44 (at $z \sim 2$, with both members of the doublet stronger than 0.15 Å) — consistent with the finding of Sargent et al. (1988). In terms of velocity space, the number of absorbers per unit velocity ($dN/d\beta$) is 7.84 ± 1.34. For radio-quiet, radio-loud, and flat-spectrum quasars, $dN/d\beta$ was found to be 6.96 ± 2.01, 6.09 ± 2.72, and 8.03 ± 2.15, respectively.

The absorption line systems found in these quasars were combined with systems of similar quality from Vanden Berk et al. (2001) to form a statistical sample. This sample is restricted to redshifts between 2.2 and 2.8. The construction of this sample is such that it has more homogeneous absorption line properties and a smaller range of redshifts than the sample studied in Paper I. As such, this sample can be used to address potential biases in Paper I. Analysis of this sample and comparison to the less homogeneous parent sample yield the following conclusions:

1) The excess of C IV absorbers in flat-spectrum quasars as compared to steep-spectrum quasars is confirmed and is found to be consistent with the 36% excess as reported in Paper I. This excess does not seem to be the result of a bias in the quality of the QSO spectra (and thus the detection limits of C IV) as a function of radio spectral index. Nor does the effect result from a redshift evolution of the C IV distribution that is reflected by the differences in the redshift distributions of the steep- and flat-spectrum populations, since the effect remains when considering only a small range in redshift ($z \sim 2.5$). No such excess is observed in the Mg II sample.

2) There is also a small excess of high velocity C IV absorbers in radio-quiet QSOs as compared to radio-loud quasars. This excess appears to be a function of velocity and remains (at 2σ significance) in the more homogeneous sample. Though the significance is small, the effect deserves further consideration. No such effect is observed for Mg II absorbers.

3) The QSO spectra from the Sloan Digital Sky Survey will allow for the detection of a high velocity, narrow, intrinsic population of absorbers that is as small as 7% of the C IV absorber population in QSOs between redshift 2 and 3.

I would like to acknowledge Don York, my advisor, for his support and guidance in this project. I thank Sally Laurent-Muehleisen and Bob Becker for their assistance on this and related projects. Dan Vanden Berk, Jean Quashnock, Arieh Königl and John Kartje were additional sources of guidance and inspiration. Comments from an anonymous referee were very helpful to the flow of the paper.

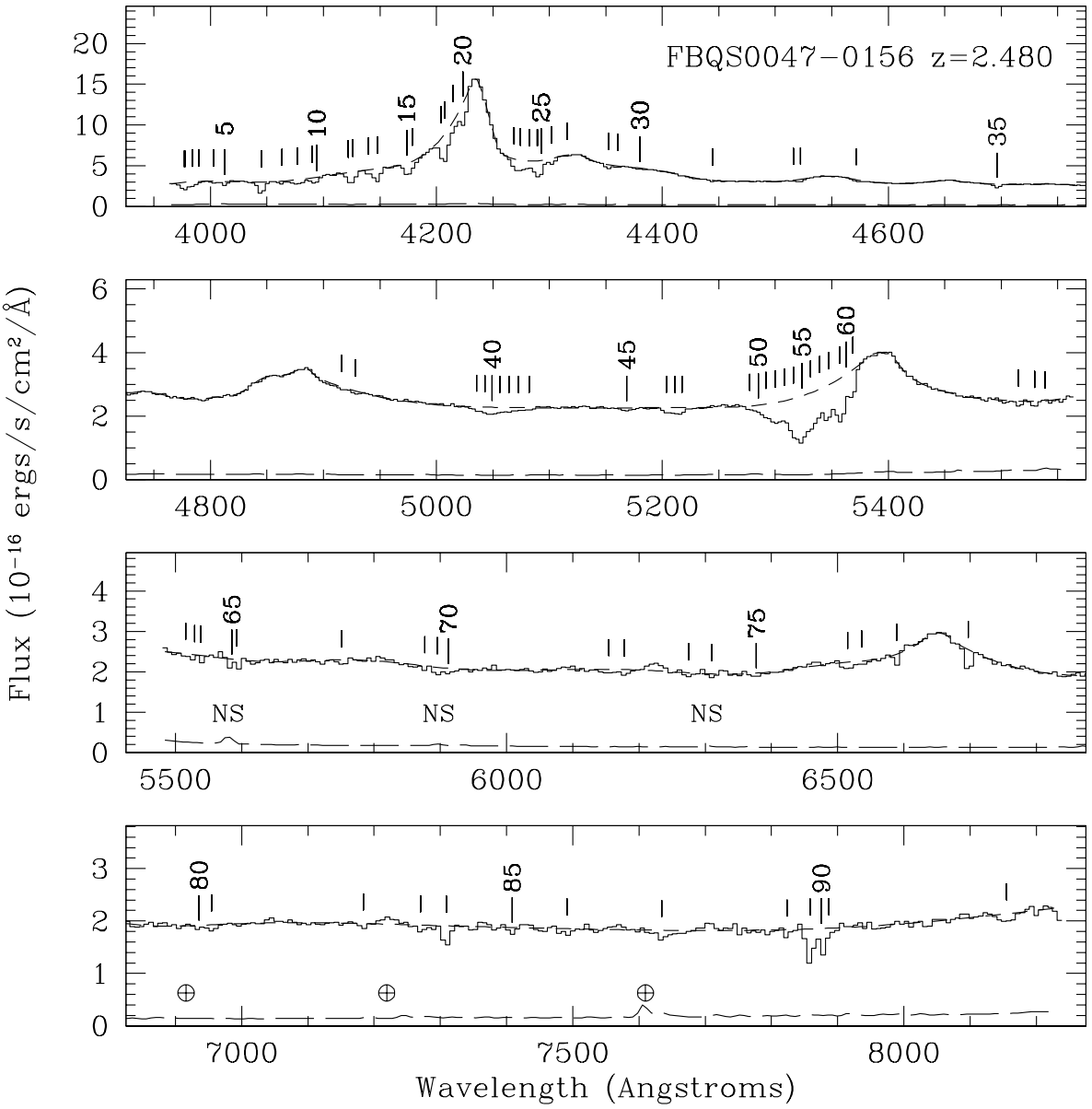

Fig. 1.— FBQS0047-0156. Coadded blue (upper panels) and red (lower panels) spectra of FBQS0047-0156. Solid line is the coadded spectrum, short dashed line is the continuum fit, and long dashed line is a 5σ error array. Absorption features with 3σ significance or better are indicated by tick marks. Regions effected by strong night sky lines are labelled with a "NS", whereas regions effected by telluric absorption are marked by a circled cross.

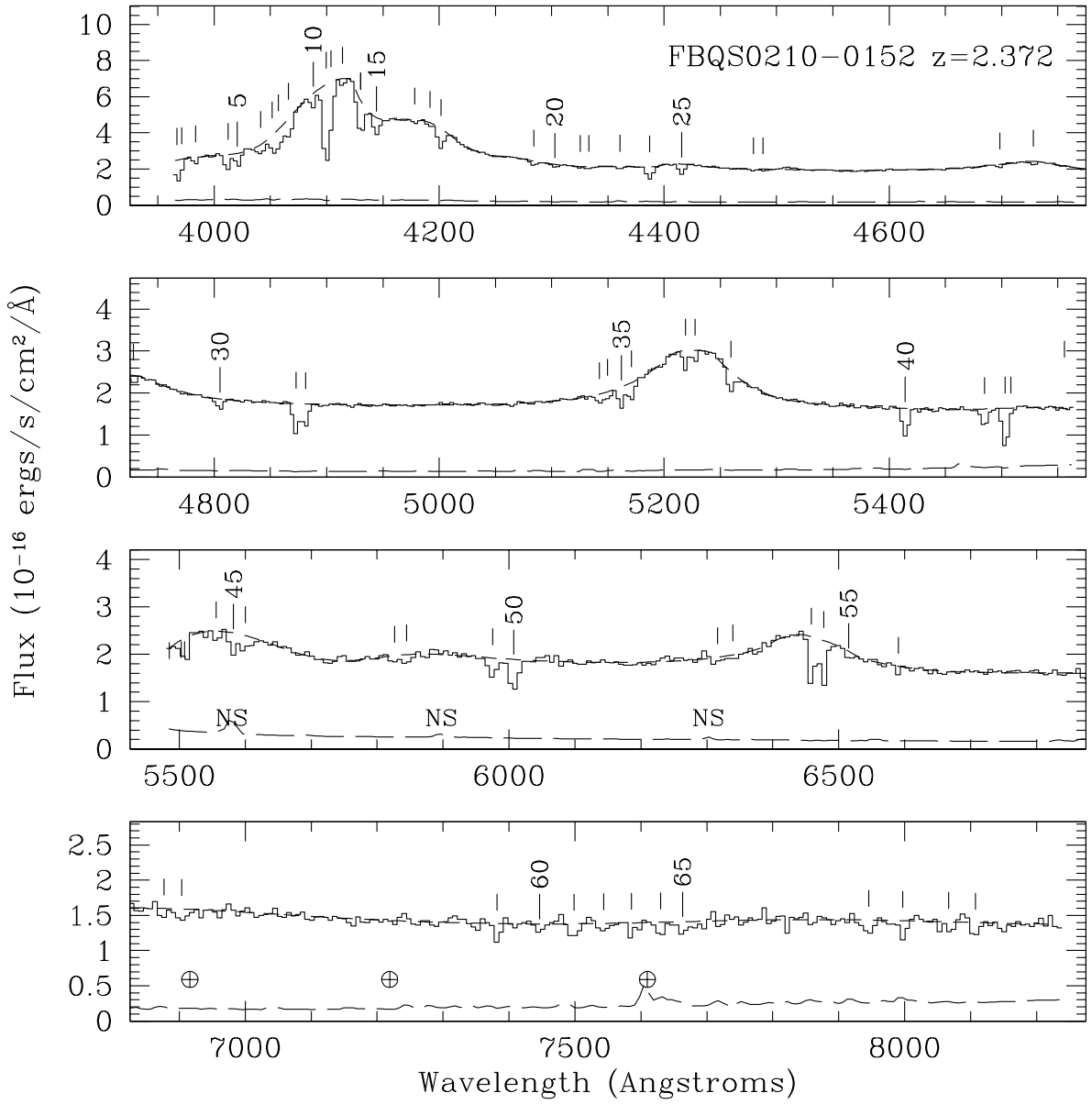

Fig. 2.— FBQS0210-0152

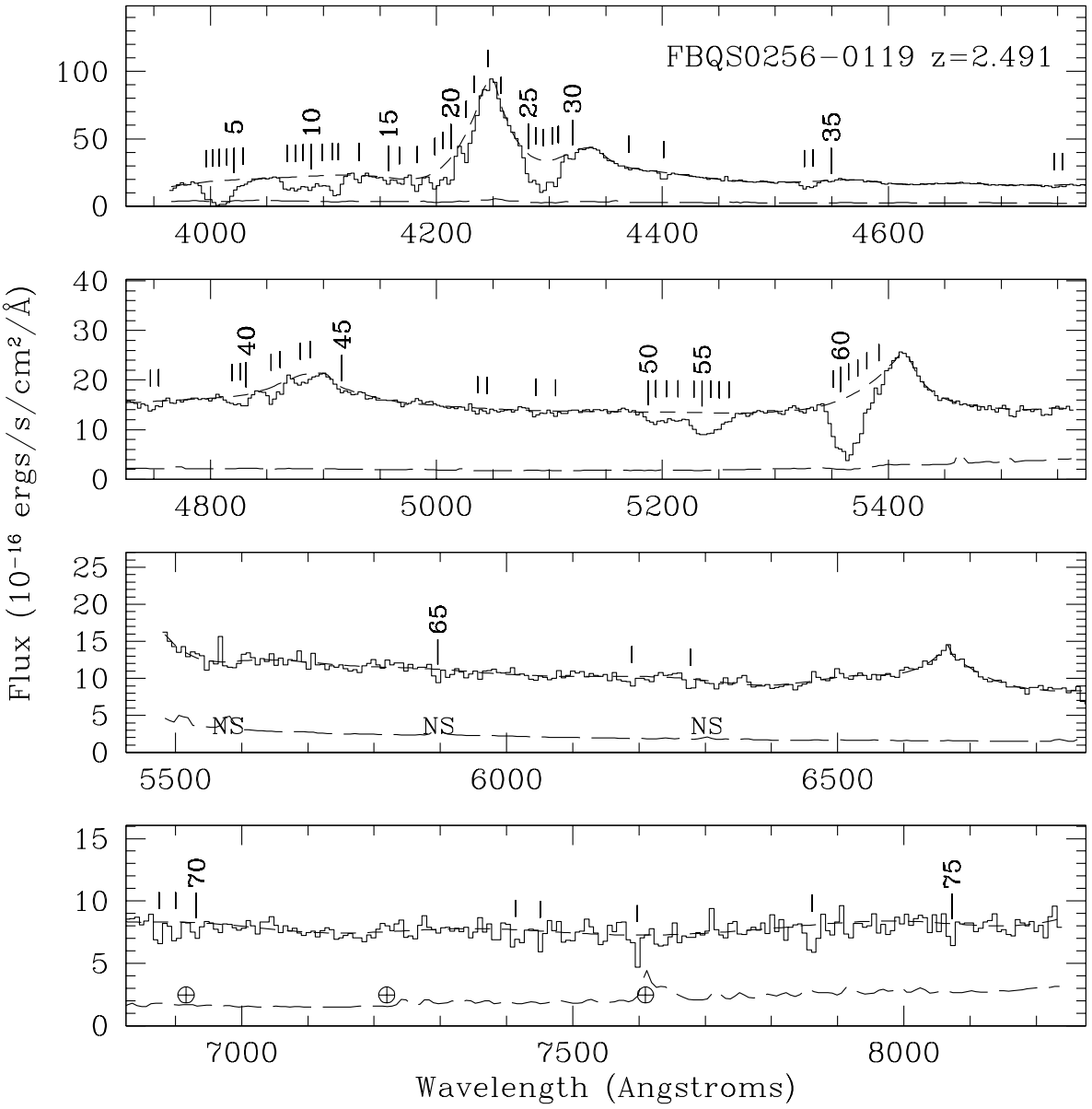

Fig. 3.— FBQS0256-0119

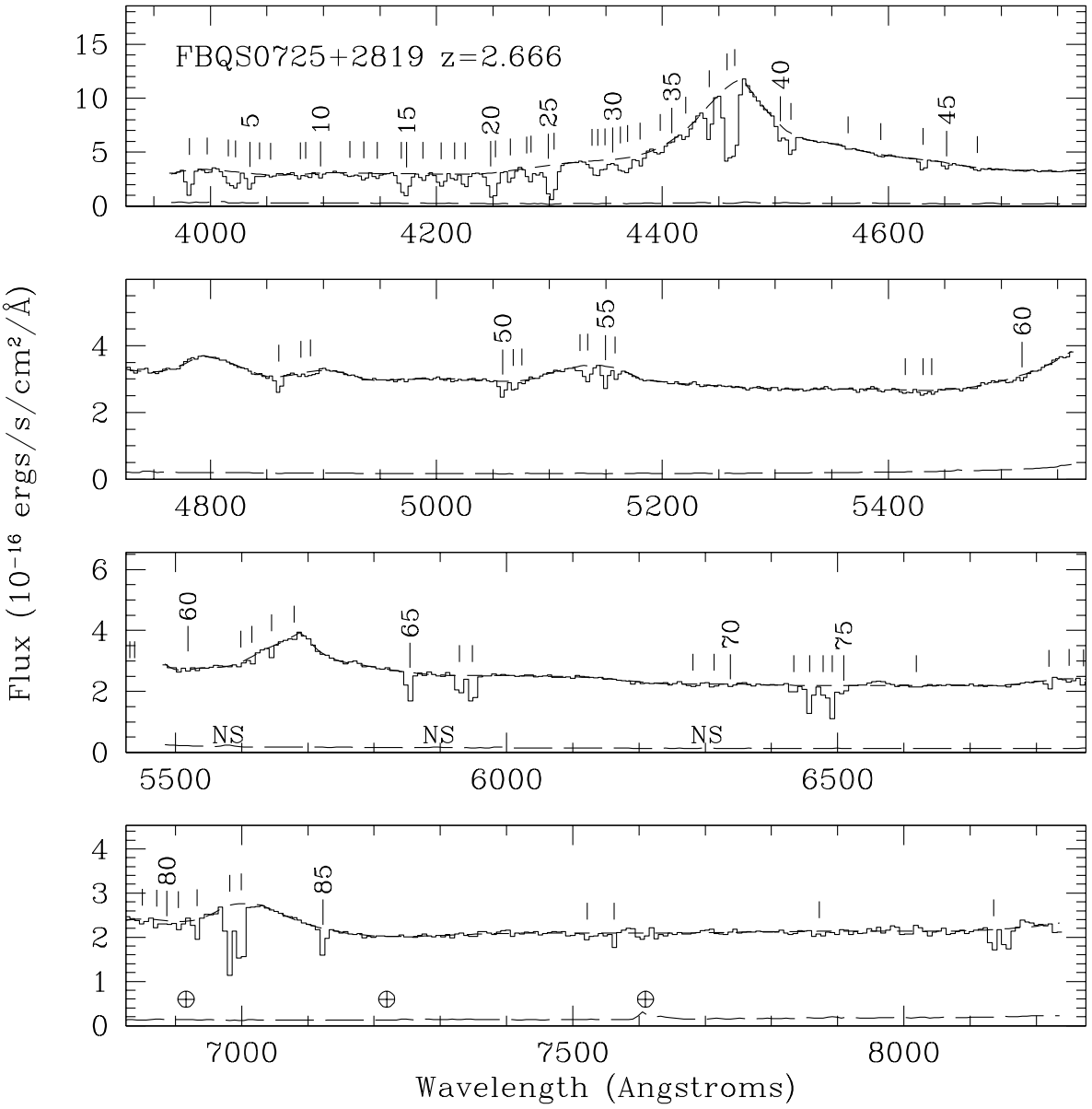

Fig. 4.— FBQS0725+2819

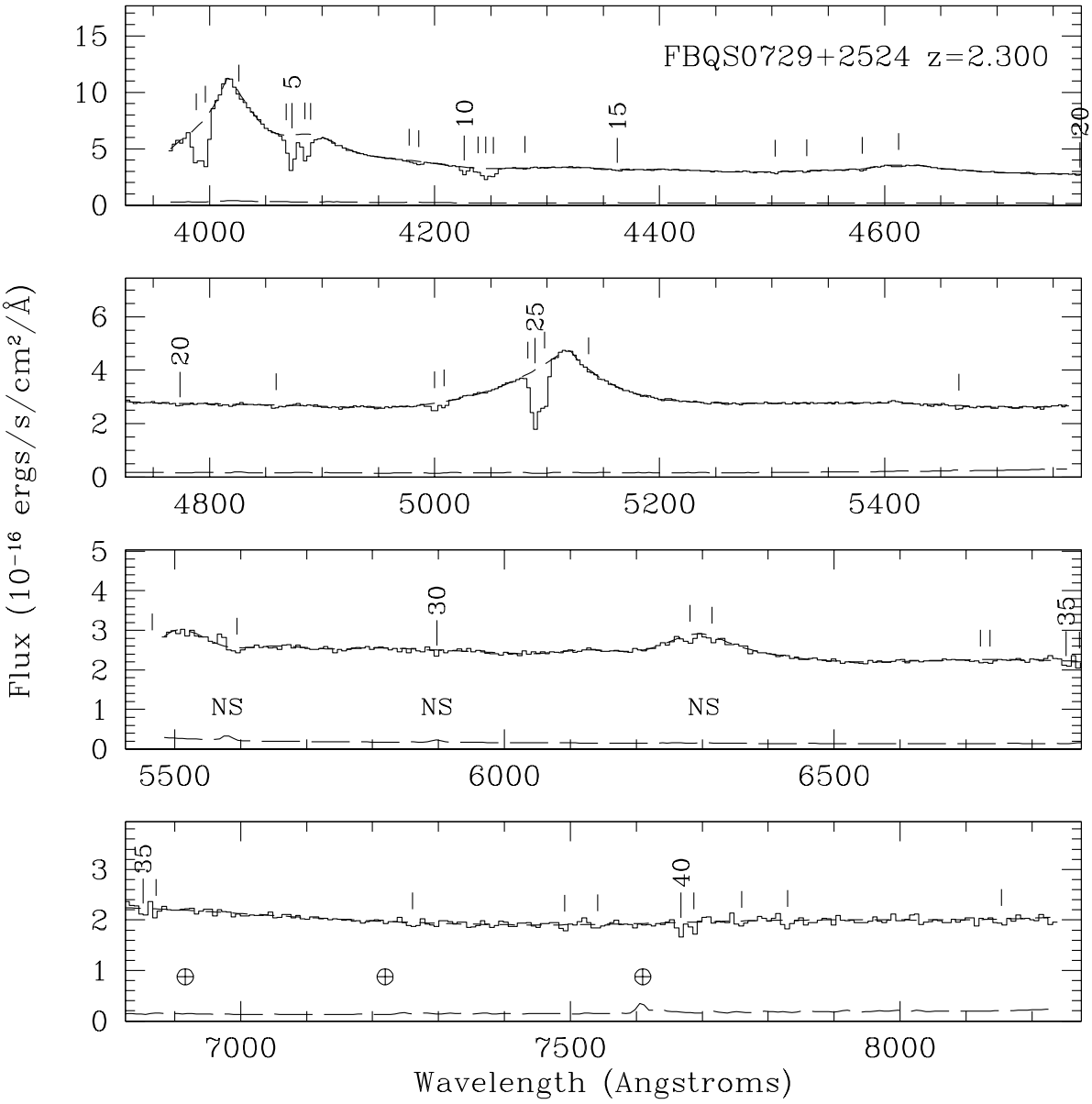

Fig. 5.— FBQS0729+2524

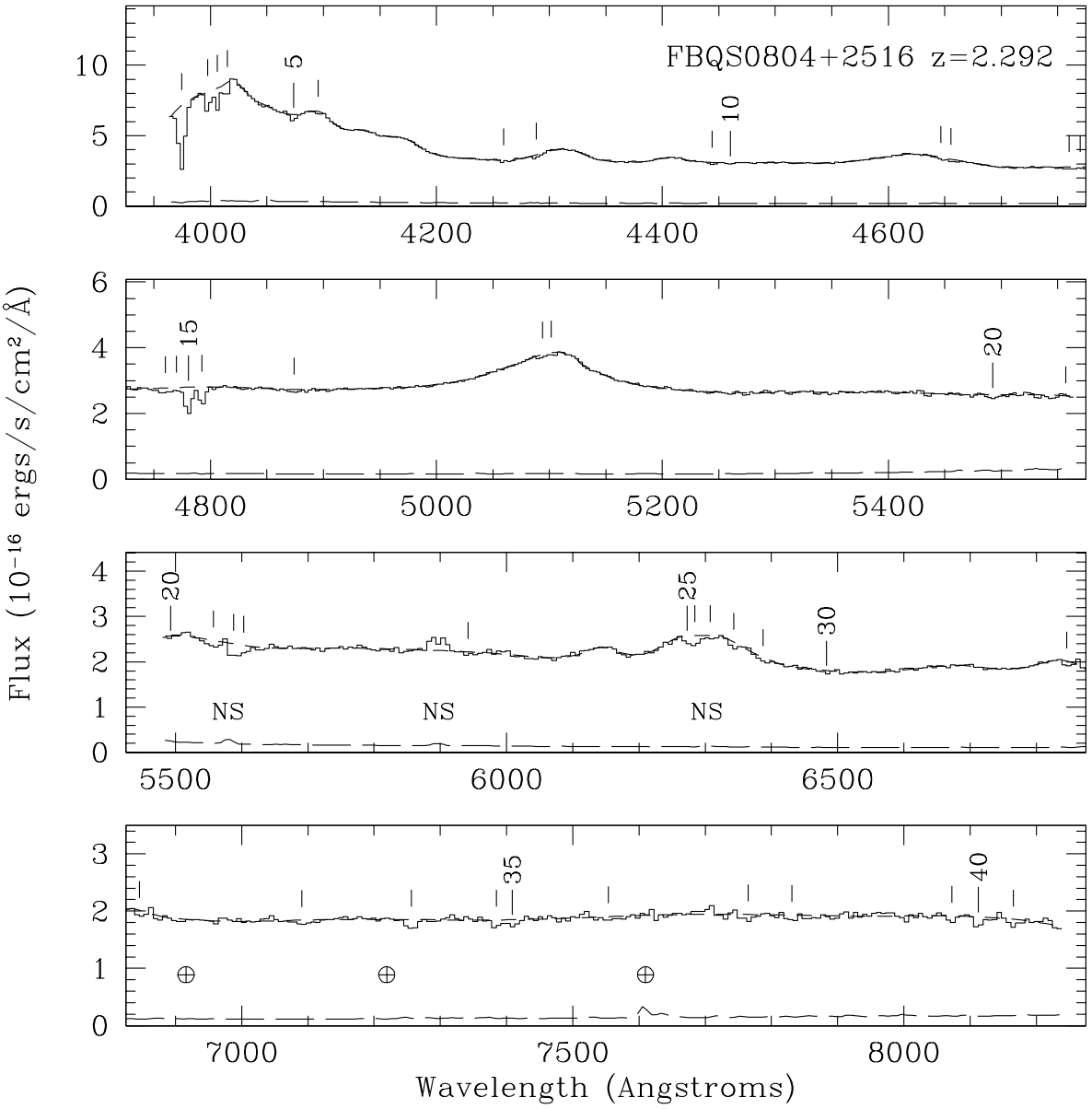

Fig. 6.— FBQS0804+2516

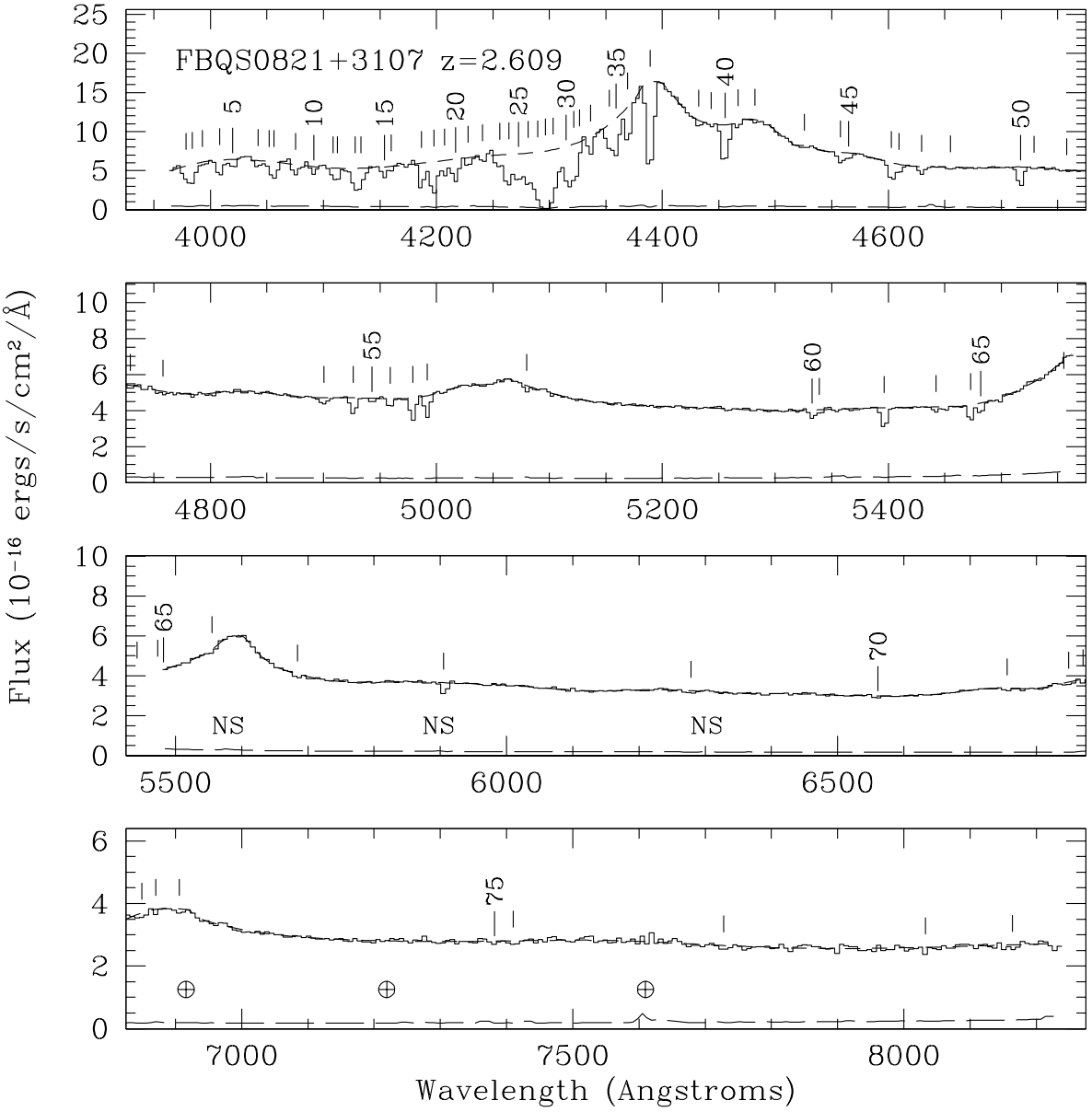

Fig. 7.— FBQS0821+3107

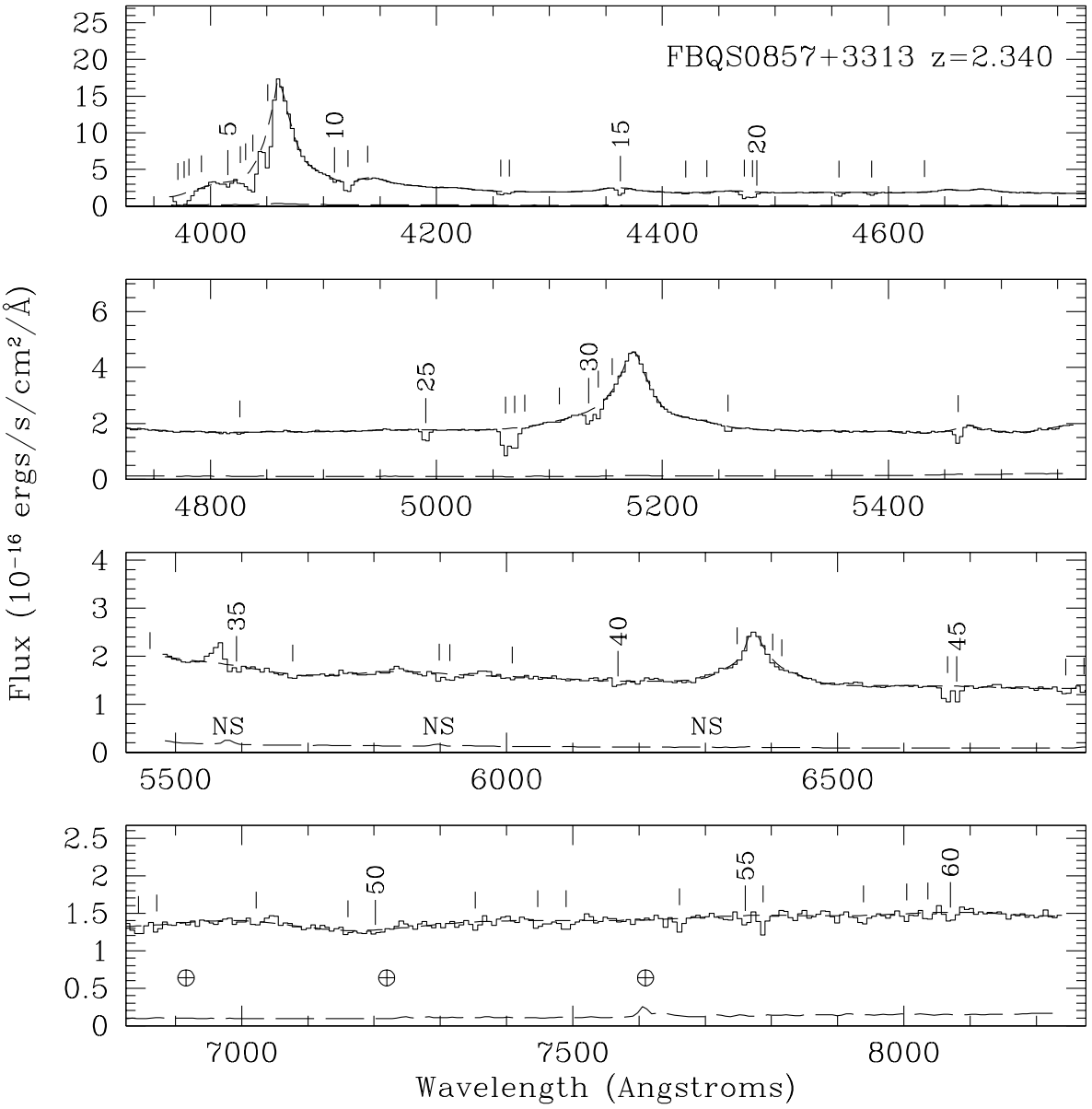

Fig. 8.— FBQS0857+3313

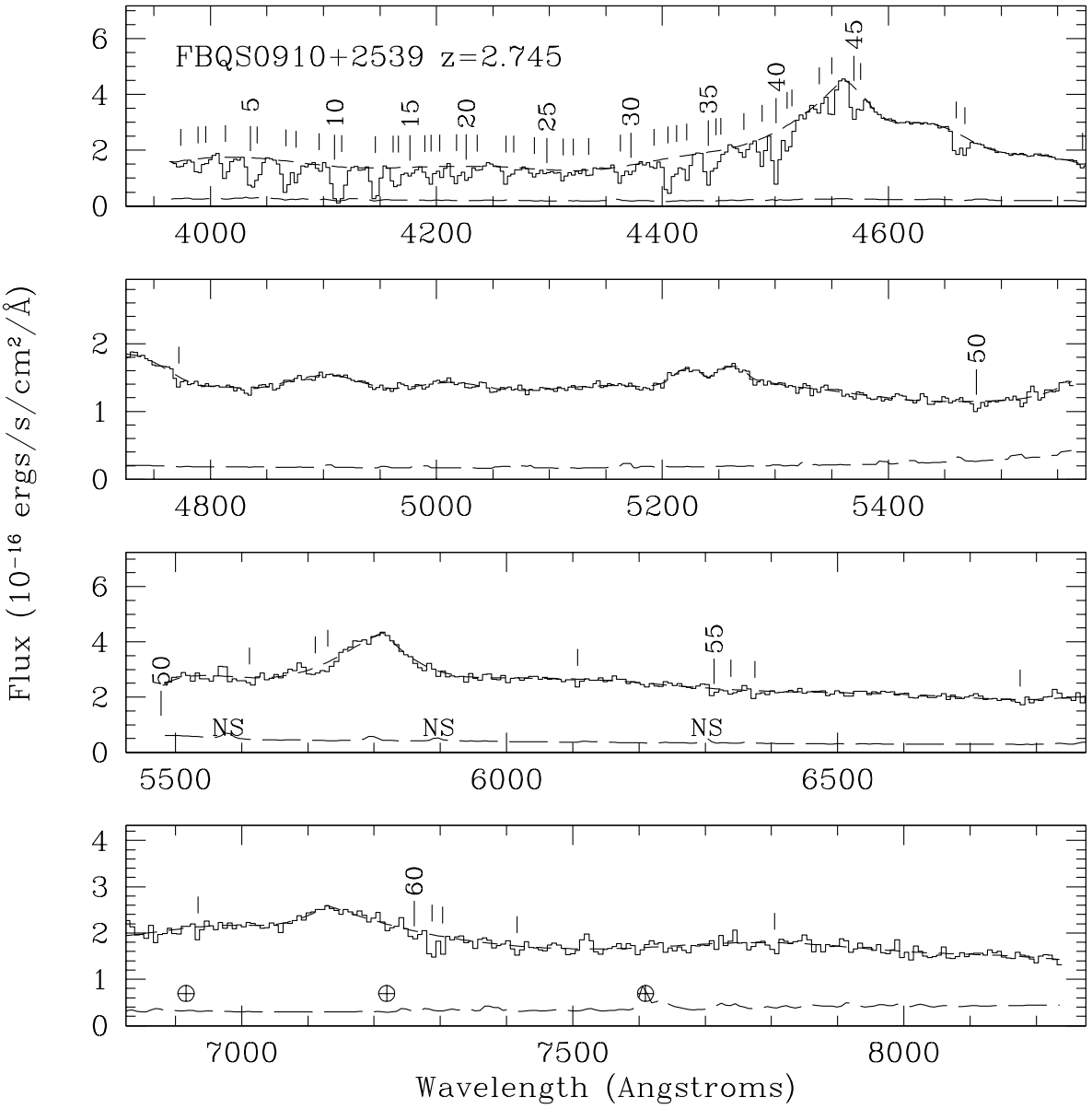

Fig. 9.— FBQS0910+2539

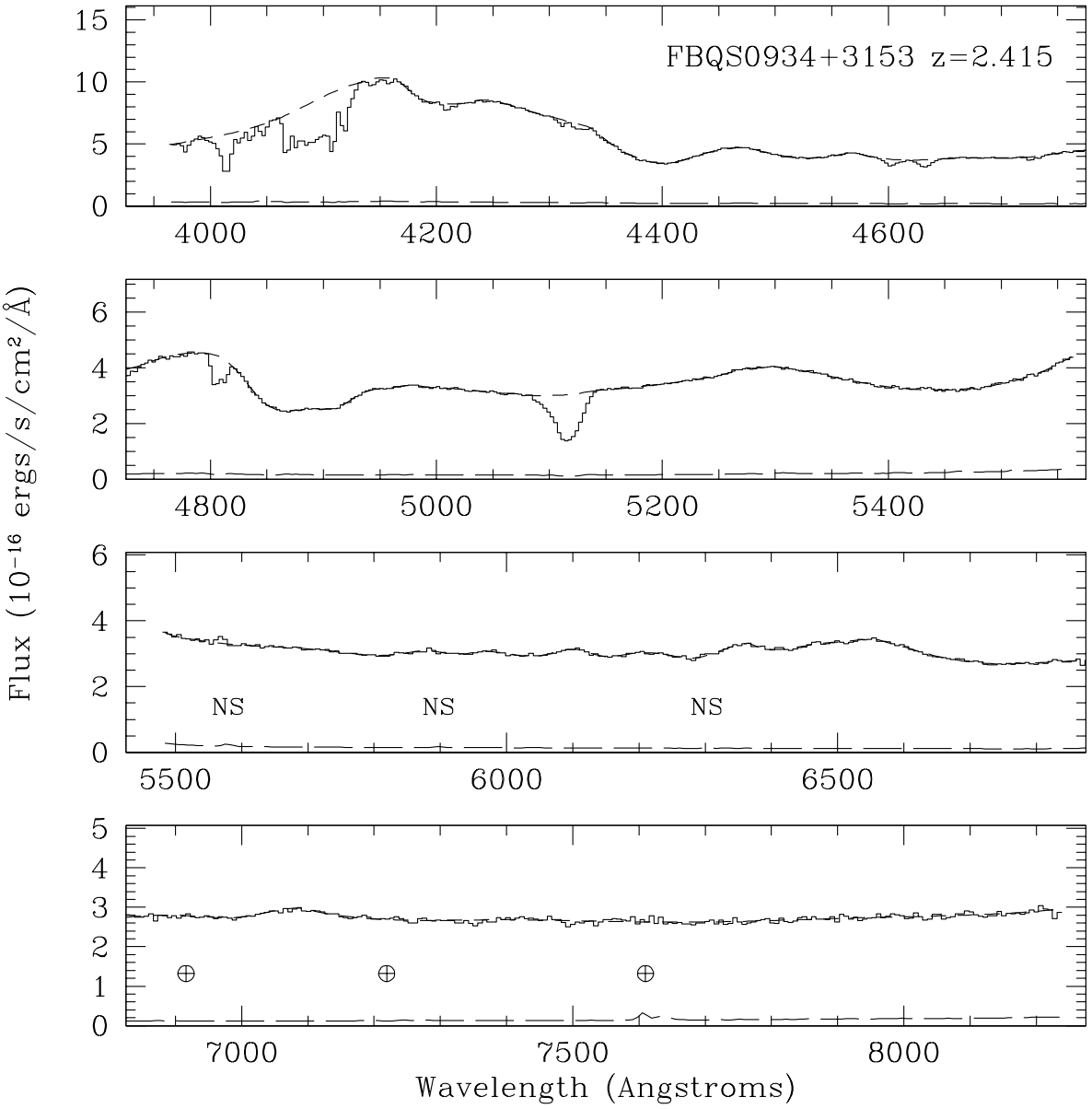

Fig. 10.— FBQS0934+3153

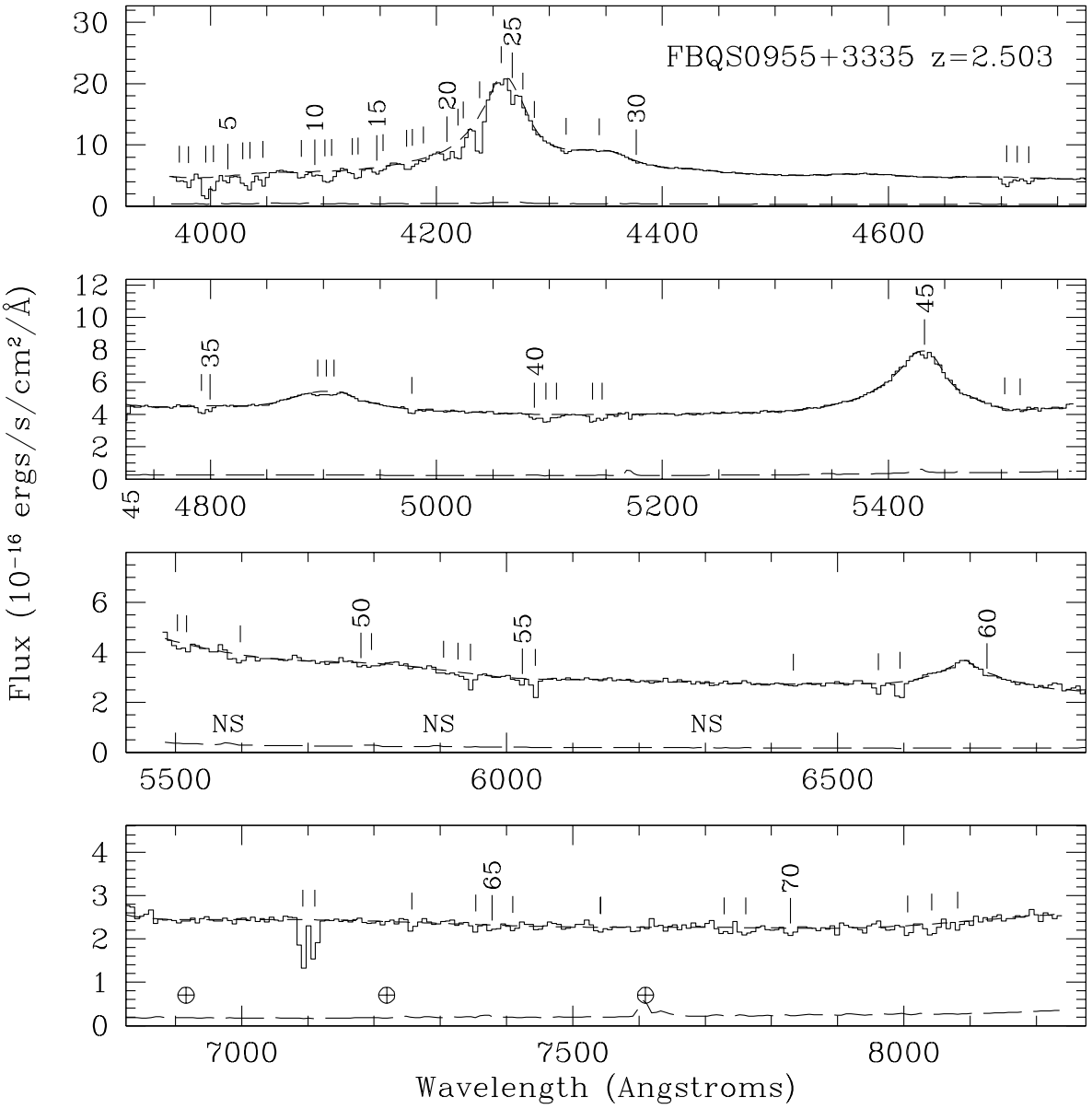

Fig. 11.— FBQS0955+3335

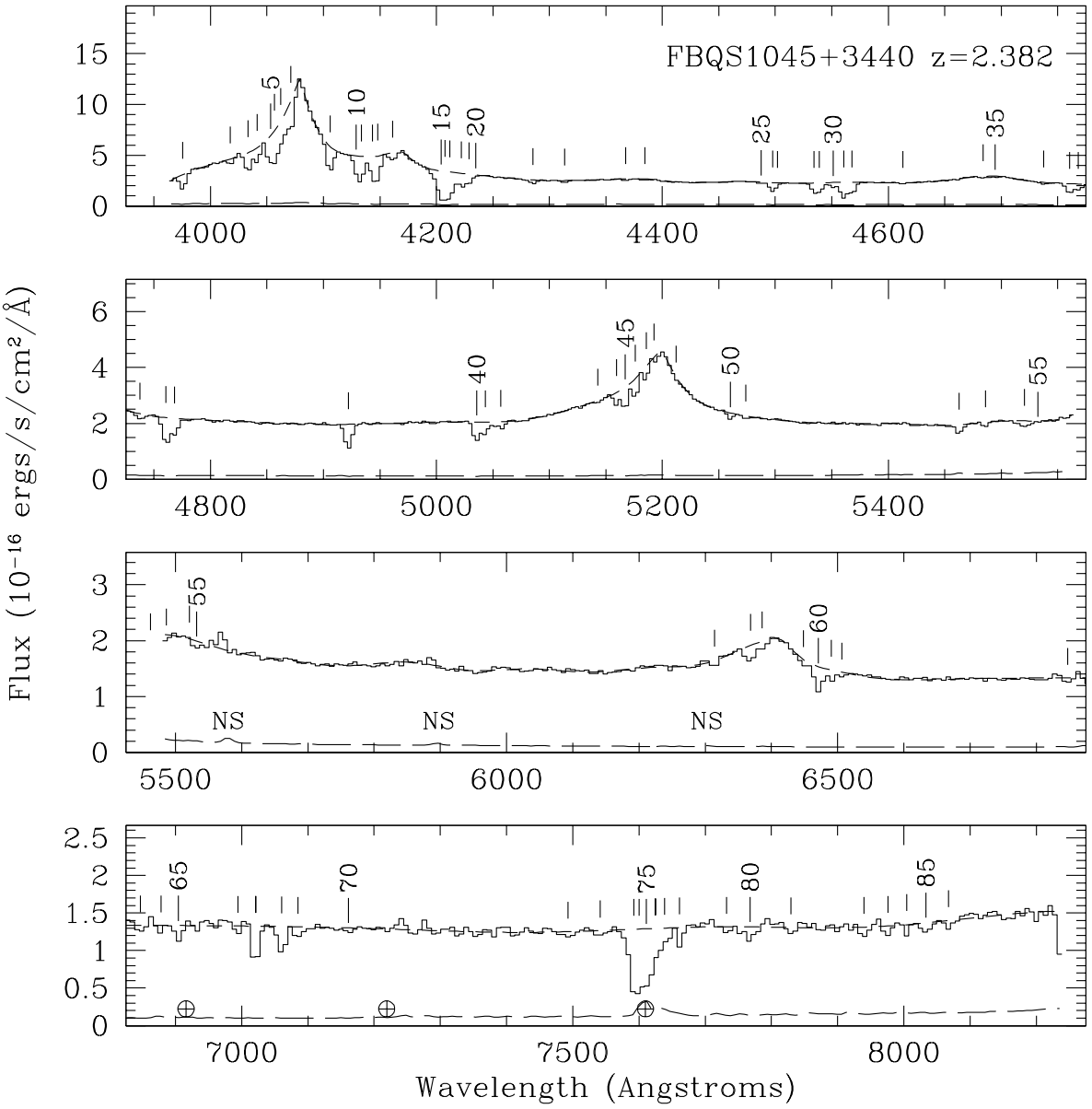

Fig. 12.— FBQS1045+3440

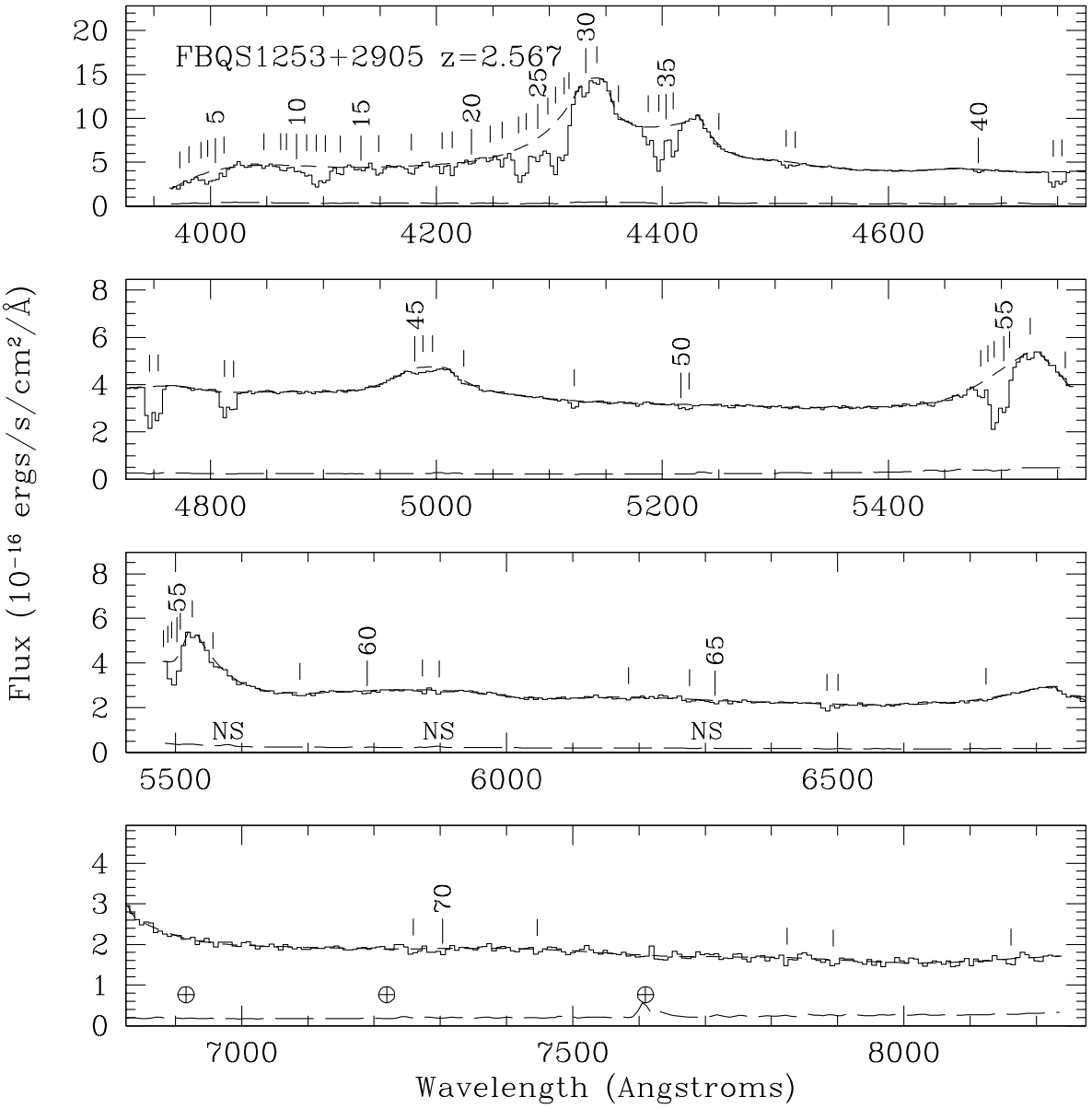

Fig. 13.— FBQS1253+2905

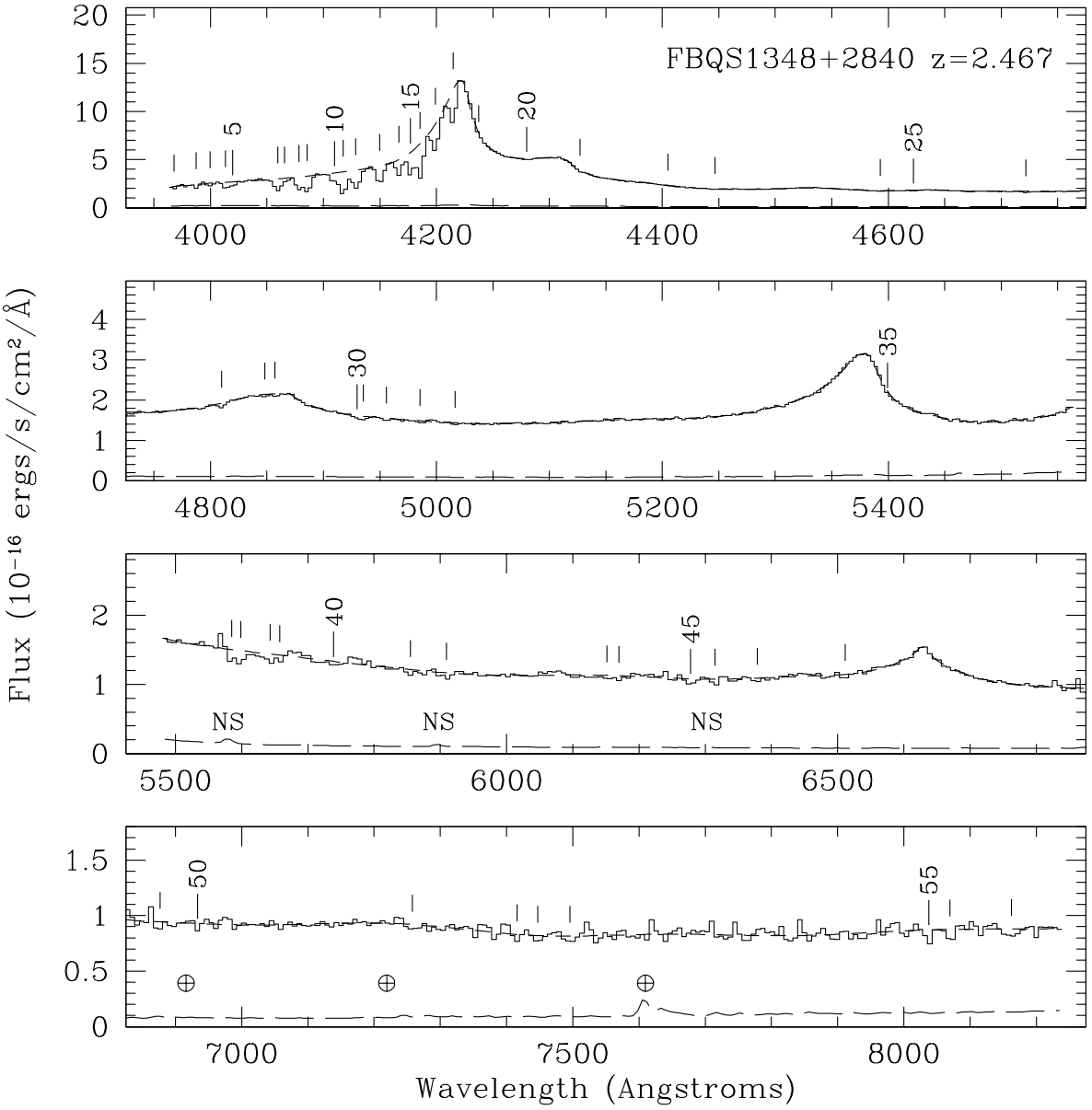

Fig. 14.— FBQS1348+2840

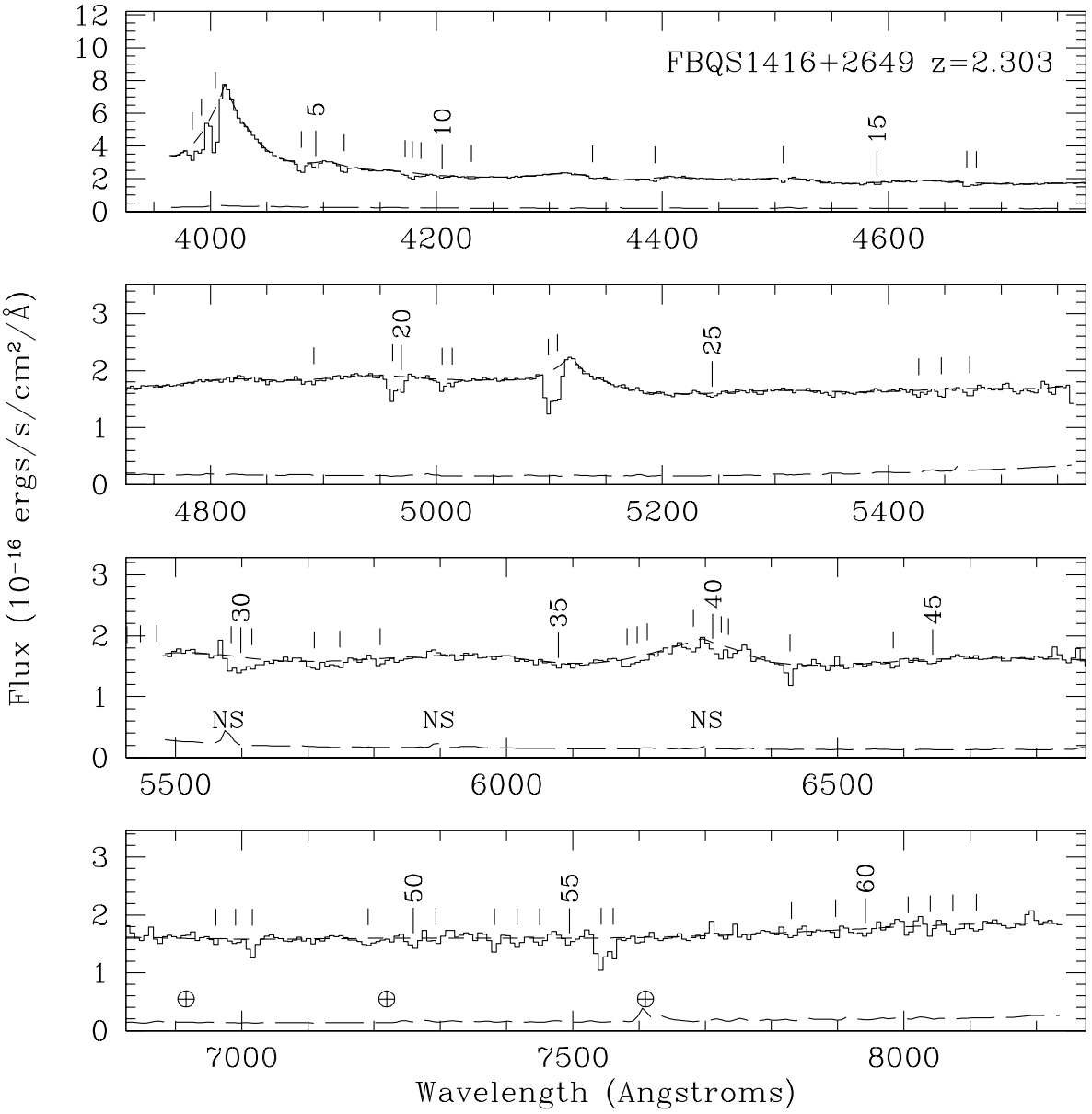

Fig. 15.— FBQS1416+2649

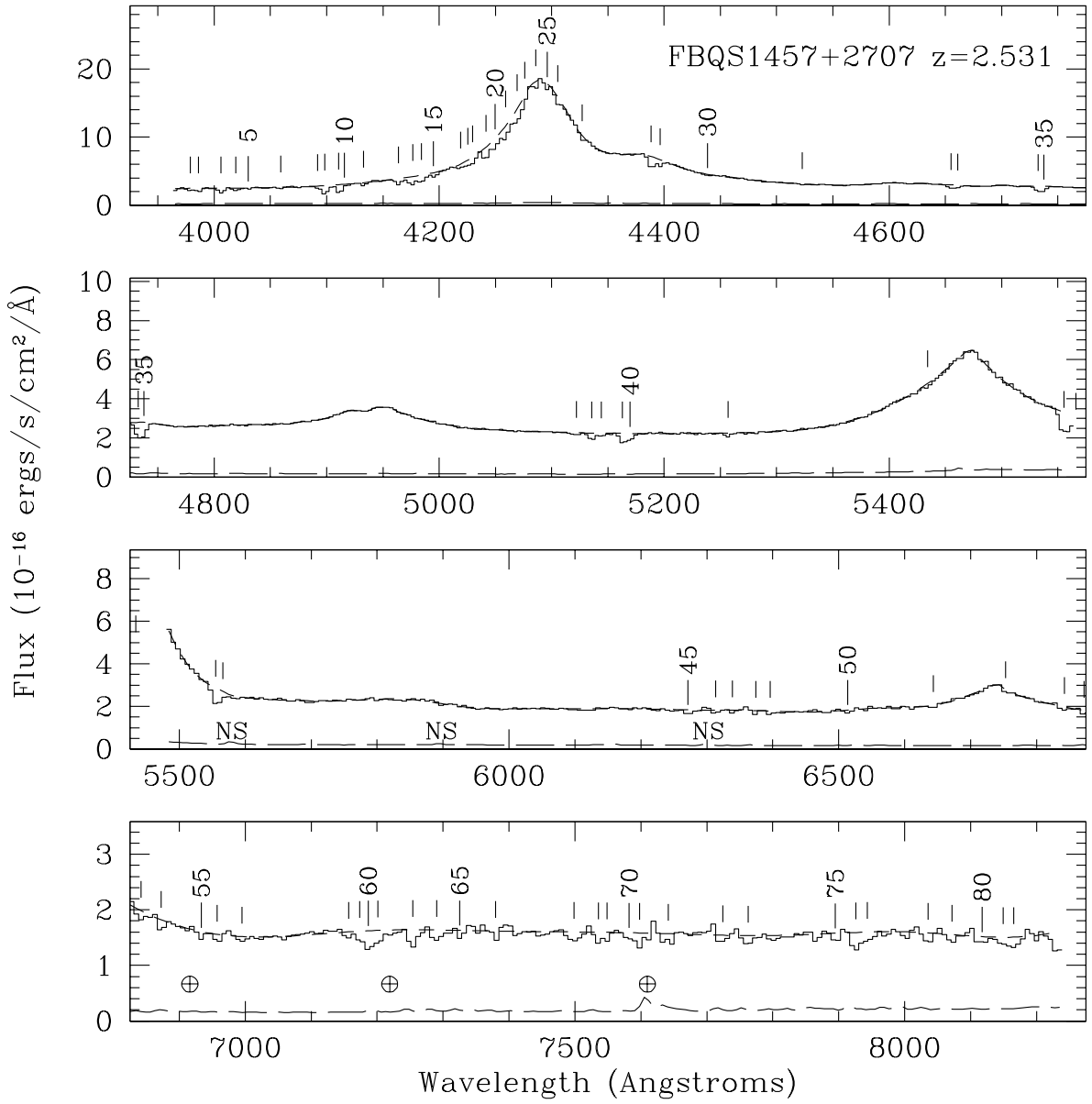

Fig. 16.— FBQS1457+2707

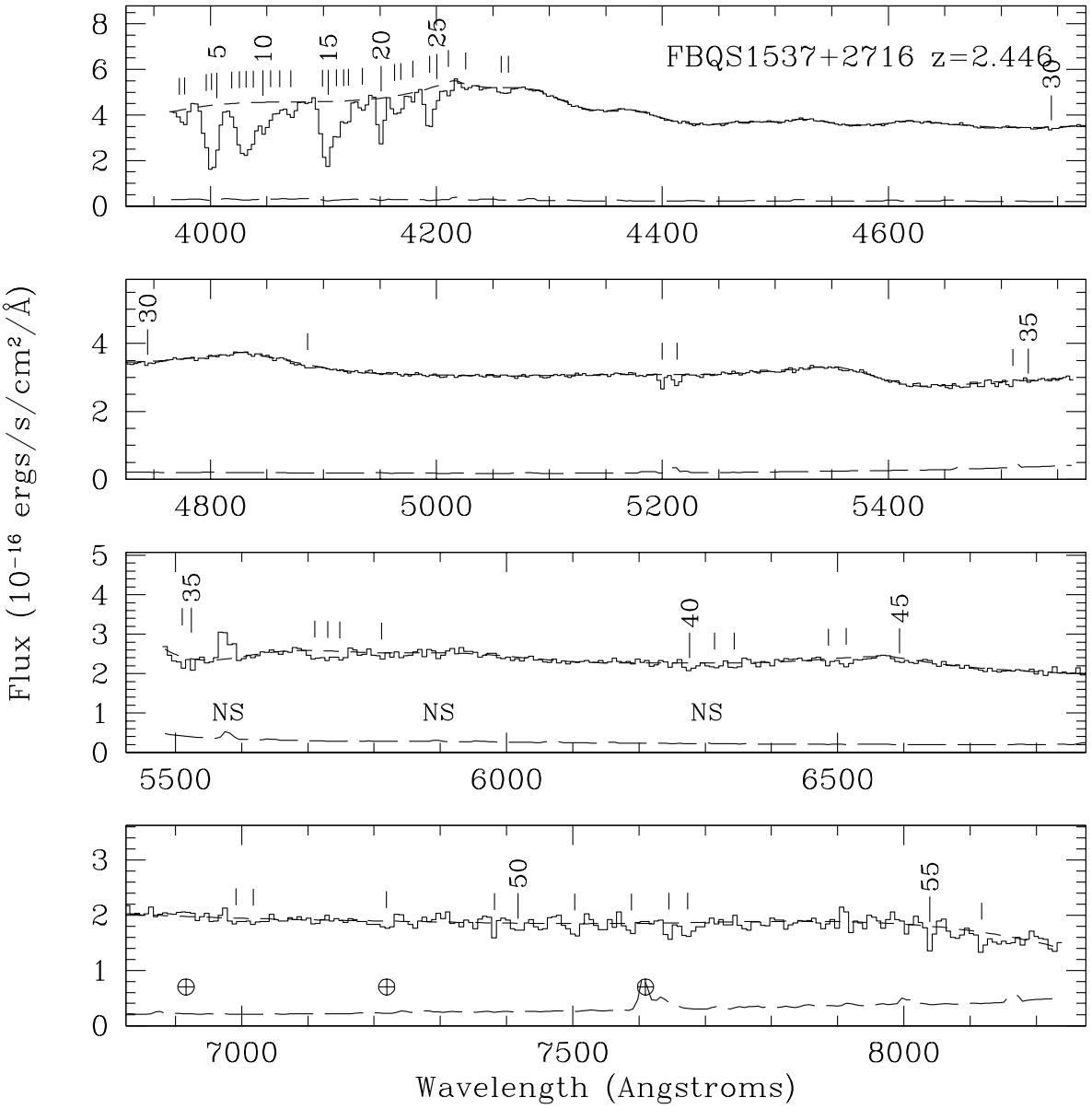

Fig. 17.— FBQS1537+2716

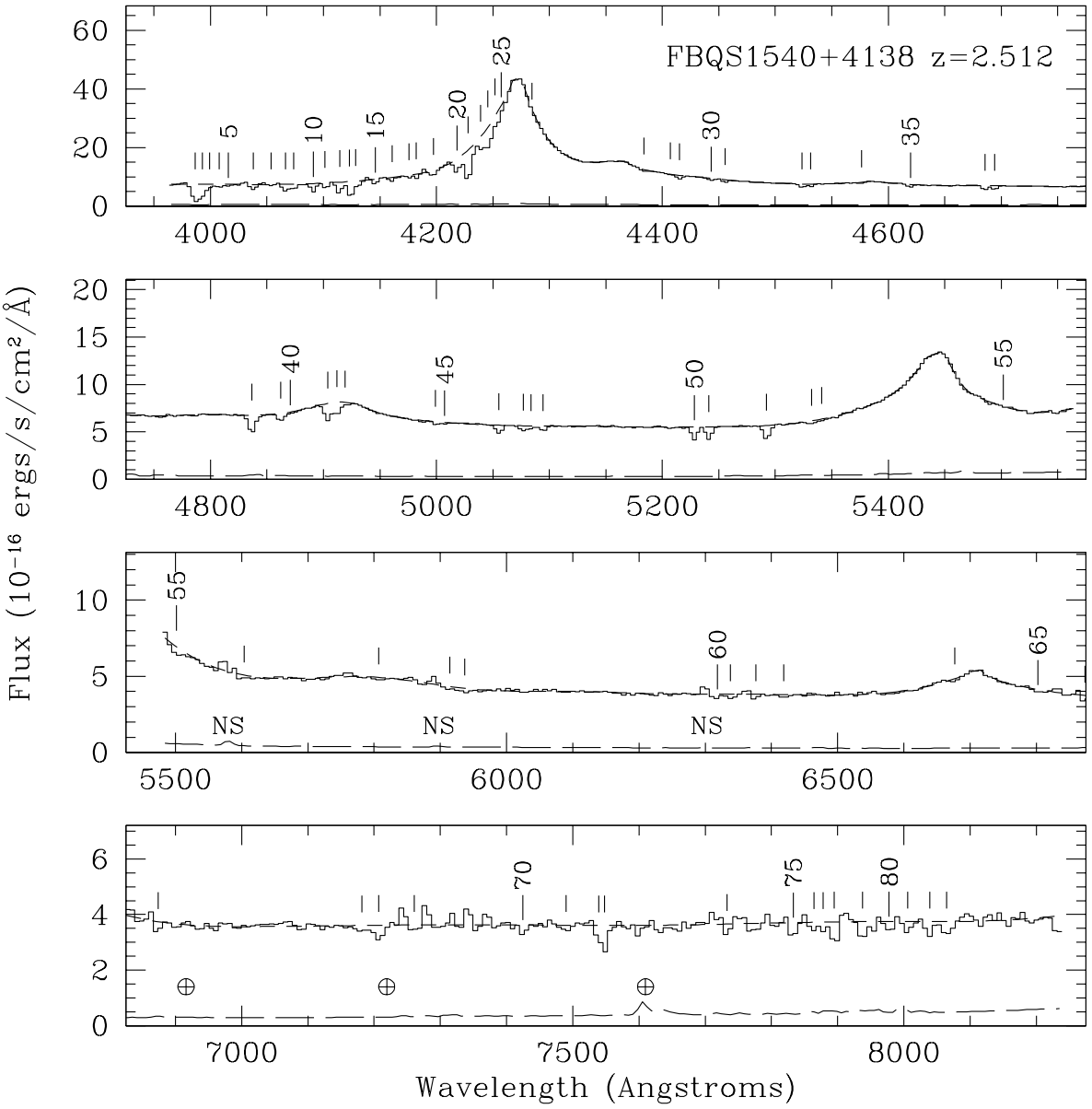

Fig. 18.— FBQS1540+4138

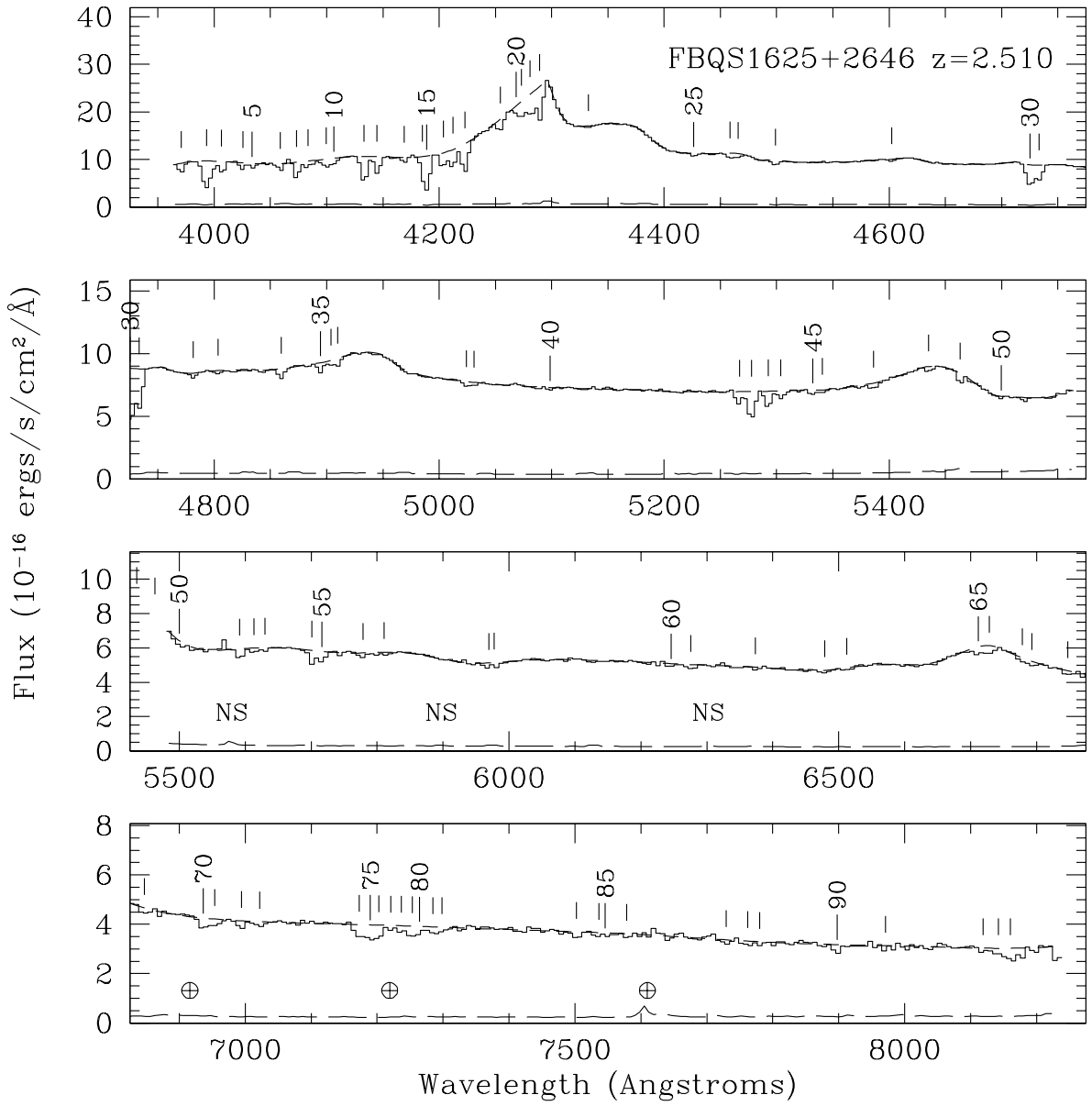

Fig. 19.— FBQS1625+2646

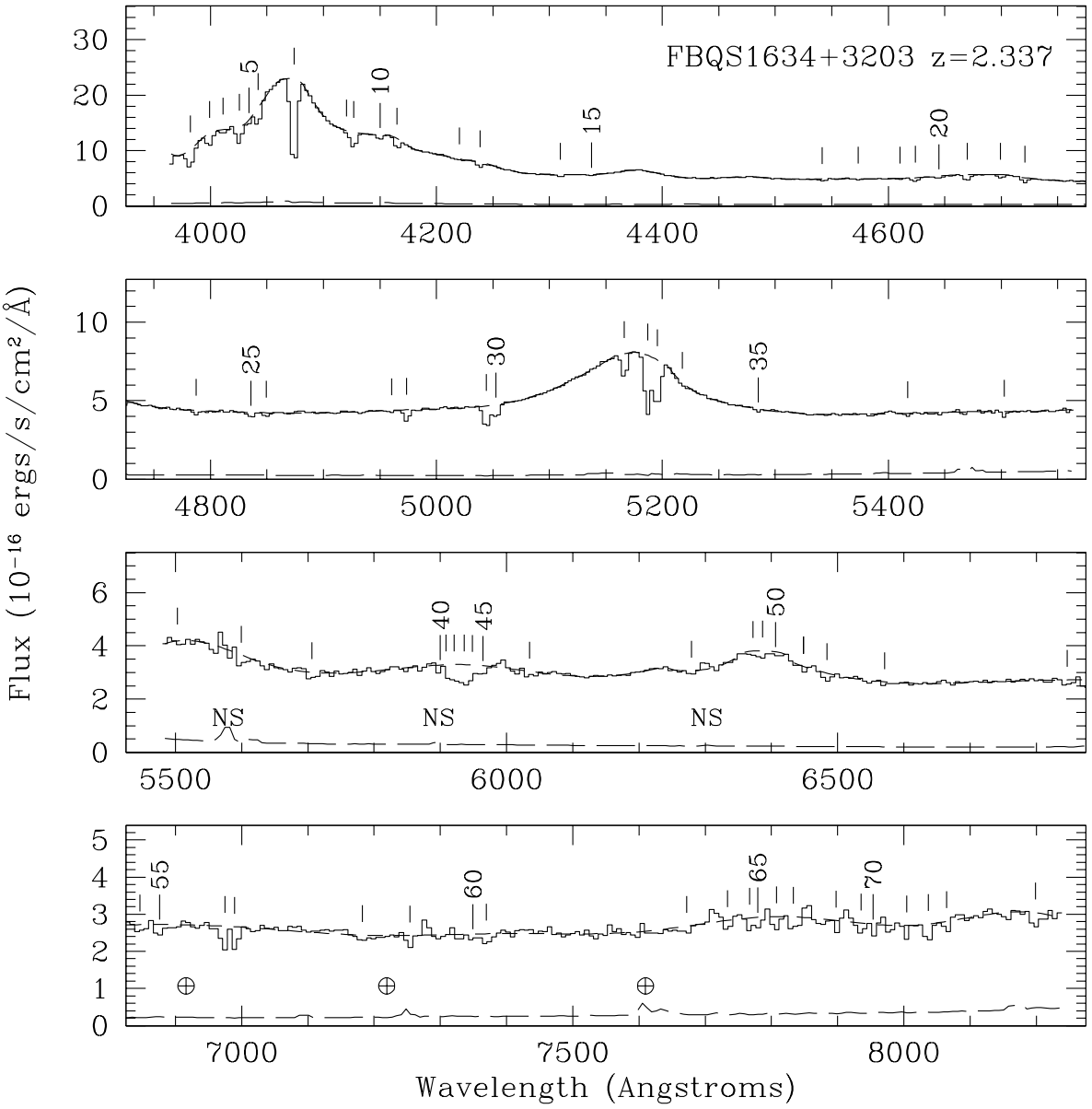

Fig. 20.— FBQS1634+3203

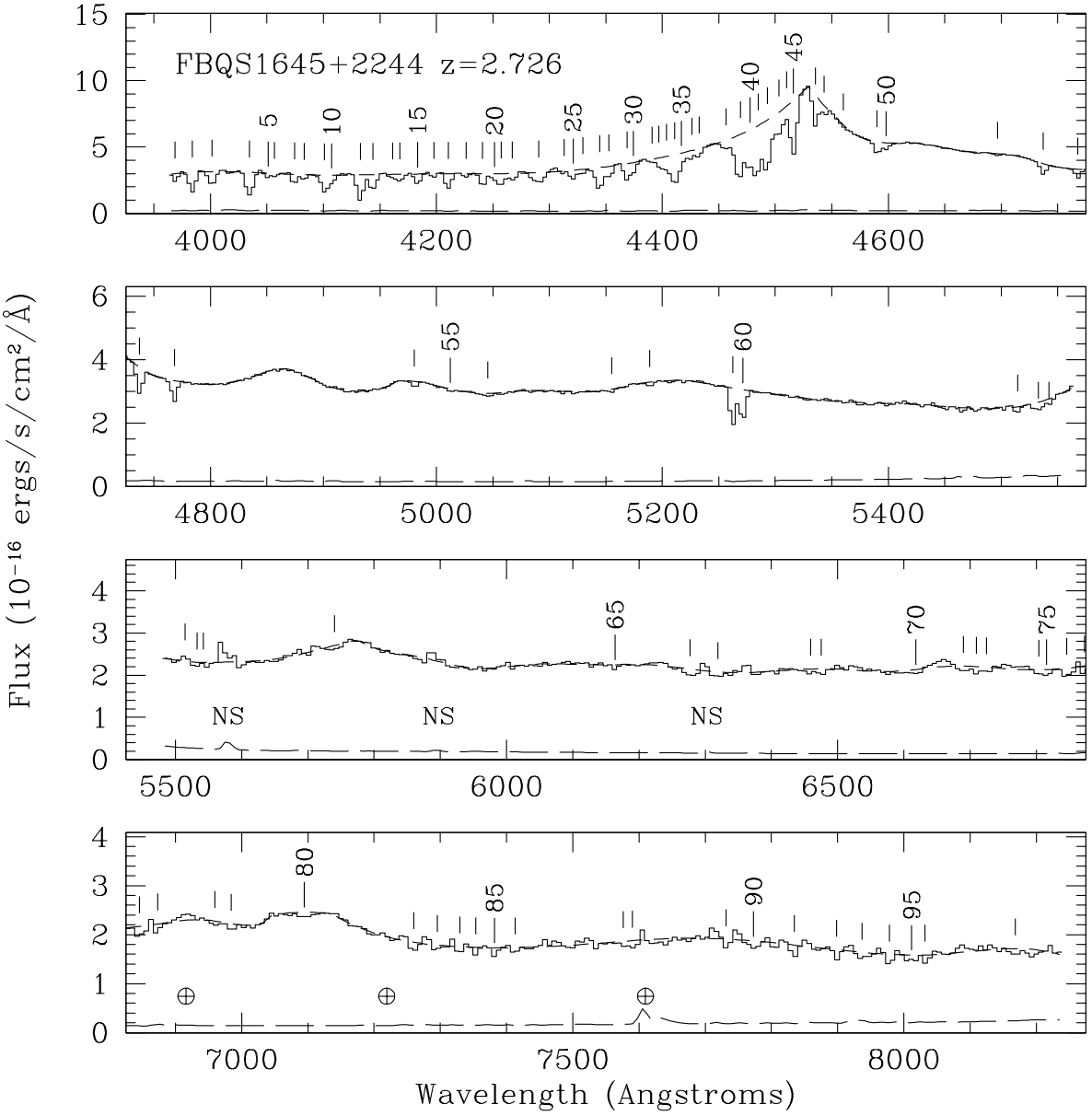

Fig. 21.— FBQS1645+2244

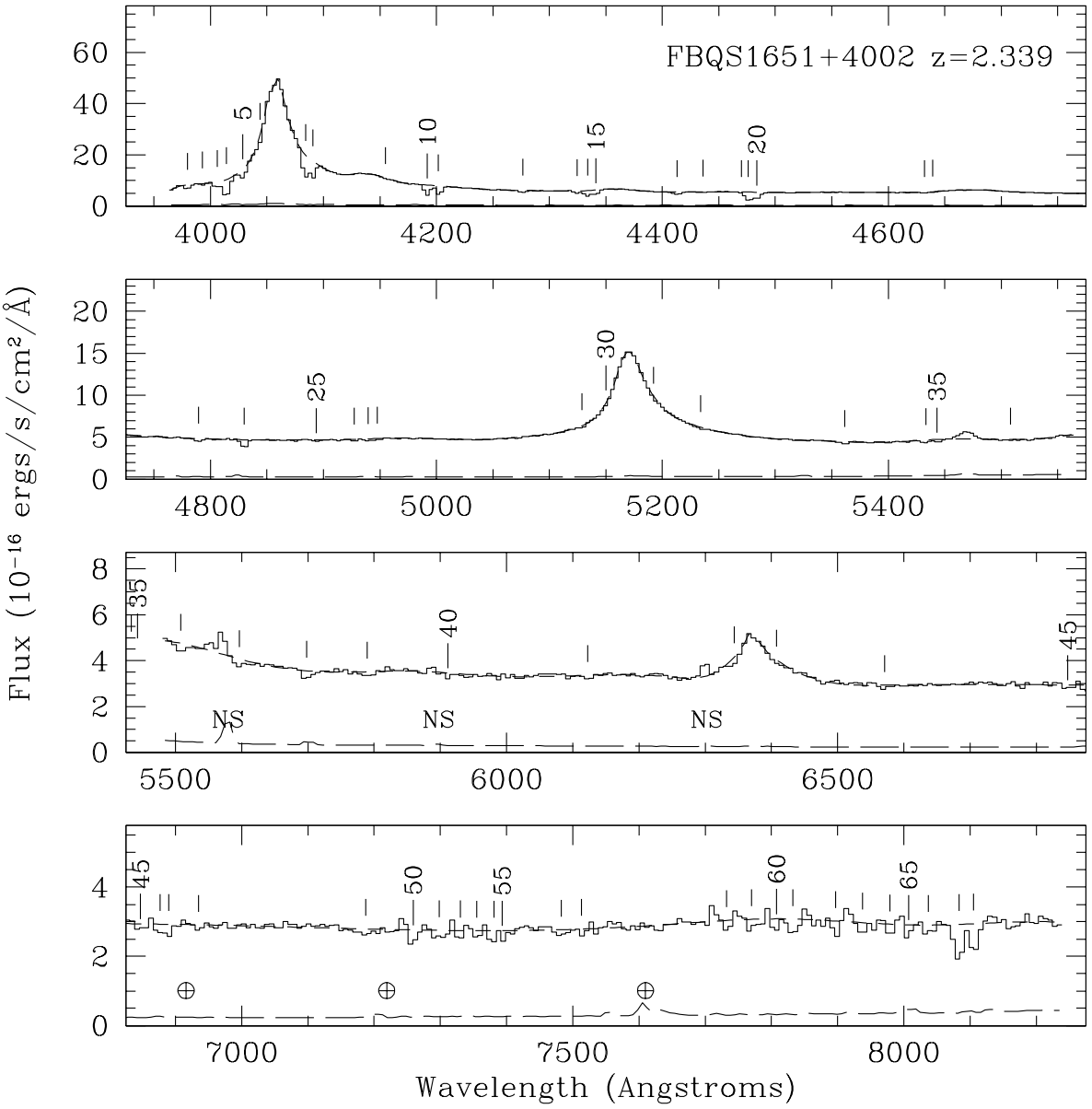

Fig. 22.— FBQS1651+4002

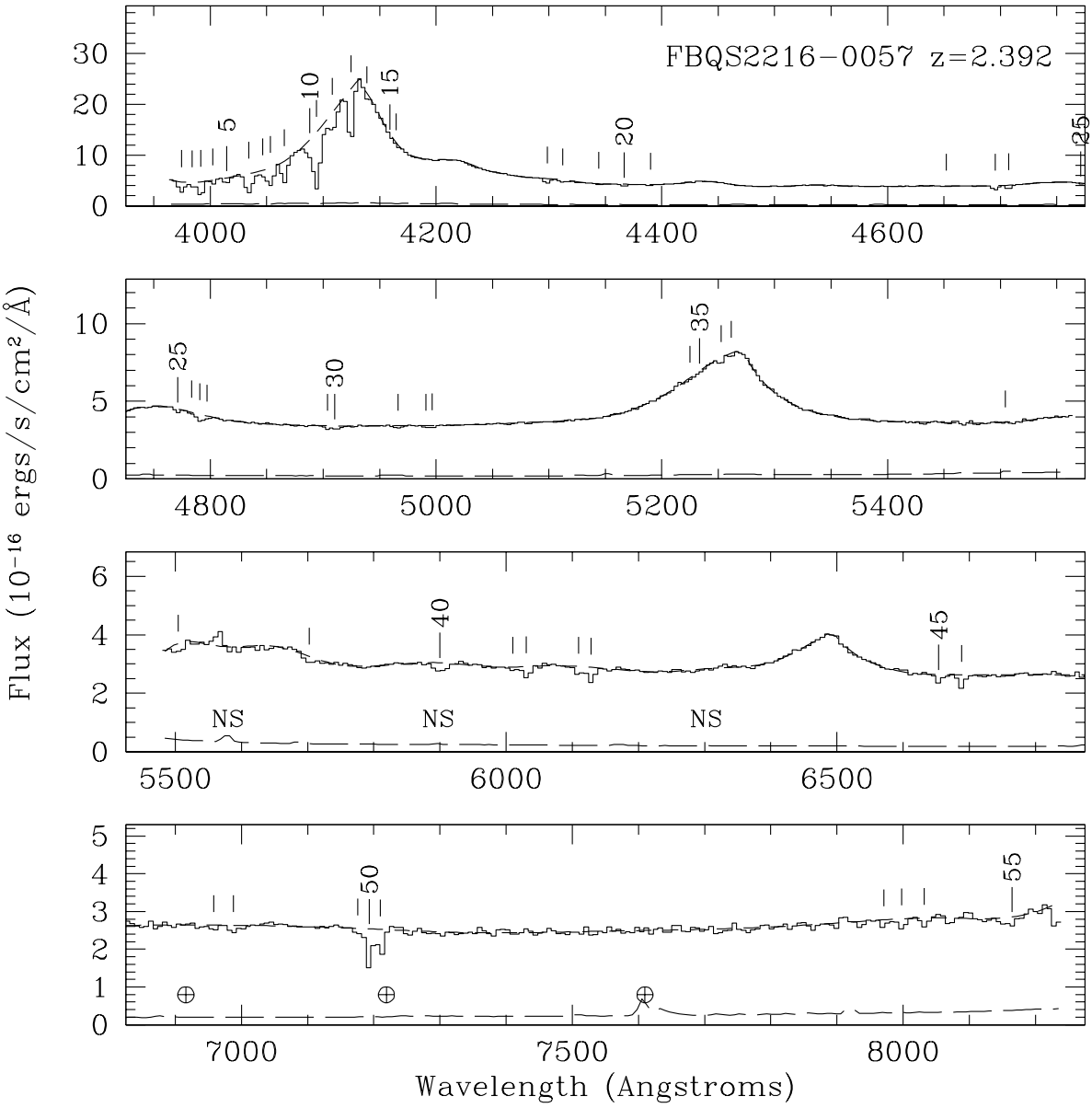

Fig. 23.— FBQS2216-0057

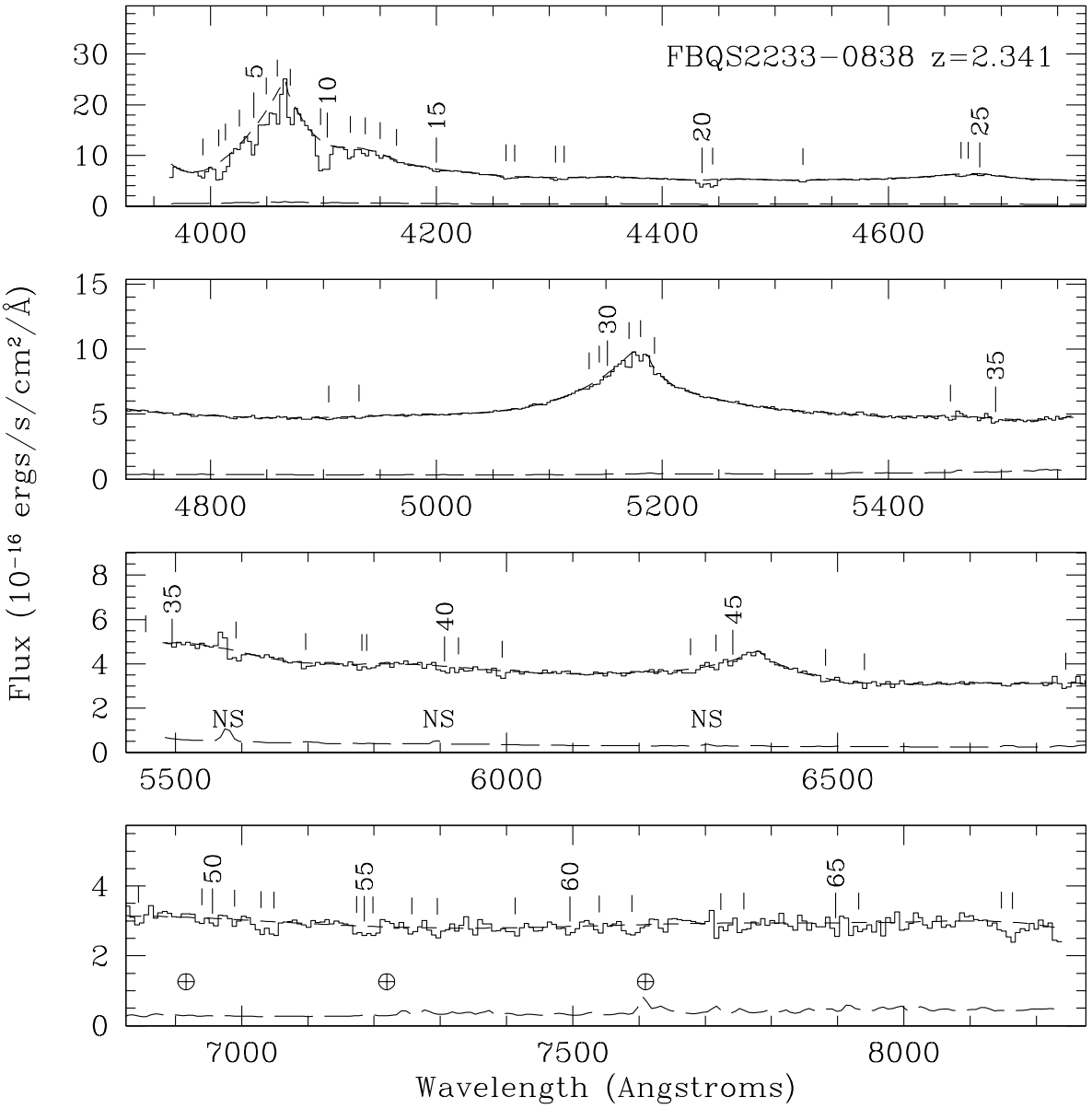

Fig. 24.— FBQS2233-0838

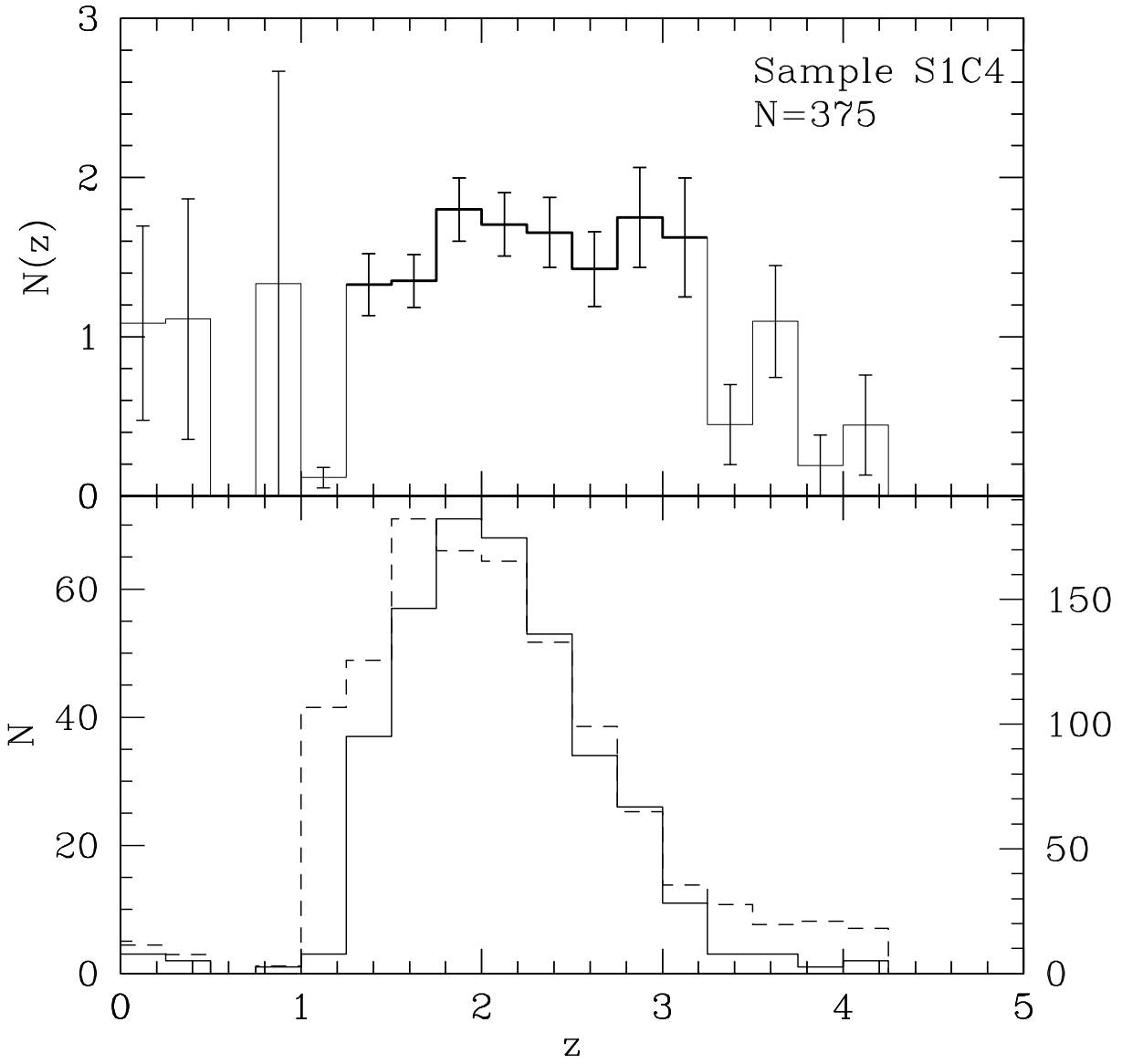

Fig. 25.— Sample S1C4 dN/dz. Normalized redshift distribution of C IV from Sample S1C4. (*Bottom*) Solid line shows the number of absorbers found in each bin (left axis). Dashed lines show the number of QSOs searched (right axis). (*Top*) Normalized number of absorbers per unit redshift: essentially the ratio of the two bottom plots. Thicker lines symbolize bins with more than ten absorbers: these bins are considered significant. Error bars are Poisson. The total number of absorbers and the sample from which they were drawn are given in the upper right hand corner. Lines within 5000 km s^{-1} of the QSO redshift have been removed.

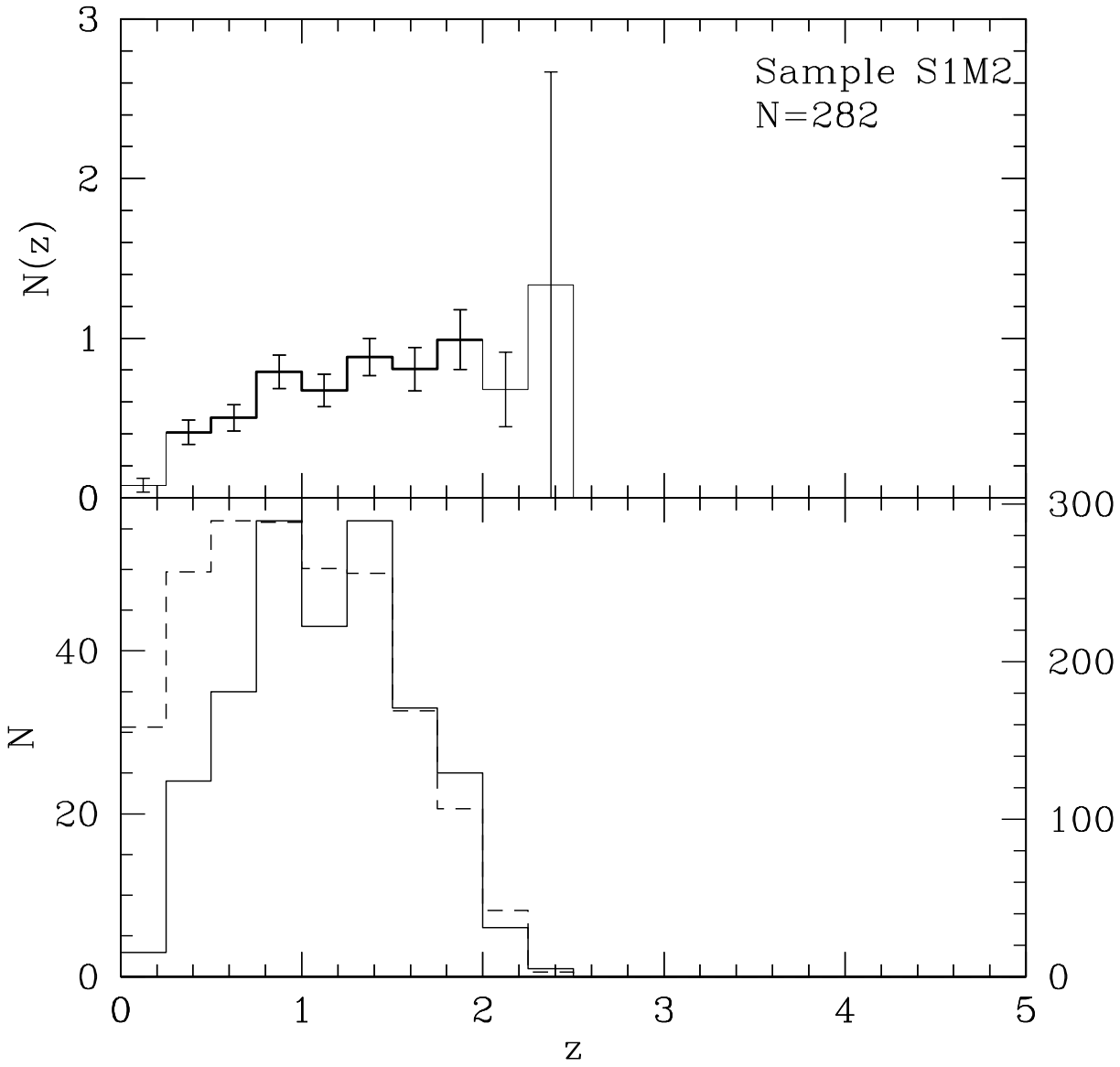

Fig. 26.— Sample S1M2 dN/dz. Normalized redshift distribution of Mg II in Sample S1M2. See Figure 25 for an explanation of the lines.

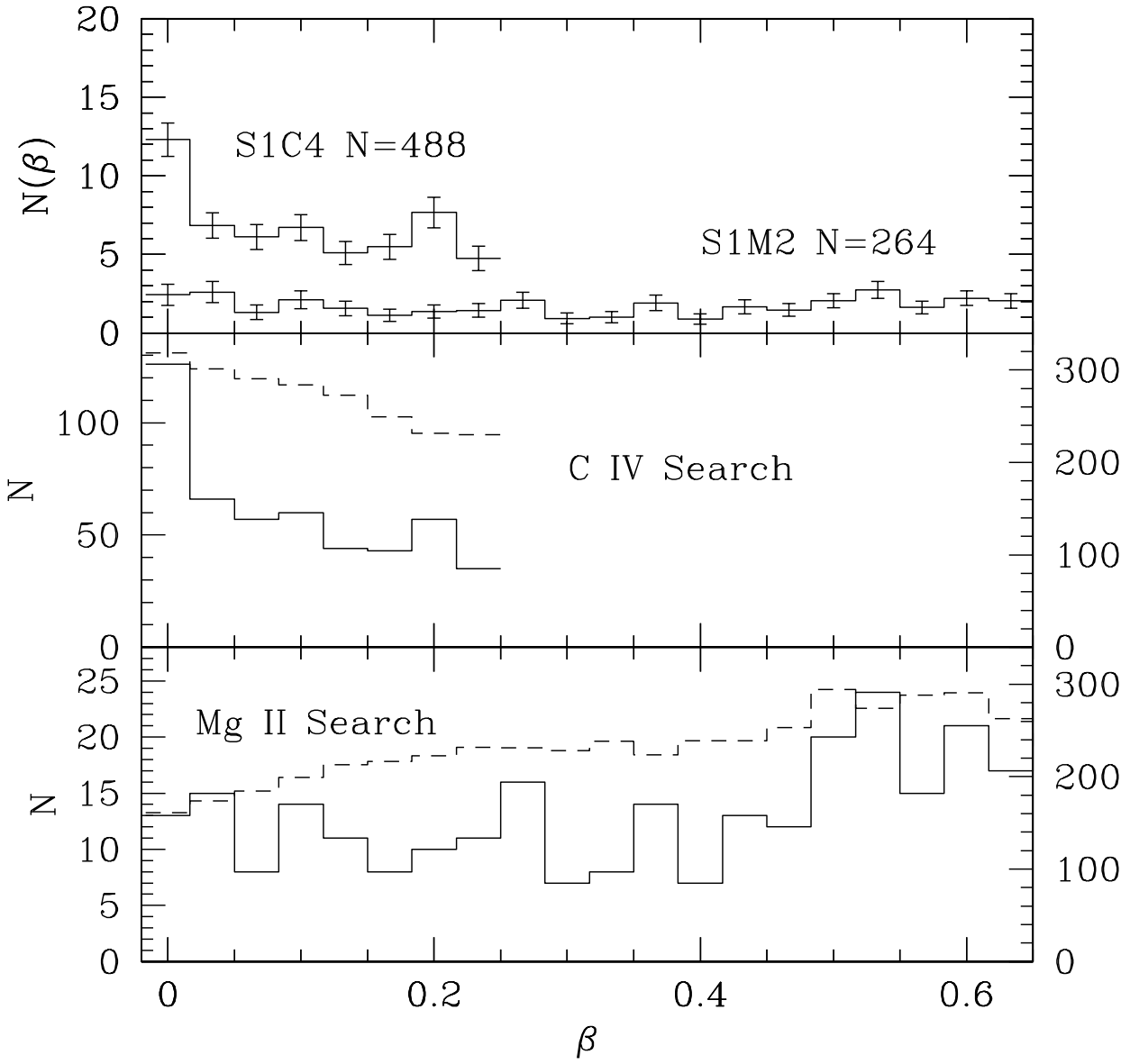

Fig. 27.— Sample S1 $dN/d\beta$. (*Top*) Normalized velocity distribution of C IV and Mg II in Sample S1. (*Middle*) Number of C IV absorbers and number of QSOs searched as a function of velocity. See Figure 25 for an explanation of the lines. (*Bottom*) Number of Mg II absorbers and number of QSOs searched as a function of velocity.

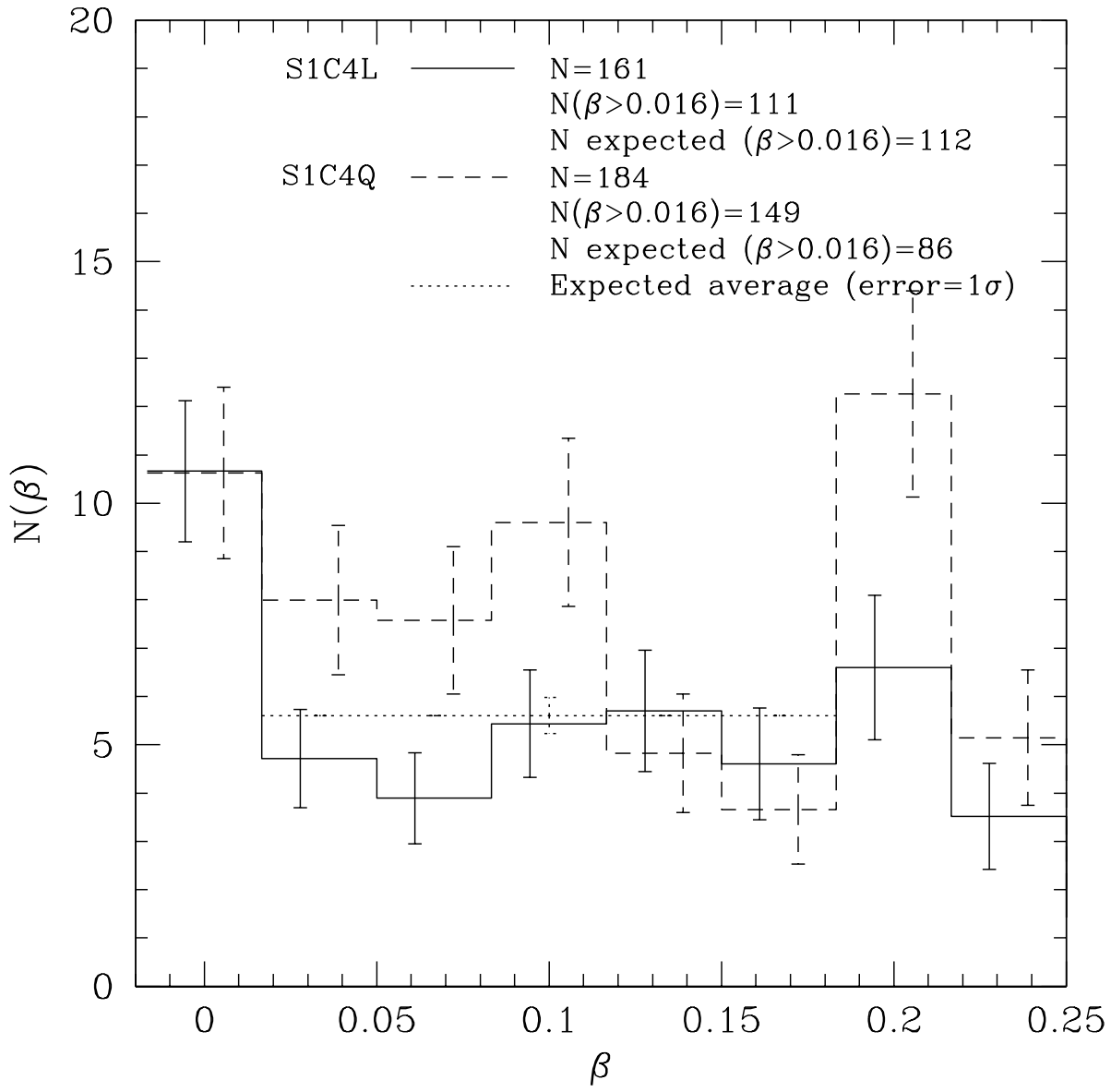

Fig. 28.— Samples S1C4L and S1C4Q $dN/d\beta$. Normalized velocity distribution of C IV for radio-loud (solid line) and radio-quiet (dashed line) quasars in Samples S1C4L and S1C4Q. In this (and similar plots) the expected level of $dN/d\beta$ is plotted in the velocity range 5000 to $55,000\,\mathrm{km\,s^{-1}}$ for comparison. The upper right hand corner gives the number of absorbers, the number of absorbers with $v > 5000\,\mathrm{km\,s^{-1}}$ and the expected number of absorbers with $v > 5000\,\mathrm{km\,s^{-1}}$.

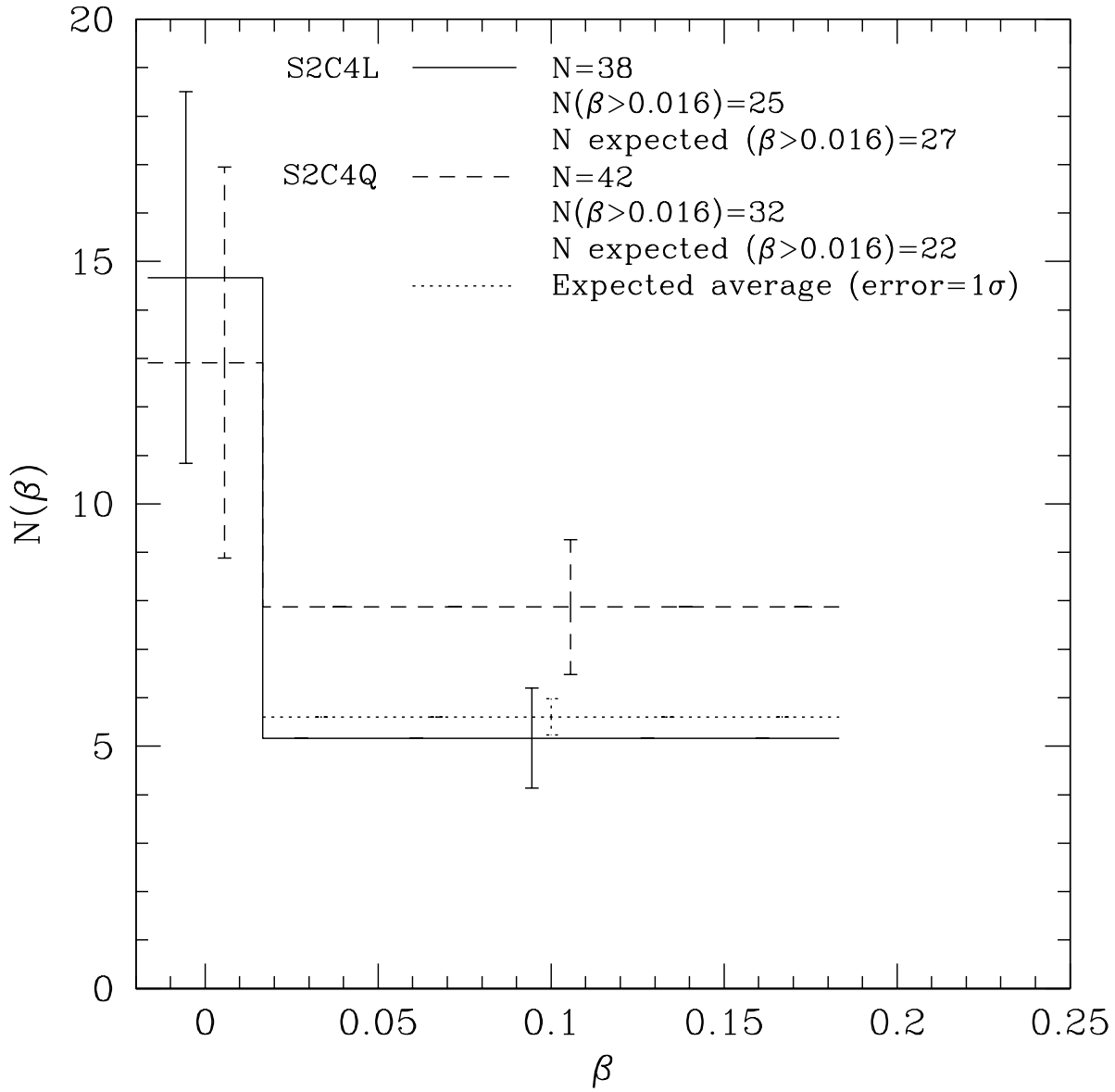

Fig. 29.— Samples S2C4L and S2C4Q $dN/d\beta$. Normalized velocity distribution of C IV from radio-loud and radio-quiet quasars in Samples S2C4L and S2C4Q.

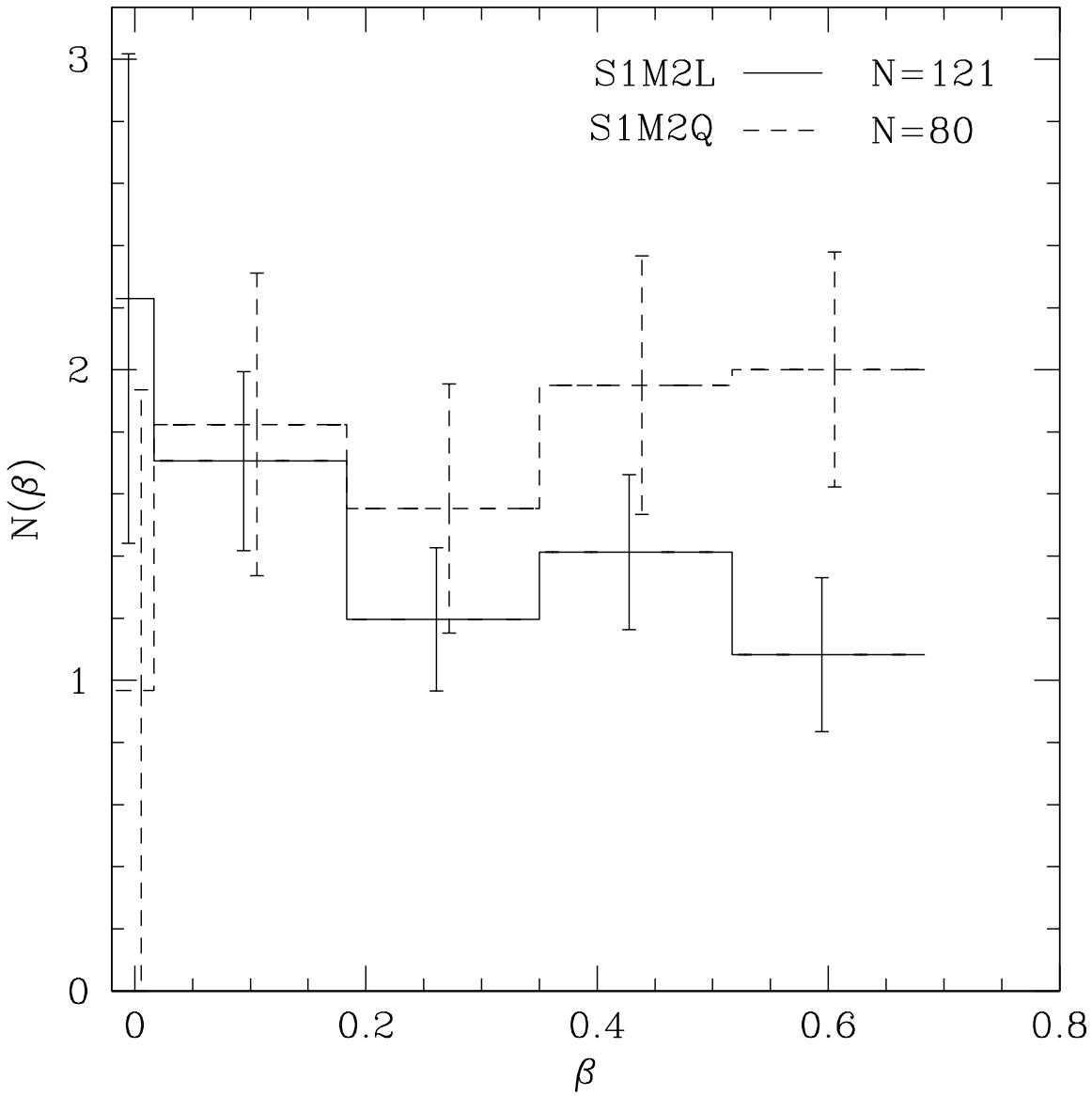

Fig. 30.— Samples S1M2L and S1M2Q $dN/d\beta$. Normalized velocity distribution of Mg II from radio-loud and radio-quiet quasars in Samples S1M2L and S1M2Q.

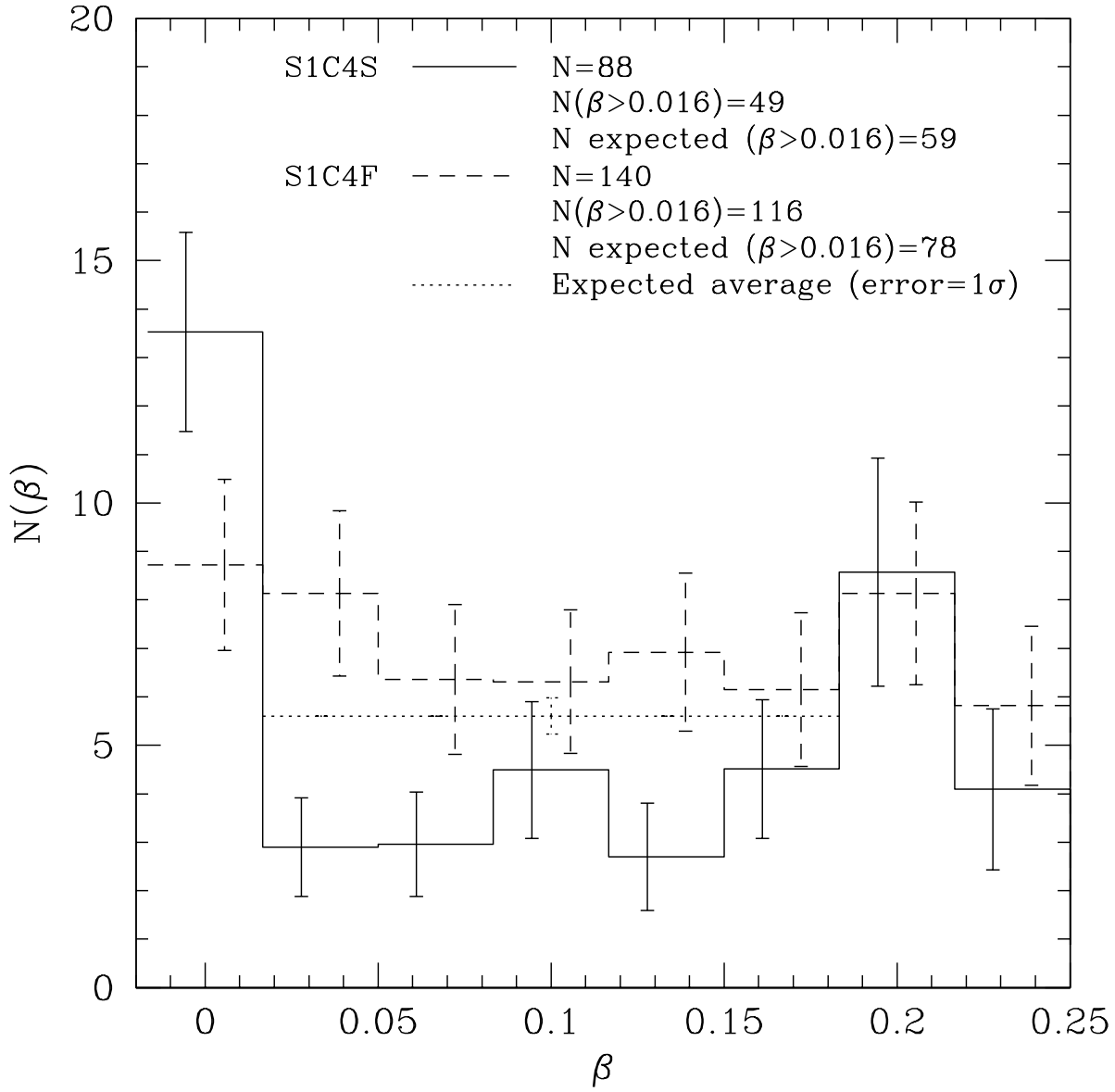

Fig. 31.— Samples S1M2S and S1M2F $dN/d\beta$. Normalized velocity distribution of C IV from steep- (solid line) and flat-spectrum (dashed line) quasars in Samples S1C4S and S1C4F.

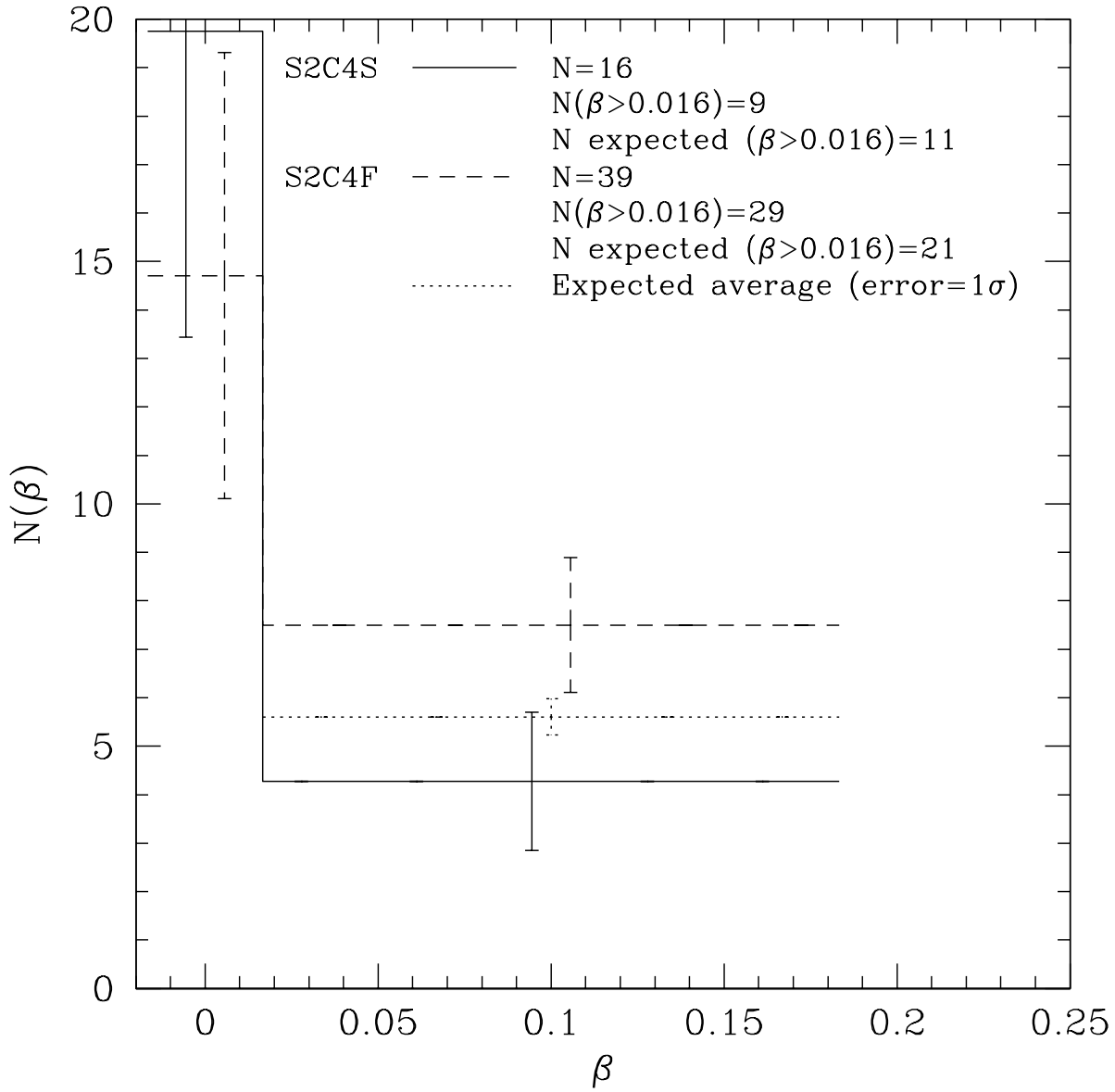

Fig. 32.— Samples S2C4S and S2C4F $dN/db\beta$. Normalized velocity distribution of C IV from steep- and flat-spectrum quasars from Samples S2C4S and S2C4F.

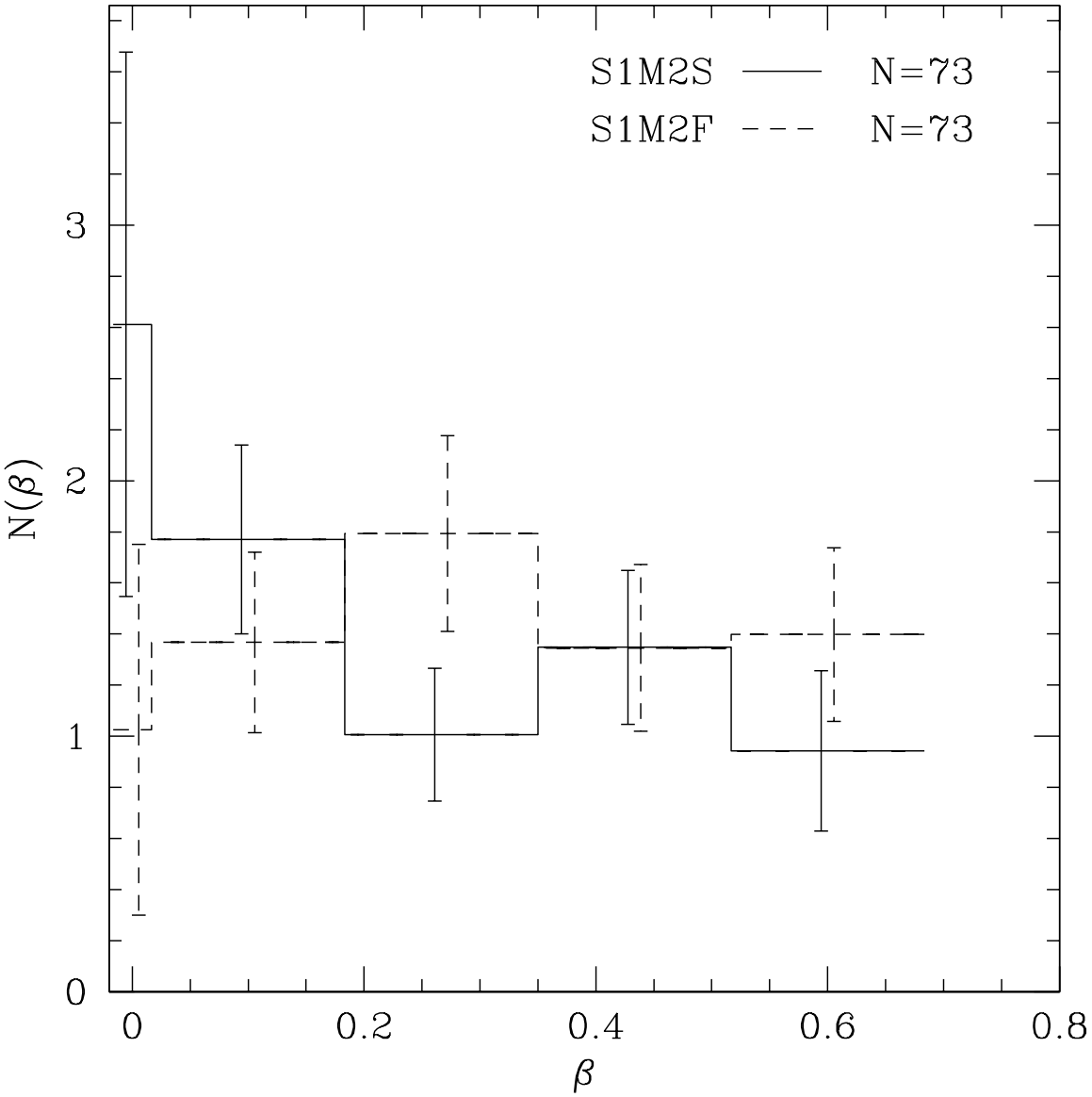

Fig. 33.— Normalized velocity distribution of Mg II from steep- and flat-spectrum quasars in Samples S1M2S and S1M2F.

Table 1. Observed Targets.

Object	z	RA	Dec	E	$O-E$	Fpeak (mJy)	Fint (mJy)	Blue S/N	Red S/N
FIRST J004717.7 − 015623	2.480	00 47 17.799	−01 56 23.85	17.60	0.50	1.53	1.27	78.0	44.0
FIRST J021039.8 − 015213	2.372	02 10 39.879	−01 52 13.81	17.97	0.44	1.51	1.76	55.5	32.5
FIRST J025625.6 − 011911	2.491	02 56 25.629	−01 19 11.91	17.99	0.16	25.78	27.56	32.0	17.5
FIRST J072550.5 + 281906	2.666	07 25 50.587	+28 19 06.12	16.98	1.18	37.99	38.85	80.0	60.0
FIRST J072928.4 + 252451	2.300	07 29 28.470	+25 24 51.80	17.22	0.91	6.83	6.47	80.5	54.0
FIRST J080413.6 + 251633	2.292	08 04 13.671	+25 16 33.63	17.49	0.58	3.48	3.68	76.5	55.0
FIRST J082107.6 + 310751	2.609	08 21 07.610	+31 07 51.41	16.40	0.45	85.41	89.98	76.0	68.5
FIRST J085726.9 + 331316	2.340	08 57 26.931	+33 13 16.86	17.15	0.55	20.69	21.29	73.5	44.0
FIRST J091055.2 + 253921	2.745	09 10 55.246	+25 39 21.21	17.28	0.92	202.60	207.22	37.5	22.0
FIRST J093404.0 + 315331	2.415	09 34 04.005	+31 53 31.17	17.49	0.70	4.68	4.41	97.0	69.0
FIRST J095537.9 + 333503	2.503	09 55 37.943	+33 35 03.95	16.72	0.51	35.73	36.61	76.5	57.5
FIRST J104541.0 + 344043	2.352	10 45 41.027	+34 40 43.38	17.38	1.19	20.35	21.16	76.0	46.0
FIRST J125306.4 + 290514	2.567	12 53 06.420	+29 05 14.14	17.26	0.26	60.91	61.78	74.0	50.0
FIRST J134804.3 + 284025	2.467	13 48 04.345	+28 40 25.50	17.31	0.52	72.45	78.07	73.5	41.5
FIRST J141617.3 + 264906	2.303	14 16 17.378	+26 49 06.51	17.33	1.02	2.94	2.60	46.5	31.5
FIRST J145705.2 + 270757	2.531	14 57 05.230	+27 07 57.28	17.07	0.69	1.64	1.22	61.0	53.0
FIRST J153714.2 + 271611	2.446	15 37 14.259	+27 16 11.52	16.79	0.80	2.01	1.56	82.0	27.0
FIRST J154042.9 + 413816	2.512	15 40 42.977	+41 38 16.40	16.72	0.83	17.67	18.28	76.0	58.0
FIRST J162548.7 + 264658	2.510	16 25 48.780	+26 46 58.51	16.94	0.42	10.12	9.69	78.5	75.5
FIRST J163412.7 + 320335	2.337	16 34 12.789	+32 03 35.27	16.74	0.75	175.25	176.52	80.0	42.0
FIRST J164552.1 + 224450	2.726	16 45 52.105	+22 44 50.08	17.01	0.84	2.30	1.94	99.0	40.0
FIRST J165137.5 + 400219	2.339	16 51 37.547	+40 02 19.09	16.74	0.55	42.73	43.90	82.0	47.0
FIRST J221608.8 − 005708	2.392	22 16 08.884	−00 57 08.28	17.74	0.26	6.56	6.30	78.0	40.0
FIRST J223338.7 − 083853	2.341	22 33 38.716	−08 38 53.00	17.98	0.23	9.39	9.28	63.0	38.5

Table 2. Observations.

QSO	UT Date	UT Time
FBQS0047-0156	1998 Aug 19	8:55[1], 9:38, 10:28
	1998 Aug 23	9:08, 10:05
	1998 Dec 12	2:57, 3:32
	1998 Dec 13	2:12, 2:47
FBQS0210-0152	1998 Dec 12	4:18, 4:56, 5:31
	1998 Dec 13	3:41, 4:16
	1998 Dec 27	2:40, 3:16
FBQS0256-0119	1998 Dec 13	6:07, 7:10
	1999 Jan 9	4:08, 4:50
FBQS0725+2819	1998 Dec 28	4:40, 5:14, 5:51
	1999 Feb 9	1:42, 2:18
	1999 Feb 13	2:41, 6:26
FBQS0729+2524	1998 Dec 12	6:18, 6:55, 7:49, 9:58, 10:35, 11:11
	1998 Dec 13	9:42, 10:17
	1998 Dec 20	8:19
FBQS0804+2516	1998 Dec 13	11:08, 11:45
	1998 Dec 20	9:04, 9:41, 10:18
	1998 Dec 27	6:21, 6:56, 9:35
FBQS0821+3107	1999 Feb 9	3:04, 3:41
	1999 Feb 13	7:07[2], 7:27[2]
FBQS0857+3313	1998 Dec 12	8:34, 9:16, 11:58
	1998 Dec 13	7:33, 8:21, 8:57
	1998 Dec 20	7:19, 10:19
	1998 Dec 28	6:55, 7;30, 10:48, 11:24
FBQS0910+2539	1999 Feb 17	3:01, 3:37, 4:12
	1999 Mar 14	1:38, 2:15
FBQS0934+3153	1998 Dec 28	8:10, 8:44
	1999 Feb 9	4:34
	1999 Feb 13	3:26, 4:01, 4:36
FBQS0955+3335	1999 Jan 14	10:03[3], 11:31[4]
	1999 Jan 15	6:43, 9:57, 10:38
FBQS1045+3440	1999 Jan 13	7:40, 11:02
	1999 Jan 14	6:57, 7:33
	1999 Jan 15	7:23, 7:58
	1999 Jan 16	7:06, 7:42
	1999 Feb 9	5:24, 6:00, 9:54, 10:43
	1999 Feb 13	5:44
FBQS1054+2536	1999 Dec 28	9:28, 10:02
	1999 Feb 13	9:14, 9:50
FBQS1217+3305	1999 Mar 14	8:37, 9:14
FBQS1253+2905	1999 Feb 13	7:53, 10:30, 11:04

Table 2—Continued

QSO	UT Date	UT Time
	1999 Feb 17	6:20, 6:54
FBQS1348+2840	1999 Jan 13	8:31
	1999 Jan 14	8:23, 8:59
	1999 Jan 15	8:37, 9:13
	1999 Jan 16	8:22, 8:57, 9:33
	1999 Feb 9	7:24, 7:55, 8:35, 9:10
	1999 Feb 13	8:34
FBQS1416+2649	1998 May 31	4:07, 4:49[5], 5:34[5]
	1999 Feb 17	7:34, 8:08
	1999 Mar 14	5:06, 5:45
	1999 Jul 13	3:41, 4:17
	1999 Jul 14	3:32, 4:06
FBQS1457+2707	1998 Jun 20	4:47, 5:34, 6:11
	1999 Jul 13	4:58, 5:32
	1999 Jul 13	4:45, 5:19
FBQS1537+2716	1999 Jun 19	5:22, 6:11, 6:47
	1999 Feb 17	8:54
FBQS1540+4138	1998 May 29	5:02, 5:41, 6:16
	1998 May 30	5:54
	1999 Feb 17	9:37
FBQS1625+2646	1999 Jul 13	6:36, 7:13
	1999 Jul 14	5:59, 6:34
FBQS1634+3203	1998 May 31	8:25, 9:00, 9:35
	1999 Feb 17	10:18, 10:45
FBQS1645+2244	1998 May 30	6:42, 7:19, 7:55, 8:31, 9:06
	1998 Aug 14	4:19, 4:59
FBQS1651+4002	1998 May 31	6:32, 7:07, 7:42
	199 Jul 13	6:11[2]
FBQS2216-0057	1998 Jun 20	9:04, 9:40
	1998 Aug 14	7:47, 8:42, 9:27
	1998 Aug 15	6:48
FBQS2233-0838	1998 Aug 22	8:00
	1998 Aug 28	4:42, 5:44, 6:29
	1998 Sep 20	3:25, 4:09, 4:50, 5:30, 6:06, 6:42

[1]1800 second exposure. Unless otherwise indicated, all exposures are 1800 seconds.

[2]900 second exposure.

[3]803 second exposure.

[4]1497 second exposure.

[4]2400 second exposure.

Table 3. Search Linelist.

Ion	λ_{vac}	f	IP (eV)	Ion	λ_{vac}	f	IP (eV)
C II	1036.3367	0.125	24.376	Ni II	1370.132	0.100	
C II	1334.5323	0.118		Ni II	1741.549	0.0679	
O VI	1031.9265	0.130	138.080	Ni II	1709.600	0.0470	
O VI	1037.6155	0.0648		Si IV	1393.755	0.528	45.13
Ar I	1048.2199	0.230	15.755	Si IV	1402.770	0.262	
Ar I	1066.6599	0.0594		C IV	1548.202	0.1940	64.476
S IV	1062.671	0.0377	47.29	C IV	1550.774	0.0970	
N II	1083.990	0.101	29.593	C I	1656.9282	0.142	11.256
Fe III	1122.526	0.056	30.643	C I	1277.2454	0.0881	
P II	1152.810	0.187	19.72	C I	1560.3095	0.0822	
S III	1190.206	0.0224	35.0	C I	1328.8332	0.0623	
N I	1199.5496	0.133	14.53	C I	1280.1353	0.0445	
N I	1200.2233	0.0885		Al II	1670.7867	1.88	18.823
N I	1200.7098	0.0442		Al III	1854.7164	0.539	28.44
N I	1134.9803	0.0402		Al III	1862.7895	0.268	
N I	1134.4149	0.0268		Zn II	2026.137	0.412	17.96
N I	1134.1653	0.0134		Zn II	2062.662	0.202	
Si III	1206.500	1.66	34.46	Cr II	2056.254	0.167	16.49
H I	1215.6701	0.4162	13.595	Cr II	2062.234	0.121	
H I	1025.7223	0.0791		Cr II	2066.161	0.0798	
N V	1238.821	0.152	97.863	Fe II	2382.7652	0.338	16.18
N V	1242.804	0.0757		Fe II	2600.1729	0.203	
S II	1259.518	0.0159	23.4	Fe II	2344.2139	0.108	
S II	1253.808	0.0107		Fe II	1608.451	0.062	
S II	1250.583	0.00535		Fe II	2586.6500	0.0573	
Si II	1260.4223	0.959	16.34	Fe II	2374.4612	0.0395	
Si II	1193.2898	0.501		Fe I	2484.0210	0.557	7.87
Si II	1190.4160	0.251		Mn II	2576.877	0.288	15.636
Si II	1526.7071	0.230		Mn II	2594.499	0.223	
Si II	1304.3711	0.147		Mn II	2606.462	0.158	
Si II	1808.0129	0.0055		Mg II	2796.352	0.592	15.031
O I	1302.1685	0.0486	13.614	Mg II	2803.531	0.295	
O I	1025.7618	0.0203		Ca II	3934.777	0.688	11.868
O I	1039.2304	0.0092		Ca II	3968.468	0.341	
Ni II	1317.217	0.121	18.15	Na I	5891.5833	0.655	5.138
Ni II	1370.132	0.100		Na I	5897.5581	0.327	

Table 4. All absorption lines.

N	λ	σ_λ	W_{obs}	σ_W	fwhm	SL	ID	z
				FBQS0047-0156 ($z = 2.479$)				
1	3977.09[a]	0.15	1.99	0.08	6.87	21.2		
2	3984.01[a]	0.25	1.19	0.08	6.88	13.0		
5	4012.43[a]	0.41	0.94	0.11	5.01	8.3		
6	4044.96[a]	0.11	3.14	0.10	6.85	26.4		
7	4063.58[a]	0.46	0.68	0.09	5.99	7.6		
8	4076.98[a]	0.23	1.28	0.08	13.19	14.6		
9	4089.69[a]	0.30	0.91	0.07	8.83	11.3		
10	4094.06[a]	0.29	0.89	0.07	5.10	11.3		
11	4121.97[a]	0.22	0.99	0.06	5.93	14.3		
12	4125.79[a]	0.12	1.81	0.06	6.97	26.2		
13	4140.14[a]	0.29	0.72	0.06	7.51	11.5		
14	4147.48[a]	0.09	2.22	0.05	6.34	35.7		
15	4173.64[a]	0.12	1.60	0.05	6.57	26.5		
16	4178.89[a]	0.18	1.04	0.05	7.35	18.1		
17	4203.99[a]	0.16	0.79	0.04	6.25	19.3		
18	4207.62[a]	0.05	2.29	0.03	6.50	56.8		
19	4214.70[a]	0.15	0.81	0.03	8.26	22.9		
20	4223.26[a]	0.06	1.52	0.03	7.16	51.8		
21	4268.99	0.13	1.21	0.04	7.11	24.7	N V BAL	
22	4274.56	0.11	1.42	0.04	7.75	28.4	N V BAL	
23	4281.93	0.14	1.11	0.04	10.71	23.2	N V BAL	
24	4289.24	0.07	1.90	0.04	7.33	40.9	N V BAL	
25	4292.58	0.12	1.15	0.04	4.99	24.6	N V BAL	
							Si II 1526[c]	1.8117
26	4302.06	0.20	0.84	0.05	6.73	17.3	N V BAL	
28	4352.24	0.27	0.59	0.04	6.00	12.7	C IV 1548	1.8112
29	4360.12	0.89	0.22	0.05	6.06	4.0	C IV 1550	1.8116
33	4522.48	0.35	0.62	0.06	6.61	9.7	Fe II 1608	1.8117
34	4571.79	0.51	0.42	0.06	10.38	6.9		
35	4696.42	0.24	1.07	0.07	6.18	14.2	Al II 1670	1.8109
38	5035.87	0.61	0.39	0.07	7.14	5.7	C IV BAL	
39	5042.90	0.43	0.52	0.06	7.46	8.1	C IV BAL	
40	5049.11	0.33	0.67	0.06	7.73	10.4	C IV BAL	
41	5056.15	0.41	0.54	0.06	8.31	8.4	C IV BAL	
42	5064.24	0.47	0.48	0.06	8.40	7.4	C IV BAL	
43	5072.65	0.69	0.35	0.07	10.04	5.1	C IV BAL	
44	5081.89	0.93	0.26	0.07	10.44	3.8	C IV BAL	
45	5168.19[b]	0.69	0.34	0.06	11.59	5.1		
46	5203.77	0.48	0.52	0.07	8.53	7.2	C IV BAL	

Table 4—Continued

N	λ	σ_λ	W_{obs}	σ_W	fwhm	SL	ID	z
47	5211.45	0.41	0.58	0.07	7.93	8.3	C IV BAL	
48	5217.38	0.50	0.49	0.07	7.18	6.9	C IV BAL	
49	5277.22	0.94	0.30	0.08	6.71	3.7	C IV BAL	
50	5284.72	0.42	0.67	0.08	7.94	8.0	C IV BAL	
51	5291.86	0.19	1.32	0.07	8.51	17.1	C IV BAL	
52	5299.96	0.13	2.03	0.07	8.72	23.6	C IV BAL	
53	5307.82	0.12	2.04	0.07	9.46	25.7	C IV BAL	
54	5316.14	0.06	3.48	0.06	8.35	41.3	C IV BAL	
55	5323.54	0.05	4.05	0.06	8.34	46.9	C IV BAL	
56	5331.48	0.07	3.21	0.06	8.84	39.8	C IV BAL	
57	5339.40	0.10	2.34	0.06	9.69	30.8	C IV BAL	
58	5347.57	0.08	2.71	0.06	9.15	36.3	C IV BAL	
59	5356.85	0.07	3.03	0.06	8.47	40.7	C IV BAL	
60	5362.56	0.16	1.34	0.06	7.32	19.0	C IV BAL	
61	5368.65	0.15	1.44	0.06	6.59	21.6	C IV BAL	
69	5895.48[e]	1.34	1.20	0.22	14.69	5.1		
72	6177.50[b]	1.18	0.97	0.16	15.77	5.9		
76	6515.31[b]	0.85	1.12	0.13	21.47	8.1		
78	6589.02	0.76	1.15	0.12	3.18	9.0	Fe II 2344	1.8108
79	6697.14	0.32	2.59	0.12	13.42	20.4	Fe II 2382	1.8107
81	6954.32	1.39	0.85	0.16	16.96	5.0		
83	7270.08	1.47	0.90	0.18	12.04	4.7	Fe II 2586	1.8106
84	7309.26	0.50	2.66	0.19	14.06	13.1	Fe II 2600	1.8111
89	7858.73	0.40	4.69	0.26	13.49	15.2	Mg II 2796	1.8103
90	7875.47	0.53	3.28	0.24	10.14	12.0	Mg II 2803	1.8091
				FBQS0210-0152 ($z = 2.372$)				
1	3966.89[a]	0.15	3.08	0.12	0.00	20.2		
2	3970.95[a]	0.62	0.74	0.12	5.02	5.2		
3	3983.54[a]	0.59	0.81	0.13	1.98	6.1		
4	4012.25[a]	0.24	1.97	0.12	6.27	14.0		
5	4020.62[a]	0.28	1.63	0.12	1.68	12.3		
6	4041.34[a]	0.34	1.12	0.10	8.60	10.4	Ly-a 1216	2.3244
7	4051.68[a]	0.26	1.27	0.09	7.30	12.9		
8	4057.16[a]	0.19	1.70	0.09	8.36	17.3	Ly-a 1216	2.3374
9	4066.01[a]	0.19	1.62	0.08	8.46	18.3		
10	4087.93[a]	0.29	0.76	0.06	4.94	12.2		
11	4099.38[a]	0.04	4.06	0.04	7.42	64.0		
12	4103.70[a]	0.12	1.53	0.05	5.58	25.3	Ly-a 1216	2.3757
13	4114.22	0.69	0.29	0.05	5.12	5.4	N V 1238[c]	2.3211
14	4130.14	0.10	2.12	0.06	7.45	33.8	N V 1238	2.3339

Table 4—Continued

N	λ	σ_λ	W_{obs}	σ_W	fwhm	SL	ID	z
							N V 1242[c]	2.3232
15	4144.34	0.18	1.30	0.06	4.21	19.2	N V 1242	2.3347
16	4178.46	0.80	0.31	0.06	1.68	4.7	N V 1238[c]	2.3729
17	4191.75	0.86	0.28	0.06	5.53	4.3	N V 1242[c]	2.3728
18	4201.56	0.15	1.78	0.07	6.57	22.8	C II 1334	2.1483
19	4284.12	0.49	0.69	0.09	6.82	7.4	Al III 1854	1.3099
20	4302.68	0.70	0.48	0.09	6.33	5.3	Al III 1862	1.3098
24	4387.23	0.19	2.11	0.11	9.45	17.2	Si IV 1393	2.1478
25	4415.56	0.20	1.64	0.09	2.71	17.2	Si IV 1402	2.1477
28	4698.51	0.63	0.49	0.08	1.91	5.9	Si IV 1393	2.3711
29	4728.13	0.53	0.55	0.08	7.61	6.9	Si IV 1402	2.3706
30	4805.03	0.36	0.90	0.09	6.92	9.9	Si II 1526	2.1473
31	4872.78	0.12	2.61	0.08	5.71	27.0	C IV 1548	2.1474
32	4881.18	0.15	2.05	0.08	6.43	21.3	C IV 1550	2.1476
33	5142.55	0.40	0.73	0.08	6.97	9.0	C IV 1548	2.3216
34	5149.79	0.57	0.56	0.09	7.33	6.4	C IV 1550	2.3208
35	5162.05	0.18	1.51	0.07	5.48	18.8	C IV 1548	2.3342
36	5171.09	0.21	1.21	0.07	6.26	16.4	C IV 1550	2.3345
37	5218.90	0.25	0.90	0.06	4.46	14.1	C IV 1548	2.3709
38	5227.65	0.47	0.50	0.06	4.99	7.8	C IV 1550	2.3710
39	5259.29	0.21	1.30	0.07	6.88	17.0	Al II 1670	2.1478
40	5414.41	0.17	2.75	0.12	6.62	18.7	Fe II 2344	1.3097
41	5484.62	0.34	1.72	0.16	7.31	10.0	Fe II 2374	1.3098
42	5503.28	0.15	3.84	0.15	6.92	19.4	Fe II 2382	1.3096
43	5508.05	1.06	2.80	0.38	16.62	6.7		
45	5582.17[be]	1.60	2.57	0.53	11.69	4.5	Mg II 2796[c]	0.9962
46	5600.41[be]	1.36	1.80	0.32	22.49	5.4	Mg II 2803[c]	0.9976
49	5974.99	0.74	3.05	0.29	14.94	9.6	Fe II 2586	1.3099
50	6007.37	0.42	5.20	0.28	16.59	15.6	Fe II 2600	1.3104
53	6458.73	0.26	5.37	0.18	11.56	24.8	Mg II 2796	1.3097
54	6477.07	0.27	5.24	0.18	10.93	23.4	Mg II 2803	1.3103
55	6515.24	1.52	1.03	0.20	13.06	5.0		
56	6590.25	1.89	0.94	0.23	3.36	4.0	Mg I 2852	1.3100
58	6903.81	1.25	1.63	0.26	20.80	5.9		
59	7381.66	1.04	2.35	0.31	4.59	6.9		
61	7498.32	1.30	2.05	0.34	18.83	5.6		
				FBQS0256-0119 ($z = 2.491$)				
1	3996.02[a]	0.18	4.26	0.21	6.84	12.0		
2	4002.27[a]	0.15	4.60	0.20	6.60	8.3		
3	4007.80[a]	0.11	6.10	0.19	7.54	7.4		

Table 4—Continued

N	λ	σ_λ	W_{obs}	σ_W	fwhm	SL	ID	z
4	4014.42[a]	0.12	5.96	0.19	7.53	10.1		
5	4020.99[a]	0.27	2.85	0.21	8.08	9.3		
6	4028.99[a]	0.45	1.74	0.22	9.26	7.1		
7	4067.48[a]	0.21	3.12	0.19	7.95	13.2		
8	4075.28[a]	0.20	3.25	0.18	7.53	13.5		
9	4082.05[a]	0.28	2.29	0.18	7.95	10.2		
10	4089.20[a]	0.19	3.20	0.17	7.77	14.8		
11	4098.57[a]	0.22	2.67	0.16	9.45	13.6		
12	4107.45[a]	0.15	3.53	0.15	8.44	16.3		
13	4113.19[a]	0.13	3.93	0.14	6.59	17.7		
14	4131.56[a]	0.42	1.37	0.16	2.25	7.8		
15	4157.27[a]	0.41	1.45	0.17	5.16	8.0		
16	4167.10[a]	0.50	1.27	0.18	7.55	6.7		
17	4182.86[a]	0.21	3.08	0.18	41.38	13.4		
18	4198.75[a]	0.12	3.55	0.12	7.79	22.3		
19	4206.04[a]	0.19	2.06	0.11	8.21	15.3		
20	4212.58[a]	0.09	3.51	0.09	6.92	29.3		
21	4226.48[a]	0.09	2.57	0.07	6.03	31.9		
22	4233.15[a]	0.25	0.89	0.06	5.87	13.1		
23	4245.24[a]	0.60	0.32	0.05	1.64	5.9		
25	4281.35	0.10	2.97	0.08	7.44	27.8	N V BAL	
26	4287.84	0.09	3.18	0.08	8.34	26.9	N V BAL	
27	4294.62	0.06	4.95	0.08	8.08	37.1	N V BAL	
28	4302.43	0.09	3.28	0.08	8.44	28.8	N V BAL	
29	4307.84	0.11	2.53	0.08	6.32	23.9	N V BAL	
30	4320.36	0.32	0.94	0.08	7.64	10.6		
32	4401.29	0.27	1.44	0.11	7.09	12.1		
33	4525.80	0.25	1.93	0.14	6.28	12.4		
34	4533.46	0.31	1.60	0.14	7.31	10.3		
36	4746.93	0.64	0.82	0.15	6.79	5.4		
38	4819.16	0.71	0.69	0.14	10.29	4.9	Si IV BAL[c]	
39	4826.61	0.74	0.68	0.14	8.74	4.6	Si IV BAL[c]	
40	4831.60	0.71	0.70	0.14	5.29	4.8	Si IV BAL[c]	
41	4853.84	0.34	1.25	0.12	6.64	9.7	Si IV BAL[c]	
42	4861.85	0.57	0.72	0.11	5.90	6.0	Si IV BAL[c]	
43	4879.40	0.56	0.69	0.11	10.77	6.1	Si IV BAL[c]	
44	4888.08	0.87	0.44	0.11	11.04	4.0	Si IV BAL[c]	
50	5187.50	0.55	0.91	0.14	7.90	6.1	C IV BAL	
51	5194.51	0.39	1.29	0.14	7.78	8.3	C IV BAL	
52	5203.55	0.46	1.14	0.15	10.57	7.3	C IV BAL	
53	5214.08	0.45	1.14	0.14	14.68	7.4	C IV BAL	
54	5227.71	0.27	1.91	0.14	9.91	11.7	C IV BAL	

Table 4—Continued

N	λ	σ_λ	W_{obs}	σ_W	fwhm	SL	ID	z
55	5235.30	0.20	2.48	0.14	8.68	14.4	C IV BAL	
56	5242.82	0.23	2.25	0.14	8.07	13.1	C IV BAL	
57	5250.39	0.30	1.74	0.15	7.77	10.4	C IV BAL	
58	5258.90	0.55	1.00	0.15	9.02	6.1	C IV BAL	
59	5351.06	0.18	2.97	0.15	8.13	15.2	C IV BAL	
60	5357.64	0.11	4.30	0.14	8.00	19.4	C IV BAL	
61	5364.85	0.08	5.51	0.12	8.00	23.4	C IV BAL	
62	5372.91	0.10	4.44	0.13	8.81	22.6	C IV BAL	
63	5380.99	0.22	2.25	0.14	11.33	13.9	C IV BAL	
64	5391.52	0.40	1.25	0.14	6.97	8.3	C IV BAL	
68	6875.20	1.16	2.68	0.46	12.69	5.3		
69	6900.33	1.17	2.48	0.43	14.60	5.3		
				FBQS0725+2819 ($z = 2.662$)				
1	3981.22[a]	0.07	4.52	0.09	6.42	38.1	Ly-a 1216[c]	2.2749
3	4015.85[a]	0.16	2.27	0.10	6.88	17.7		
4	4022.29[a]	0.11	3.10	0.10	7.26	26.1		
5	4034.96[a]	0.11	3.06	0.10	6.16	27.0		
8	4079.50[a]	0.47	0.80	0.11	4.34	7.4		
9	4084.20[a]	0.56	0.66	0.11	14.20	6.2		
10	4097.57[a]	0.45	0.76	0.10	1.56	7.7		
11	4123.59[a]	0.41	0.80	0.09	10.85	8.3		
12	4135.54[a]	0.23	1.36	0.09	6.97	14.2		
13	4147.44[a]	0.34	0.95	0.09	3.81	9.4		
14	4168.98[a]	0.13	2.48	0.09	6.47	23.8		
15	4173.68[a]	0.08	3.82	0.09	6.60	36.8		
16	4188.11[a]	0.28	1.23	0.10	1.90	12.8		
17	4204.37[a]	0.12	2.63	0.09	7.80	28.3		
18	4216.21[a]	0.28	1.05	0.08	5.44	11.4		
19	4225.67[a]	0.11	2.56	0.08	6.24	29.7		
20	4248.16[a]	0.06	3.76	0.07	6.58	46.1		
21	4252.39[a]	0.07	3.11	0.07	6.09	38.5		
22	4265.42[a]	0.13	1.96	0.07	1.83	25.8		
24	4283.89[a]	0.10	2.29	0.06	6.04	32.3		
25	4299.02[a]	0.05	3.86	0.05	6.03	57.4		
26	4304.14[a]	0.04	4.27	0.05	7.27	64.5		
27	4337.91[a]	0.19	1.04	0.06	8.27	16.7		
28	4342.72[a]	0.10	1.99	0.05	6.49	31.7		
29	4349.27[a]	0.17	1.19	0.06	5.72	18.9		
30	4356.11[a]	0.49	0.44	0.06	5.83	7.0		
31	4362.78[a]	0.14	1.59	0.06	6.81	25.1		

Table 4—Continued

N	λ	σ_λ	W_{obs}	σ_W	fwhm	SL	ID	z
32	4369.31[a]	0.09	2.06	0.05	7.43	32.7		
33	4380.49[a]	0.15	1.36	0.06	5.59	22.2		
34	4398.13[a]	0.21	0.82	0.05	8.57	15.6		
36	4420.90[a]	0.18	0.79	0.04	7.56	18.4		
37	4441.43[a]	0.06	2.11	0.03	5.92	56.8	Si II 1526	1.9092
38	4457.21[a]	0.02	4.15	0.02	6.79	129.2		
39	4464.12[a]	0.02	4.03	0.02	7.59	125.6		
40	4504.46	0.12	1.26	0.04	6.20	30.3	C IV 1548	1.9095
41	4513.90	0.08	1.93	0.05	6.70	42.0	C IV 1550	1.9107
							Si II 1808	1.4966
44	4630.61	0.13	1.47	0.05	6.50	26.1	Al III 1854	1.4967
45	4651.48	0.23	0.85	0.06	4.00	14.4	Al III 1862	1.4970
46	4678.85	0.45	0.50	0.06	6.73	7.3	Fe II 1608	1.9089
47	4860.35	0.22	0.93	0.06	4.21	14.6	Al II 1670[c]	1.4980
49	4888.57	0.66	0.31	0.06	11.13	5.3		
50	5058.69	0.20	1.01	0.06	6.01	17.2	C IV 1548[c]	2.2675
							Mg I 2026	1.4963
							Zn II 2026	1.4967
51	5067.97	0.34	0.59	0.06	6.18	9.7	C IV 1548[c]	2.2735
							C IV 1550[c]	2.2680
53	5127.33	0.68	0.30	0.06	9.48	5.7		
54	5134.01	0.20	0.91	0.05	6.71	17.3	Cr II 2056	1.4968
55	5149.66	0.15	1.20	0.05	5.32	22.5	Cr II 2062	1.4971
							Zn II 2062	1.4966
56	5158.37	0.31	0.61	0.05	5.28	11.2	Cr II 2066	1.4966
62	5615.64	1.00	0.83	0.12	2.76	6.7		
63	5645.21	0.71	1.04	0.11	2.85	9.3		
65	5853.92	0.20	4.12	0.12	10.27	32.0	Fe II 2344	1.4972
66	5929.00	0.30	2.92	0.13	13.27	22.0	Fe II 2374	1.4970
67	5948.42	0.18	4.50	0.12	11.13	34.3	Fe II 2382	1.4964
71	6433.71	0.62	1.33	0.12	14.30	10.7	Mn II 2576	1.4967
72	6457.53	0.17	4.70	0.12	9.41	37.7	Fe II 2586	1.4965
73	6478.21	0.58	1.42	0.12	7.84	11.4	Mn II 2594	1.4969
74	6491.63	0.15	5.54	0.13	9.22	44.8	Fe II 2600	1.4966
75	6509.04	0.59	1.39	0.12	11.69	11.4	Mn II 2606	1.4973
77	6819.19	0.60	1.27	0.11	3.40	10.6	Fe II 2344	1.9089
79	6871.55	1.06	0.84	0.13	9.62	6.9		
81	6904.75	0.86	0.94	0.12	9.66	7.7	Fe II 2374	1.9079
82	6932.41	0.38	1.98	0.11	3.02	16.8	Fe II 2382	1.9094
83	6981.99	0.09	6.92	0.09	10.42	66.8	Mg II 2796	1.4968
84	6999.47	0.10	6.26	0.09	14.42	61.1	Mg II 2803	1.4967
85	7122.70	0.25	3.07	0.12	3.21	25.4	Mg I 2852	1.4966

Table 4—Continued

N	λ	σ_λ	W_{obs}	σ_W	fwhm	SL	ID	z
86	7521.72	1.13	0.85	0.14	9.95	6.0	Fe II 2586	1.9079
87	7562.25	0.58	1.57	0.14	2.83	11.2	Fe II 2600	1.9084
89	8135.78	0.50	2.56	0.19	11.92	12.7	Mg II 2796	1.9094
				FBQS0729+2524 ($z = 2.300$)				
1	3988.18[a]	0.05	3.47	0.04	7.94	66.1		
2	3996.26[a]	0.04	4.13	0.04	7.56	84.8	Ly-a 1216	2.2873
3	4025.95	0.71	0.24	0.04	8.95	5.7		
4	4068.05	0.40	0.55	0.06	7.32	9.9		
5	4073.17	0.06	3.54	0.05	7.13	65.3	N V 1238	2.2879
6	4084.50	0.07	2.58	0.05	7.01	49.2	N V 1242	2.2865
7	4089.86	0.21	0.94	0.05	10.53	18.1		
9	4185.99	0.53	0.57	0.07	8.16	7.8	Si II 1526	1.7418
10	4226.52	0.19	1.35	0.07	1.84	19.4	Mg II 2796[c]	0.5114
11	4238.72	0.35	0.76	0.07	8.45	10.8	Mg II 2803[c]	0.5119
12	4245.46	0.13	1.96	0.07	6.18	27.9	C IV 1548	1.7422
13	4252.37	0.18	1.47	0.07	6.54	21.0	C IV 1550	1.7421
16	4502.90	0.69	0.40	0.07	1.91	5.7	Si IV 1393	2.2308
17	4530.67	1.12	0.27	0.08	4.33	3.6	Si IV 1402	2.2298
18	4580.28	0.67	0.38	0.06	3.95	5.9	Si IV 1393[c]	2.2863
							Al II 1670	1.7414
19	4612.34[b]	0.57	0.41	0.06	11.56	6.8	Si IV 1402[c]	2.2880
22	4999.99	0.31	0.77	0.06	6.82	11.7	C IV 1548	2.2295
23	5008.40	0.48	0.51	0.06	6.08	7.3	C IV 1550	2.2296
24	5082.79	0.55	0.35	0.05	4.46	6.9		
25	5089.17	0.04	4.11	0.04	7.88	83.5	C IV 1548	2.2871
26	5097.64	0.05	3.05	0.04	8.31	64.2	C IV 1550	2.2872
31	6281.41[b]	0.74	1.00	0.11	16.84	8.4		
32	6315.21[b]	1.27	0.60	0.11	9.84	5.2		
40	7667.89	0.77	1.66	0.19	7.87	8.5	Mg II 2796	1.7421
41	7687.11	0.87	1.34	0.17	2.98	7.6	Mg II 2803	1.7419
43	7829.52	1.19	1.07	0.19	23.96	5.6	Mg I 2852	1.7443
				FBQS0804+2516 ($z = 2.290$)				
1	3974.52[a]	0.03	4.49	0.04	6.75	79.6		
2	3997.47[a]	0.20	0.96	0.05	5.03	18.6		
3	4006.17[a]	0.18	1.04	0.05	4.10	19.9		
4	4014.78[a]	0.34	0.58	0.05	5.25	11.4		
5	4073.43	0.48	0.45	0.05	1.88	8.1	Fe II 2382	0.7095
8	4288.59	0.62	0.47	0.07	9.64	6.3		

Table 4—Continued

N	λ	σ_λ	W_{obs}	σ_W	fwhm	SL	ID	z
9	4444.23	0.81	0.36	0.07	2.33	4.8	Fe II 2600	0.7092
12	4655.48	0.59	0.46	0.07	6.61	6.6		
13	4760.11[b]	0.67	0.41	0.07	10.61	5.8		
15	4780.60	0.13	2.10	0.07	7.17	25.8	Mg II 2796	0.7096
16	4792.41	0.20	1.34	0.07	6.88	18.6	Mg II 2803	0.7094
17	4874.10	0.92	0.28	0.07	11.47	4.3	Mg I 2852[c]	0.7084
22	5587.86[be]	0.98	1.77	0.23	18.23	7.3		
23	5603.01[b]	1.17	1.15	0.18	18.56	6.2		
25	6272.70[b]	1.20	0.71	0.11	13.40	6.1		
26	6284.61[b]	0.70	1.23	0.11	17.58	10.4		
27	6307.71[b]	1.95	0.50	0.13	25.00	3.8	Fe II 2382[c]	1.6472
28	6343.00	1.09	0.80	0.11	13.98	6.8		
29	6387.39	1.45	0.68	0.13	23.23	5.1		
31	6845.98	1.30	0.76	0.13	16.31	5.7		
33	7256.24	0.86	1.40	0.16	20.31	8.4		
34	7384.50	1.16	1.04	0.16	3.81	6.3	Mg II 2796[c]	1.6408
35	7408.60	1.25	0.97	0.16	16.28	5.9	Mg II 2803[c]	1.6426
40	8112.43	1.16	1.33	0.20	14.20	6.3		
				FBQS0821+3107 ($z = 2.604$)				
1	3978.23[a]	0.14	1.95	0.08	7.25	20.5		
2	3984.00[a]	0.10	2.61	0.07	6.43	27.3		
3	3992.93[a]	0.64	0.47	0.09	9.52	5.2		
4	4008.35[a]	0.13	2.01	0.08	6.95	23.0		
5	4019.40[a]	0.28	0.97	0.08	7.96	11.4		
6	4042.30[a]	0.35	0.81	0.08	6.74	9.3		
7	4051.76[a]	0.40	0.69	0.08	8.07	7.8		
8	4056.35[a]	0.12	2.10	0.07	6.71	23.6		
9	4075.52[a]	0.20	1.35	0.08	11.14	15.3		
10	4091.31[a]	0.30	0.93	0.08	1.64	10.7		
11	4108.38[a]	0.27	0.98	0.08	6.61	11.2		
12	4112.43[a]	0.18	1.49	0.08	5.77	16.8		
13	4127.88[a]	0.08	2.90	0.07	6.91	31.1		
14	4133.06[a]	0.09	2.59	0.07	6.58	28.3		
15	4154.01[a]	0.18	1.38	0.07	4.59	16.8		
16	4160.00[a]	0.57	0.45	0.08	3.06	5.6		
17	4186.94[a]	0.06	3.22	0.06	5.96	41.5	Ly-a 1216	2.4441
18	4197.65[a]	0.04	4.49	0.05	6.68	56.3		
19	4207.33[a]	0.10	2.04	0.06	6.94	29.0		
20	4216.85[a]	0.08	2.88	0.07	6.65	33.3		
21	4227.96[a]	0.28	0.90	0.07	6.36	11.3	Fe II 2374[c]	0.7806

Table 4—Continued

N	λ	σ_λ	W_{obs}	σ_W	fwhm	SL	ID	z
22	4240.91[a]	0.39	0.52	0.06	2.02	8.4	Fe II 2382[c]	0.7798
23	4256.31[a]	0.12	1.58	0.05	10.69	25.7		
24	4264.17[a]	0.04	3.85	0.04	7.82	59.5		
25	4272.84[a]	0.05	3.42	0.05	9.01	55.2	Ly-a 1216	2.5148
26	4281.28[a]	0.04	4.01	0.04	8.85	63.4		
27	4289.49[a]	0.02	5.72	0.03	8.13	69.8		
28	4296.32[a]	0.01	6.81	0.02	7.96	22.9		
29	4303.22[a]	0.02	5.82	0.03	8.78	62.2	Ly-a 1216	2.5398
30	4314.80[a]	0.03	3.91	0.04	10.91	68.0		
31	4321.59[a]	0.03	3.92	0.04	8.55	69.6		
32	4326.74[a]	0.26	0.56	0.04	4.66	11.1		
33	4336.55[a]	0.11	1.36	0.04	1.83	28.2		
34	4352.89[a]	0.07	1.76	0.04	6.96	39.6		
35	4359.21[a]	0.05	2.49	0.04	6.23	51.9		
36	4369.24[a]	0.06	2.09	0.03	4.77	52.4		
37	4389.07[a]	0.02	4.64	0.02	6.69	129.7		
38	4432.01	0.37	0.36	0.04	2.07	8.9		
40	4455.36	0.04	2.95	0.03	6.83	68.9	Si II 1260	2.5348
41	4466.92	0.43	0.32	0.04	5.16	7.7		
42	4481.99	0.62	0.21	0.04	1.75	5.4		
43	4525.58	0.64	0.25	0.05	9.40	5.3		
44	4557.86	0.15	1.16	0.05	6.61	21.4	C IV 1548	1.9440
45	4565.10	0.25	0.67	0.05	7.84	12.9	C IV 1550	1.9438
46	4602.86	0.08	2.25	0.05	6.96	37.7	O I 1302	2.5348
47	4609.49	0.17	1.12	0.05	7.69	18.7	Si II 1304	2.5339
48	4629.68	0.23	1.07	0.07	5.62	13.9	Fe II 2600[c]	0.7805
50	4717.11	0.06	2.79	0.05	5.68	44.7	C II 1334	2.5347
53	4900.28	0.37	0.51	0.06	7.62	8.8	Si IV 1393[c]	2.5159
54	4926.51	0.15	1.19	0.05	6.34	20.8	Si IV 1393	2.5347
							Si IV 1402[c]	2.5120
56	4959.23	0.33	0.56	0.05	6.43	10.0	Si IV 1402	2.5353
57	4979.12	0.11	1.59	0.05	5.67	27.4	Mg II 2796	0.7806
58	4991.92	0.12	1.46	0.05	1.76	25.9	Mg II 2803	0.7806
59	5079.96	0.61	0.33	0.06	1.70	5.4	Mg I 2852	0.7806
60	5332.75	0.35	0.69	0.07	5.55	9.3	C IV 1548	2.4445
61	5339.06	0.89	0.28	0.07	6.68	3.7	C IV 1550	2.4428
62	5396.28	0.15	1.66	0.07	6.61	20.0	Si II 1526	2.5346
63	5442.26	0.71	0.41	0.09	5.28	4.6	C IV 1548	2.5152
64	5473.12	0.24	1.22	0.09	6.09	12.7	C IV 1548	2.5351
65	5481.94	0.42	0.74	0.09	6.71	7.7	C IV 1550	2.5350
67	5684.40	1.85	0.45	0.12	12.52	3.6	Fe II 1608	2.5341
68	5905.06	0.47	1.78	0.13	11.27	13.3	Al II 1670	2.5343

Table 4—Continued

N	λ	σ_λ	W_{obs}	σ_W	fwhm	SL	ID	z
72	6849.00	1.29	0.55	0.11	17.89	5.1		
				FBQS0857+3313 ($z = 2.340$)				
1	3971.31[a]	0.05	5.56	0.08	6.70	17.7		
2	3976.67[a]	0.06	4.62	0.08	7.15	13.9	Ly-a 1216	2.2712
3	3980.98[a]	0.11	2.62	0.08	6.72	19.0		
5	4015.16[a]	0.18	1.28	0.06	1.79	18.8		
6	4026.59[a]	0.60	0.34	0.06	2.36	5.6		
7	4031.02[a]	0.08	2.10	0.05	6.77	35.1	Si IV 1393[c]	1.8922
8	4037.27[a]	0.03	4.38	0.04	7.08	78.7	Ly-a 1216	2.3210
9	4050.84[a]	0.03	3.32	0.03	6.34	91.1	Si IV 1402[c]	1.8877
10	4109.65	0.29	0.67	0.05	4.54	12.1	N V 1238	2.3174
11	4121.87	0.07	2.84	0.05	7.16	44.0	N V 1242	2.3166
							Si II 1260	2.2702
12	4139.27	0.43	0.44	0.05	6.59	8.3		
13	4257.04	0.15	1.65	0.07	6.66	21.4	O I 1302	2.2692
14	4264.54	0.25	1.04	0.07	5.09	13.6	Si II 1304	2.2694
15	4362.94	0.08	2.76	0.06	6.69	36.5	C II 1334	2.2693
16	4420.50	0.39	0.70	0.07	6.26	9.0	Al III 1854	1.3834
17	4439.49	0.41	0.62	0.07	7.66	8.8	Al III 1862	1.3832
18	4472.44	0.07	3.36	0.07	6.46	38.0	C IV 1548	1.8888
19	4479.67	0.08	2.83	0.06	7.40	34.7	C IV 1550	1.8887
21	4556.56	0.14	1.83	0.07	6.74	24.1	Si IV 1393	2.2693
22	4585.51	0.17	1.41	0.07	6.84	19.2	Si IV 1402	2.2689
25	4990.73	0.14	1.63	0.06	6.87	24.4	Si II 1526	2.2690
26	5061.19	0.05	3.65	0.05	7.06	50.0	C IV 1548	2.2691
27	5069.47	0.07	2.95	0.05	7.35	44.7	C IV 1550	2.2690
30	5134.90	0.13	1.27	0.05	6.53	25.3	C IV 1548	2.3167
31	5143.37	0.14	1.13	0.04	5.60	24.0	C IV 1550	2.3166
33	5258.18	0.35	0.67	0.06	6.68	10.0	Fe II 1608	2.2691
34	5461.94	0.20	1.98	0.11	6.38	16.2	Al II 1670	2.2691
37	5898.15[b]	1.31	1.17	0.22	9.86	5.1		
38	5914.29[b]	1.18	1.06	0.18	14.19	5.7		
40	6168.44	1.19	0.95	0.16	18.81	5.7		
44	6666.06	0.30	3.31	0.14	9.56	20.5	Mg II 2796	1.3838
45	6679.74	0.35	2.85	0.14	9.75	17.9	Mg II 2803	1.3826
46	6844.26	0.87	1.22	0.15	18.00	7.7		
51	7352.96	1.20	0.96	0.17	8.19	5.6		
52	7447.19[b]	1.13	0.99	0.16	13.49	5.9		
53	7490.01[b]	0.88	1.32	0.17	18.12	7.6		
54	7661.50	0.90	1.53	0.20	3.28	7.3	Fe II 2344	2.2683

Table 4—Continued

N	λ	σ_λ	W_{obs}	σ_W	fwhm	SL	ID	z
55	7760.37	1.22	1.14	0.20	17.66	5.5	Fe II 2374	2.2683
56	7787.16	0.64	2.10	0.19	3.71	10.0	Fe II 2382	2.2681
57	7938.74	1.34	1.12	0.22	16.61	5.0		
60	8070.14	1.31	1.12	0.21	16.06	5.1		
				FBQS0910+2539 ($z = 2.744$)				
1	3973.81[a]	0.66	0.98	0.18	8.57	5.2		
2	3988.91[a]	0.27	2.09	0.16	6.99	11.6		
4	4013.32[a]	0.19	2.88	0.15	6.54	15.4		
5	4035.18[a]	0.17	3.84	0.18	6.72	14.8		
6	4041.48[a]	0.22	3.07	0.19	8.18	12.2		
7	4066.65[a]	0.12	4.66	0.15	6.70	20.2		
8	4075.61[a]	0.20	2.99	0.16	6.09	14.6		
10	4110.01[a]	0.12	4.49	0.15	6.77	13.3		
11	4116.02[a]	0.09	5.73	0.15	8.26	16.2		
12	4145.93[a]	0.09	6.04	0.15	6.96	21.8		
13	4161.79[a]	0.30	1.99	0.17	6.11	9.5		
14	4166.36[a]	0.21	2.82	0.16	6.79	13.1		
15	4176.56[a]	0.37	1.61	0.17	8.20	8.7		
17	4195.39[a]	0.20	2.67	0.15	5.46	14.3		
18	4203.12[a]	0.34	1.66	0.16	1.94	9.7		
19	4217.63[a]	0.18	2.94	0.15	7.10	16.3		
20	4226.52[a]	0.21	2.50	0.14	6.99	14.6		
22	4261.65[a]	0.23	2.55	0.16	4.87	12.9		
24	4286.55[a]	0.37	1.46	0.15	7.04	8.9		
26	4312.03[a]	0.30	1.79	0.15	5.26	10.7		
28	4334.95[a]	0.59	0.92	0.15	5.63	5.7		
29	4362.67[a]	0.24	2.56	0.17	5.66	12.3		
30	4372.03[a]	0.31	1.59	0.14	7.07	10.4		
31	4392.82[a]	0.40	1.13	0.12	6.57	8.5		
32	4404.90[a]	0.07	5.19	0.10	7.29	30.8		
33	4412.43[a]	0.17	2.35	0.11	7.53	17.0		
34	4421.71[a]	0.12	3.16	0.11	6.02	23.1		
35	4440.60[a]	0.09	3.96	0.10	6.33	29.0		
36	4447.39[a]	0.21	1.76	0.10	5.55	14.4		
38	4472.21[a]	0.28	1.37	0.11	6.36	11.8		
39	4488.26[a]	0.12	2.64	0.09	4.02	25.4		
40	4500.73[a]	0.07	4.68	0.08	6.74	36.4		
41	4510.39[a]	0.15	1.93	0.08	6.57	21.1		
42	4514.61[a]	0.37	0.76	0.08	6.47	8.7		
43	4539.00[a]	0.40	0.63	0.07	3.31	8.6		

Table 4—Continued

N	λ	σ_λ	W_{obs}	σ_W	fwhm	SL	ID	z
44	4549.90[a]	0.15	1.49	0.06	4.39	21.6		
45	4569.40	0.12	1.74	0.06	6.47	25.4		
46	4575.61	0.31	0.77	0.07	4.97	10.9		
47	4660.23	0.15	2.01	0.09	6.88	20.5	C IV 1548	2.0101
48	4667.95	0.20	1.66	0.09	6.07	16.3	C IV 1550	2.0101
53	5730.25[b]	1.46	1.56	0.30	19.30	5.0		
61	7287.17	0.87	3.45	0.40	13.16	7.7	Mg II 2796	1.6060
62	7303.57	1.48	1.94	0.38	7.08	4.7	Mg II 2803	1.6051
				FBQS0955+3335 ($z = 2.503$)				
1	3972.24[a]	0.36	0.87	0.09	5.30	9.5		
2	3980.40[a]	0.16	1.99	0.09	4.57	20.5		
3	3995.71[a]	0.05	5.06	0.07	6.69	41.9	Ly-a 1216[c]	2.2868
4	4002.74[a]	0.12	2.65	0.08	5.06	24.6	Ly-a 1216[c]	2.2926
5	4015.19[a]	0.21	1.50	0.09	5.76	15.8		
6	4028.74[a]	0.18	1.62	0.08	6.03	17.1		
7	4034.80[a]	0.09	3.18	0.07	6.04	33.7	Ly-a 1216[c]	2.3190
8	4046.59[a]	0.12	2.57	0.08	5.91	25.8		
9	4080.44[a]	0.21	1.37	0.08	8.40	16.1		
10	4092.17[a]	0.35	0.92	0.09	6.91	9.8		
11	4101.44[a]	0.13	1.95	0.07	7.09	24.2		
12	4107.34[a]	0.15	1.70	0.07	7.00	21.3		
13	4125.71[a]	0.51	0.52	0.07	9.03	6.8		
14	4130.75[a]	0.15	1.63	0.07	6.72	21.7		
15	4147.08[a]	0.22	1.09	0.07	6.59	15.5		
16	4152.83[a]	0.53	0.46	0.07	6.23	6.7		
17	4173.61[a]	0.24	0.90	0.06	5.68	14.0		
18	4178.79[a]	0.24	0.89	0.06	8.91	14.2		
19	4188.42[a]	0.43	0.48	0.06	6.55	8.2		
20	4209.53[a]	0.13	1.33	0.05	7.28	25.7		
21	4219.11[a]	0.09	1.77	0.04	7.10	37.2		
22	4223.67[a]	0.28	0.54	0.04	6.58	12.0		
23	4238.22[a]	0.04	3.12	0.03	7.27	81.6	Al II 1670	1.5367
24	4257.32[a]	0.38	0.29	0.03	4.61	9.5		
25	4267.18[a]	0.11	1.01	0.03	5.44	31.5	Ly-a 1216[c]	2.5101
27	4286.84	0.68	0.21	0.04	5.68	5.3		
28	4314.89	0.34	0.49	0.05	6.44	10.4	Si IV 1393	2.0959
29	4344.10	0.95	0.18	0.05	4.66	3.8	Si IV 1402	2.0968
31	4705.01	0.10	2.41	0.07	6.95	31.0	Al III 1854	1.5368
32	4714.15	0.32	0.74	0.06	6.71	11.2		
33	4724.44	0.16	1.39	0.06	6.46	20.8	Si II 1526	2.0945

Table 4—Continued

N	λ	σ_λ	W_{obs}	σ_W	fwhm	SL	ID	z
							Al III 1862	1.5362
34	4792.19	0.33	0.69	0.06	6.82	10.6	C IV 1548	2.0953
35	4799.76	0.54	0.43	0.06	4.77	6.7	C IV 1550	2.0951
36	4894.70	0.66	0.30	0.05	7.55	5.5		
37	4902.65	0.71	0.28	0.05	8.53	5.1		
39	4978.43	0.48	0.47	0.06	6.86	7.6	Fe II 1608	2.0952
40	5086.93	0.47	0.57	0.07	8.53	7.6	C IV 1548[c]	2.2857
41	5097.13	0.24	0.90	0.06	7.94	14.4	C IV 1548[c]	2.2923
							C IV 1550[c]	2.2868
42	5106.09	0.58	0.39	0.06	9.58	6.2	C IV 1550[c]	2.2926
43	5138.11	0.28	0.80	0.06	6.84	12.7	C IV 1548	2.3188
44	5146.88	0.43	0.61	0.07	6.66	8.2	C IV 1550	2.3189
45	5432.24	0.88	0.30	0.07	4.95	4.1	C IV 1548[c]	2.5087
46	5503.15	1.88	0.76	0.19	13.20	3.9	C IV 1548[c]	2.5545
49	5597.95[be]	1.26	1.06	0.18	12.79	5.8	Si II 1808[c]	2.0962
54	5945.75	0.46	2.63	0.16	10.91	14.9	Fe II 2344	1.5363
55	6024.18	1.14	1.08	0.16	8.94	6.4	Fe II 2374	1.5371
56	6043.16	0.40	2.96	0.16	3.16	17.0	Fe II 2382	1.5362
58	6561.35	0.56	1.93	0.14	3.55	12.6	Fe II 2586	1.5366
59	6594.05	0.31	3.33	0.14	14.76	22.0	Fe II 2600	1.5360
61	7092.54	0.21	5.59	0.15	10.91	28.9	Mg II 2796	1.5364
62	7110.38	0.26	4.48	0.16	11.16	24.3	Mg II 2803	1.5362
63	7257.32	1.49	0.93	0.18	3.72	4.9	Fe II 2344	2.0958
64	7353.26	1.78	0.82	0.19	3.36	4.1	Fe II 2374	2.0968
65	7378.26	1.95	0.80	0.21	20.01	3.8	Fe II 2382	2.0965
67	7542.38	2.17	0.70	0.20	13.83	3.4	Fe II 2382	2.1654
67	7542.38	2.17	0.70	0.20	13.83	3.4	Fe II 2344	2.2174
67	7542.38	2.17	0.70	0.20	13.83	3.4	Mg II 2796	1.6972
71	8005.95	1.47	1.33	0.26	12.82	5.0	Fe II 2586	2.0951
72	8041.83	1.11	1.73	0.25	17.95	6.5	Fe II 2600	2.0928
FBQS1045+3440 ($z = 2.353$)								
1	3975.31[a]	0.09	3.07	0.07	6.71	34.8		
2	4017.52[a]	0.34	0.69	0.06	1.88	10.9		
3	4033.45[a]	0.08	2.28	0.05	6.69	38.9	N V 1238[c]	2.2559
4	4041.50[a]	0.12	1.54	0.05	5.78	28.0	N V 1242[c]	2.2519
5	4053.14[a]	0.08	1.93	0.04	18.28	37.5		
6	4056.68[a]	0.07	2.09	0.04	6.05	43.3	Ly-a 1216	2.3370
7	4062.07[a]	0.07	1.95	0.04	10.01	45.5	Ly-a 1216	2.3414
8	4070.87[a]	0.07	1.95	0.03	7.76	51.3	Ly-a 1216	2.3432
							Ly-a 1216	2.3496

Table 4—Continued

N	λ	σ_λ	W_{obs}	σ_W	fwhm	SL	ID	z
9	4105.83	0.06	2.87	0.04	7.35	53.8	Si IV 1393	1.9459
10	4129.12	0.11	1.72	0.05	5.61	28.3		
11	4133.69	0.06	2.96	0.05	7.69	47.5	Si IV 1402	1.9468
							N V 1238	2.3375
							N V 1242	2.3325
12	4143.20	0.07	2.50	0.05	7.86	43.0		
13	4148.04	0.06	2.70	0.04	6.12	46.2	N V 1238	2.3496
							N V 1242	2.3375
							N V 1238	2.3432
							N V 1242	2.3325
							Si II 1526[c]	1.7170
14	4161.13	0.19	0.96	0.05	7.78	18.8	N V 1242	2.3496
							N V 1242	2.3432
							Si II 1526[c]	1.7256
15	4204.38	0.04	4.43	0.04	18.36	45.3	C IV 1548	1.7157
							Fe II 2586[c]	0.6254
16	4207.57	0.05	3.56	0.04	5.97	34.4	C IV 1550	1.7132
17	4211.74	0.04	4.62	0.05	18.31	49.5		
18	4221.98	0.07	2.92	0.06	8.32	41.1	C IV 1548	1.7270
19	4228.79	0.12	1.92	0.06	7.04	27.3	C IV 1550	1.7269
							Fe II 2600[c]	0.6263
21	4285.65	0.27	0.94	0.07	6.79	13.2	Si IV 1393	2.0749
22	4313.61	0.52	0.51	0.07	6.43	7.0	Si IV 1402	2.0751
23	4367.48	0.73	0.36	0.07	6.59	5.1	Fe II 1608[c]	1.7153
25	4487.44	0.60	0.43	0.07	6.80	6.1		
26	4497.50	0.10	2.54	0.07	6.83	31.2		
27	4502.16	0.79	0.33	0.07	6.54	4.4	Si II 1526	1.9489
28	4534.08	0.12	2.06	0.06	6.53	25.6		
29	4539.10	0.09	2.58	0.06	7.98	31.7	Si IV 1393[c]	2.2567
							Mg II 2796[c]	0.6232
							Al II 1670 [c]	1.7167
30	4551.09	0.17	1.48	0.07	7.64	20.0	Mg II 2803[c]	0.6233
31	4560.43	0.05	4.58	0.06	7.21	50.4	C IV 1548	1.9456
							Al II 1670[c]	1.7295
32	4568.03	0.07	3.10	0.06	7.71	39.1	C IV 1550	1.9456
							Si IV 1402[c]	2.2564
34	4684.07	0.56	0.39	0.06	10.37	6.7		
35	4694.69	0.66	0.33	0.06	10.59	5.7		
36	4737.58	0.44	0.57	0.07	8.02	8.3	Fe II 1608	1.9454
37	4760.65	0.08	2.89	0.06	7.57	38.7	C IV 1548	2.0750
38	4768.36	0.12	1.89	0.06	7.38	26.2	C IV 1550	2.0748
39	4922.17	0.07	3.09	0.06	6.71	40.3	Al II 1670	1.9460

Table 4—Continued

N	λ	σ_λ	W_{obs}	σ_W	fwhm	SL	ID	z
40	5035.59	0.10	2.23	0.06	6.84	33.5	C IV 1548	2.2525
							Al III 1854[c]	1.7150
41	5043.26	0.17	1.39	0.06	6.32	20.1	C IV 1550	2.2521
42	5056.98	0.27	0.86	0.06	10.06	13.5	Al III 1854[c]	1.7265
							Al III 1862[c]	1.7147
44	5159.42	0.21	0.86	0.05	4.84	16.6	C IV 1548	2.3325
45	5167.08	0.11	1.47	0.04	6.40	31.5	C IV 1548	2.3375
							C IV 1550	2.3325
46	5176.02	0.14	1.11	0.04	6.12	25.5	C IV 1548	2.3432
							C IV 1550	2.3377
47	5185.81	0.25	0.61	0.04	5.45	14.5	C IV 1548	2.3496
							C IV 1550	2.3440
48	5192.74	0.48	0.31	0.04	4.90	7.7	C IV 1550	2.3485
50	5260.25	0.39	0.57	0.06	1.78	9.3	Mg II 2796[c]	0.8811
51	5273.97	0.84	0.28	0.06	7.31	4.5	Mg II 2803[c]	0.8812
52	5462.67	0.42	1.06	0.12	7.10	8.3	Al III 1854	1.9453
53	5486.07	0.82	0.48	0.10	3.87	4.5	Al III 1862	1.9451
54	5520.77	0.63	0.69	0.11	7.23	5.7		
57	6368.41	0.43	2.32	0.13	16.81	16.3	Fe II 2344	1.7167
58	6386.08	0.94	1.01	0.13	15.24	7.7	Fe II 2344[c]	1.7242
59	6448.60	1.20	0.86	0.14	14.53	6.1	Fe II 2374	1.7158
60	6471.13	0.27	4.07	0.15	13.65	23.8	Fe II 2382	1.7158
61	6490.56	0.63	1.79	0.15	12.44	11.3		
62	6506.72	1.68	0.71	0.16	10.33	4.4	Fe II 2382[c]	1.7307
65	6904.43	0.70	1.99	0.19	3.72	10.0	Fe II 2344	1.9453
66	6994.23	1.87	0.71	0.17	4.31	3.9	Fe II 2374	1.9456
67	7021.14	0.27	4.76	0.17	14.46	23.7	Fe II 2382	1.9466
67	7021.14	0.27	4.76	0.17	14.46	23.7	Fe II 2586	1.7144
68	7060.41	0.36	3.69	0.17	14.42	18.8	Fe II 2600	1.7154
69	7085.30	0.86	1.56	0.18	17.10	8.4	Fe II 2600[c]	1.7249
73	7591.95	0.30	7.73	0.30	13.24	15.2		
74	7600.45	0.58	6.10	0.47	14.70	7.8	Mg II 2796	1.7180
75	7611.11	0.53	7.84	0.55	20.61	9.1		
76	7625.02	0.71	4.17	0.39	17.26	8.6	Fe II 2586	1.9478
							Mg II 2803	1.7198
77	7638.61	1.27	2.29	0.39	18.62	5.4	Mg II 2796[c]	1.7316
78	7661.36	0.98	2.19	0.28	8.42	7.1	Fe II 2600	1.9465
							Mg II 2803[c]	1.7328
79	7732.49	2.41	0.75	0.24	11.21	3.1	Mg I 2852	1.7103
80	7767.98	0.99	1.84	0.24	12.49	7.2	Mg I 2852[c]	1.7228

FBQS1253+2905 ($z = 2.565$)

Table 4—Continued

N	λ	σ_λ	W_{obs}	σ_W	fwhm	SL	ID	z
1	3972.65[a]	0.46	1.01	0.12	1.70	7.7		
3	3991.48[a]	0.38	1.01	0.10	6.02	9.2		
4	3997.62[a]	0.17	2.11	0.09	6.25	18.9		
5	4004.32[a]	0.20	1.77	0.09	6.90	16.1		
6	4012.04[a]	0.33	1.18	0.10	4.24	10.5		
8	4062.06[a]	0.57	0.57	0.09	5.88	6.3		
9	4067.07[a]	0.42	0.78	0.09	7.98	8.5		
10	4076.38[a]	0.28	1.13	0.08	7.52	12.5		
11	4085.19[a]	0.17	1.81	0.08	8.00	19.5		
12	4093.56[a]	0.07	3.82	0.07	7.71	38.9		
13	4101.80[a]	0.10	2.97	0.07	7.99	31.7		
14	4114.73[a]	0.25	1.26	0.08	6.53	14.2		
15	4133.11[a]	0.63	0.53	0.09	10.78	5.9		
16	4149.12[a]	0.22	1.40	0.08	2.38	16.0		
17	4178.03[a]	0.18	1.57	0.08	7.40	18.9		
18	4204.99[a]	0.23	1.23	0.07	3.98	15.4		
19	4214.10[a]	0.19	1.57	0.08	1.56	18.0		
21	4247.53[a]	0.66	0.38	0.07	5.79	5.6		
22	4258.39[a]	0.16	1.43	0.06	1.66	22.0		
23	4272.49[a]	0.04	3.85	0.05	7.33	59.3	Si IV 1393[c]	2.0655
24	4279.47[a]	0.05	3.32	0.05	7.37	54.4		
25	4289.66[a]	0.07	2.62	0.04	8.68	48.2		
26	4298.51[a]	0.07	2.13	0.04	8.93	42.2	Si IV 1402[c]	2.0643
27	4305.42[a]	0.03	4.31	0.03	7.33	85.9	Ly-a 1216	2.5416
28	4313.25[a]	0.04	3.48	0.03	7.44	77.0		
29	4317.31[a]	0.29	0.46	0.04	5.09	10.8	Ly-a 1216	2.5514
30	4332.21[a]	0.16	0.80	0.03	6.68	22.1	Si IV 1393	2.1083
31	4342.07[a]	0.42	0.31	0.03	5.60	8.7		
32	4361.12	1.14	0.15	0.05	1.59	3.3	Si IV 1402	2.1089
33	4387.66	0.10	1.59	0.04	7.57	33.3	N V 1238	2.5418
34	4396.71	0.03	4.00	0.03	7.72	80.4	N V 1238	2.5491
35	4403.44	0.15	1.05	0.04	7.11	22.3	N V 1242	2.5431
36	4409.77	0.05	2.94	0.04	6.40	61.8	N V 1242	2.5482
38	4509.51	0.27	0.89	0.06	6.25	13.5	C IV 1548	1.9127
39	4517.50	0.52	0.47	0.06	6.41	7.1	C IV 1550	1.9131
40	4679.93	0.43	0.62	0.07	6.31	8.5	Si II 1526	2.0654
41	4745.93	0.08	3.05	0.06	6.55	37.3	C IV 1548	2.0654
42	4753.70	0.11	2.50	0.07	6.75	28.9	C IV 1550	2.0654
43	4812.30	0.13	1.98	0.07	6.44	25.9	C IV 1548	2.1083
44	4820.30	0.18	1.43	0.07	6.98	18.8	C IV 1550	2.1083
45	4980.88[b]	0.66	0.33	0.06	8.40	5.6	Mg II 2796[c]	0.7812

Table 4—Continued

N	λ	σ_λ	W_{obs}	σ_W	fwhm	SL	ID	z
46	4987.98[b]	0.61	0.36	0.06	8.36	6.1		
47	4996.35[b]	0.72	0.32	0.06	9.20	5.2	C IV 1550[c]	2.2218
49	5122.07	0.40	0.66	0.07	6.73	9.2	Al II 1670	2.0657
51	5223.80	0.67	0.44	0.08	7.16	5.5		
52	5481.88	0.40	0.99	0.10	7.25	8.8	C IV 1548	2.5408
53	5488.23	0.65	0.59	0.10	6.34	5.2		
54	5493.97	0.09	3.84	0.09	7.63	31.7	C IV 1548	2.5486
							C IV 1550	2.5427
55	5502.21	0.12	2.81	0.09	8.23	24.6	C IV 1550	2.5480
56	5507.48	0.34	1.05	0.09	7.50	9.7		
57	5525.77	0.94	0.39	0.10	6.15	3.9	Fe II 2382	1.3191
58	5556.71	1.24	0.88	0.16	14.11	5.4		
66	6483.59	0.61	1.87	0.16	11.82	10.7	Mg II 2796	1.3186
67	6500.23	1.29	0.91	0.17	8.74	5.2	Mg II 2803	1.3186
70	7303.16	1.69	0.89	0.22	9.52	4.0	Fe II 2382	2.0650
				FBQS1348+2840 ($z = 2.466$)				
1	3967.70[a]	0.53	0.59	0.09	1.51	6.2		
2	3987.21[a]	0.35	0.85	0.09	1.63	9.2		
3	3999.81[a]	0.45	0.64	0.09	3.83	7.3		
4	4013.33[a]	0.20	1.37	0.08	6.04	15.0		
5	4019.45[a]	0.29	0.95	0.08	7.13	10.7		
6	4059.79[a]	0.08	2.76	0.07	6.19	33.1		
7	4065.77[a]	0.36	0.70	0.07	10.55	8.7		
8	4078.40[a]	0.08	2.69	0.06	7.04	33.2		
9	4085.72[a]	0.06	3.24	0.06	7.11	41.1		
10	4109.71[a]	0.11	1.76	0.06	9.04	27.2		
11	4117.44[a]	0.04	4.21	0.05	8.20	60.8		
12	4128.62[a]	0.05	3.42	0.05	22.45	54.0		
13	4149.92[a]	0.06	2.64	0.05	6.50	48.2		
14	4166.87[a]	0.07	1.96	0.04	5.34	40.2		
15	4177.14[a]	0.05	2.57	0.04	6.62	58.5		
16	4185.51[a]	0.03	3.44	0.03	6.42	86.2		
17	4198.90[a]	0.05	2.01	0.03	5.91	64.0		
18	4214.71[a]	0.04	1.72	0.02	6.05	69.2		
20	4280.04	0.81	0.16	0.04	8.61	4.1	Fe II 1608[c]	1.6610
26	4721.82	0.43	0.53	0.07	6.43	7.7		
27	4809.81	0.53	0.36	0.06	6.14	6.3	Si II 1808[c]	1.6603
							Fe II 2382[c]	1.0186
31	4935.41	0.60	0.34	0.06	6.72	5.5	Al III 1854[c]	1.6610
32	4955.85	0.81	0.25	0.06	6.93	4.1	Al III 1862[c]	1.6604

Table 4—Continued

N	λ	σ_λ	W_{obs}	σ_W	fwhm	SL	ID	z
37	5598.53	0.93	1.58	0.21	13.63	7.0		
38	5642.72[be]	1.21	1.12	0.20	12.97	5.5	Mg II 2796[c]	1.0179
39	5657.39[b]	1.78	0.75	0.19	8.69	3.8	Mg II 2803[c]	1.0180
45	6277.62	1.25	0.97	0.17	15.65	5.4		
55	8037.96	1.30	1.64	0.31	3.48	5.0		
				FBQS1416+2649 ($z = 2.303$)				
1	3984.08[a]	0.16	1.47	0.07	5.77	19.6		
2	3991.78[a]	0.13	1.59	0.06	6.76	23.3		
3	4004.15[a]	0.06	2.74	0.05	6.58	44.1	Ly-a 1216	2.2938
4	4080.54	0.24	1.30	0.09	7.02	13.0	N V 1238	2.2939
5	4093.30	0.40	0.76	0.09	6.69	8.1	N V 1242	2.2936
6	4118.09	0.32	0.96	0.09	7.21	10.0	Si II 1526	1.6974
7	4172.43	0.60	0.56	0.10	7.96	5.4		
8	4178.83	0.33	1.01	0.10	6.45	9.7	C IV 1548	1.6991
9	4186.25	0.64	0.52	0.10	6.42	5.1	C IV 1550	1.6995
10	4205.09	0.74	0.46	0.10	8.23	4.5	Si IV 1393	2.0171
11	4231.06	0.91	0.37	0.10	10.35	3.7	Si IV 1402	2.0162
13	4393.41	0.47	0.67	0.09	8.08	6.9	C II 1334[c]	2.2921
14	4506.90	0.48	0.78	0.11	5.51	6.7	Al II 1670	1.6975
15	4590.01	0.80	0.46	0.11	5.81	4.2	Si IV 1393	2.2933
16	4669.71	0.38	0.97	0.11	7.61	8.4	C IV 1548	2.0162
17	4677.87	0.63	0.58	0.11	8.54	5.2	C IV 1550	2.0165
19	4961.12	0.18	1.55	0.08	6.00	17.4	C IV 1548	2.2044
20	4969.06	0.30	0.94	0.08	6.50	10.6	C IV 1550	2.2042
21	5005.07	0.42	0.69	0.09	5.69	7.8	C IV 1548	2.2328
22	5014.15	0.72	0.40	0.08	5.51	4.6	C IV 1550	2.2333
23	5099.23	0.11	2.46	0.08	7.23	25.5	C IV 1548	2.2936
24	5107.24	0.13	2.04	0.08	8.08	23.0	C IV 1550	2.2934
30	5598.43[be]	0.95	2.11	0.29	14.32	6.8		
31	5615.11[b]	1.29	1.46	0.27	15.05	5.1		
36	6182.18	1.15	1.16	0.19	17.35	5.8		
39	6282.01	0.89	1.32	0.17	19.19	7.4		
41	6324.49	0.78	1.51	0.17	11.02	8.4	Fe II 2344	1.6979
42	6335.41	0.99	1.20	0.17	10.96	6.7		
43	6428.17	0.48	2.71	0.19	10.44	13.1	Fe II 2382	1.6978
48	7016.12	0.49	2.59	0.18	12.53	13.0	Fe II 2600	1.6983
49	7190.93	1.34	1.00	0.19	14.41	5.0	Fe II 2382[c]	2.0179
50	7259.49	0.97	1.46	0.20	15.44	6.8		
52	7381.66	0.81	1.74	0.20	3.57	8.1		
53	7416.01	1.04	1.33	0.20	13.83	6.4		

Table 4—Continued

N	λ	σ_λ	W_{obs}	σ_W	fwhm	SL	ID	z
56	7543.06	0.35	3.98	0.20	14.11	16.4	Mg II 2796[c]	1.6975
57	7560.95	0.50	2.82	0.20	12.59	12.4	Mg II 2803[c]	1.6969
63	8074.17	1.32	1.30	0.25	14.17	5.0		
				FBQS1457+2707 ($z = 2.531$)				
1	3978.73[a]	0.35	0.85	0.09	6.26	9.0		
2	3986.23[a]	0.28	1.10	0.09	5.92	11.5		
3	4006.15[a]	0.18	1.76	0.09	5.65	16.5		
4	4019.22[a]	0.35	0.93	0.10	1.75	9.1		
7	4091.95[a]	0.55	0.58	0.09	4.03	5.8		
8	4098.17[a]	0.10	2.82	0.08	7.37	27.5		
9	4110.79[a]	0.11	2.38	0.08	6.27	25.1		
10	4115.89[a]	0.62	0.46	0.08	10.84	5.1		
11	4132.80[a]	0.37	0.72	0.08	2.45	8.7		
12	4163.86[a]	0.16	1.43	0.07	6.08	19.3		
13	4176.57[a]	0.10	2.00	0.06	6.14	30.0		
14	4184.38[a]	0.12	1.53	0.06	7.97	24.6		
15	4194.89[a]	0.20	0.91	0.05	6.42	16.0		
16	4219.11[a]	0.26	0.62	0.05	9.23	12.6		
17	4225.65[a]	0.27	0.58	0.05	7.18	12.0		
18	4229.65[a]	0.23	0.65	0.04	5.57	13.7		
19	4241.74[a]	0.10	1.24	0.04	6.79	31.9		
20	4249.80[a]	0.11	0.98	0.03	7.28	28.6		
21	4258.99[a]	0.09	1.11	0.03	8.42	36.4		
22	4269.26[a]	0.09	0.95	0.03	9.31	35.3		
23	4276.29[a]	0.27	0.30	0.02	5.63	12.3		
24	4285.86[a]	0.25	0.31	0.02	1.60	13.6		
25	4295.92[a]	0.31	0.25	0.02	1.51	10.9		
26	4305.36	0.19	0.42	0.02	5.16	17.2		
27	4327.34	0.35	0.30	0.03	1.57	9.6	Si II 1526	1.8344
28	4388.56	0.09	1.45	0.04	6.72	32.8	C IV 1548	1.8346
29	4396.32	0.15	0.89	0.04	6.04	21.9	C IV 1550	1.8349
32	4654.96	0.22	1.00	0.07	6.56	14.1	Fe II 2344	0.9857
33	4660.97	0.29	0.81	0.07	6.53	11.1	Fe II 2344	0.9883
34	4732.52	0.14	1.58	0.07	7.28	20.9	Fe II 2382	0.9861
35	4737.63	0.18	1.28	0.07	5.62	17.0	Fe II 2382	0.9883
							Al II 1670[c]	1.8356
36	5122.11	0.71	0.34	0.07	9.63	4.7	Si II 1808[c]	1.8330
37	5135.59	0.24	0.99	0.07	7.39	13.3	Fe II 2586	0.9854
38	5144.26	0.57	0.43	0.07	7.92	5.8	Fe II 2586	0.9888
39	5162.95	0.17	1.38	0.07	6.40	17.8	Fe II 2600	0.9856

Table 4—Continued

N	λ	σ_λ	W_{obs}	σ_W	fwhm	SL	ID	z
40	5169.68	0.25	0.97	0.07	7.54	12.7	Fe II 2600	0.9882
41	5256.66	0.53	0.52	0.08	5.57	6.2	Al III 1854[c]	1.8342
43	5555.50	0.37	3.41	0.18	14.12	16.3	Mg II 2796	0.9867
44	5566.28	1.27	1.15	0.21	15.76	5.1	Mg II 2803	0.9855
							Mg II 2796	0.9906
45	6271.63	1.01	1.42	0.21	16.46	6.5		
49	6396.09	1.30	1.07	0.20	11.45	5.1		
51	6643.47	1.76	0.68	0.17	4.46	3.8	Fe II 2344	1.8340
52	6753.01	1.63	0.56	0.13	11.76	4.2	Fe II 2382	1.8341
53	6841.99	1.19	1.08	0.19	13.23	5.6		
59	7173.63	1.18	1.28	0.22	13.58	5.6		
60	7186.89	0.63	2.69	0.25	14.02	9.9	Mg II 2796[c]	1.5701
61	7201.30	0.86	1.92	0.24	16.23	7.5	Mg II 2803[c]	1.5687
63	7254.19	0.67	2.55	0.25	14.54	9.5		
64	7290.49	1.04	1.68	0.25	18.02	6.3		
65	7325.48	2.00	0.91	0.26	4.45	3.3	Mg I 2852[c]	1.5677
67	7498.59	1.06	1.50	0.23	22.56	6.2		
68	7535.80	1.21	1.39	0.24	9.17	5.4		
71	7598.04	1.26	2.11	0.38	10.94	5.1		
76	7926.22	0.78	2.82	0.32	16.32	8.1	Mg II 2796	1.8345
77	7943.29	1.28	1.54	0.28	21.29	5.2	Mg II 2803	1.8333
82	8165.55	1.23	1.82	0.32	18.11	5.3		
				FBQS1537+2716 ($z = 2.445$)				
2	3977.07[a]	0.24	0.92	0.07	5.70	12.6		
3	3996.12[a]	0.10	2.00	0.06	7.31	25.1		
4	4000.74[a]	0.06	3.22	0.06	6.04	36.6		
5	4005.72[a]	0.07	2.66	0.06	7.47	32.0		
6	4018.73[a]	0.26	0.85	0.07	13.63	11.3		
7	4025.50[a]	0.08	2.51	0.06	6.94	31.0		
8	4031.42[a]	0.06	3.11	0.06	7.17	37.6		
9	4037.88[a]	0.08	2.57	0.06	7.71	32.5		
10	4046.56[a]	0.11	2.01	0.07	7.95	24.4		
11	4053.08[a]	0.19	1.16	0.07	7.92	15.1		
12	4061.10[a]	0.33	0.68	0.07	9.61	9.4		
13	4071.07[a]	0.23	0.96	0.07	8.42	13.1		
14	4099.25[a]	0.08	2.23	0.06	6.45	29.4		
15	4104.26[a]	0.05	3.56	0.05	6.53	44.9		
16	4111.34[a]	0.09	2.20	0.06	7.65	30.6		
17	4117.70[a]	0.19	1.02	0.06	7.62	14.8		
18	4121.98[a]	0.20	1.01	0.06	4.76	14.8		

Table 4—Continued

N	λ	σ_λ	W_{obs}	σ_W	fwhm	SL	ID	z
19	4134.62[a]	0.32	0.65	0.06	7.56	9.7		
20	4150.95[a]	0.07	2.62	0.05	6.20	38.6		
21	4162.95[a]	0.20	0.96	0.06	6.62	15.1		
22	4168.57[a]	0.23	0.84	0.06	6.51	13.3		
23	4178.95[a]	0.43	0.44	0.06	4.28	7.3		
24	4194.14[a]	0.07	2.34	0.05	8.47	39.8		
25	4200.32[a]	0.25	0.66	0.05	26.33	11.8		
26	4210.58[a]	0.24	0.72	0.05	16.34	12.6		
28	4257.50[a]	0.60	0.27	0.05	7.72	5.3		
29	4263.65[a]	0.61	0.27	0.05	6.33	5.2		
32	5199.76	0.27	0.73	0.06	1.63	11.1	Mg II 2796	0.8595
33	5212.88	0.51	0.66	0.10	6.88	6.0	Mg II 2803	0.8594
37	5729.94	1.20	1.35	0.24	37.73	5.3		
38	5748.31	1.29	1.25	0.24	38.77	5.0		
40	6276.57	1.15	1.24	0.21	19.31	5.6		
44	6512.88	0.91	1.34	0.18	17.74	7.1	Fe II 2382[c]	1.7333
51	7502.92	1.26	1.61	0.30	18.08	5.0		
53	7645.47	1.62	2.02	0.49	12.62	3.9	Mg II 2796[c]	1.7341
54	7673.41	1.20	2.02	0.36	20.77	5.2	Mg II 2803[c]	1.7371
55	8039.45	1.11	2.74	0.45	3.26	5.4		
				FBQS1540+4138 ($z = 2.512$)				
1	3986.62[a]	0.04	5.22	0.06	7.25	69.1	Ly-a 1216	2.2794
2	3992.87[a]	0.06	3.63	0.06	6.93	47.7		
3	3999.42[a]	0.27	0.96	0.07	7.81	12.5	Si II 1260	2.1731
4	4007.86[a]	0.31	0.89	0.08	7.22	11.5		
5	4015.99[a]	0.61	0.46	0.08	4.70	5.8		
6	4037.88[a]	0.18	1.47	0.07	2.30	17.8	C II 1334	2.0257
8	4066.33[a]	0.14	1.99	0.08	6.24	22.1		
9	4073.53[a]	0.20	1.33	0.07	6.83	16.0		
10	4091.06[a]	0.11	2.24	0.07	5.10	30.1		
11	4101.47[a]	0.19	1.27	0.07	6.00	17.8		
12	4114.33[a]	0.07	2.93	0.06	6.59	42.2		
13	4122.92[a]	0.06	3.59	0.06	6.29	53.1	OI 1302	2.1662
14	4128.59[a]	0.13	1.66	0.06	9.91	25.0	Si II 1304	2.1652
15	4145.80[a]	0.22	0.96	0.06	2.17	15.4		
16	4160.63[a]	0.32	0.77	0.07	3.60	10.9		
17	4175.67[a]	0.55	0.35	0.05	3.58	6.4		
18	4181.98[a]	0.26	0.72	0.05	3.89	13.5		
19	4197.35[a]	0.17	0.97	0.05	7.24	19.8		
20	4218.45[a]	0.08	1.83	0.04	7.05	43.2	Si IV 1393	2.0267

Table 4—Continued

N	λ	σ_λ	W_{obs}	σ_W	fwhm	SL	ID	z
21	4228.05[a]	0.03	3.63	0.03	7.60	94.8	C II 1334	2.1682
22	4239.11[a]	0.09	1.14	0.03	6.16	34.4		
23	4245.65[a]	0.05	1.70	0.03	7.08	56.1	Si IV 1402	2.0266
24	4251.90[a]	0.12	0.71	0.02	8.21	25.8		
25	4257.56[a]	0.17	0.51	0.02	9.56	20.0		
27	4383.78	0.47	0.31	0.04	6.62	7.5	Fe II 2344	0.8700
29	4415.35	0.21	0.80	0.05	6.25	16.5	Si IV 1393	2.1680
30	4443.04	0.38	0.46	0.05	7.00	9.3	Si IV 1402	2.1673
							Fe II 2374	0.8712
31	4455.74	0.30	0.59	0.05	6.05	11.7	Fe II 2382	0.8700
32	4523.64	0.24	0.85	0.06	6.11	13.2	C IV 1548	1.9219
33	4531.46	0.35	0.59	0.06	4.72	9.7	C IV 1550	1.9221
34	4576.26	0.58	0.33	0.05	2.43	6.1		
35	4619.64	0.25	0.80	0.06	6.10	14.2	Si II 1526	2.0259
36	4685.56	0.18	1.27	0.06	6.42	19.7	C IV 1548	2.0265
37	4694.12	0.18	1.08	0.06	6.51	18.0	C IV 1550	2.0270
38	4836.48	0.14	1.79	0.07	7.03	26.7	Si II 1526	2.1679
							Fe II 2586	0.8698
39	4862.26	0.30	0.74	0.06	7.62	12.8	Fe II 2600	0.8700
41	4903.85	0.10	1.52	0.04	6.96	33.0	C IV 1548	2.1675
42	4911.99	0.14	1.08	0.04	7.50	23.9	C IV 1550	2.1674
43	4919.28	0.64	0.25	0.04	9.61	5.6		
44	4999.30	0.62	0.31	0.05	6.04	5.7	C IV 1548	2.2291
45	5007.17	1.14	0.17	0.05	6.56	3.1	C IV 1550	2.2288
46	5055.34	0.19	0.99	0.05	6.73	18.1	Al II 1670	2.0257
47	5076.73	0.31	0.62	0.05	7.17	11.2	C IV 1548	2.2791
48	5083.76	0.54	0.37	0.06	7.42	6.7	C IV 1550	2.2782
49	5094.39	0.33	0.59	0.05	7.82	10.7	Fe II 1608	2.1673
50	5228.35	0.14	1.53	0.06	1.56	24.7	Mg II 2796	0.8697
51	5241.09	0.14	1.52	0.06	5.95	24.4	Mg II 2803	0.8695
52	5292.33	0.13	1.69	0.06	7.10	25.1	Al II 1670	2.1676
53	5332.16	0.78	0.38	0.08	9.46	4.6	Mg I 2852	0.8690
55	5501.80[b]	1.27	1.02	0.18	19.73	5.6		
60	6318.34[b]	1.27	0.95	0.17	8.30	5.5		
61	6338.23[b]	1.18	1.01	0.17	13.95	6.0		
66	6873.66[b]	1.42	0.99	0.20	12.89	5.6		
68	7206.69	0.64	2.10	0.19	16.46	11.2	Fe II 2382	2.0245
70	7424.33[b]	1.27	1.17	0.21	11.33	5.6	Fe II 2344	2.1670
73	7548.03	0.50	3.15	0.22	10.79	13.7	Fe II 2382	2.1678
75	7833.09[b]	1.11	1.60	0.25	13.55	6.1		
78	7894.80[b]	0.93	2.40	0.31	13.74	8.0		
79	7937.45[b]	1.10	2.05	0.32	14.28	6.8		

Table 4—Continued

N	λ	σ_λ	W_{obs}	σ_W	fwhm	SL	ID	z
82	8038.90[b]	1.16	1.74	0.28	8.81	5.8		
83	8064.72[b]	1.14	1.82	0.29	19.08	6.4		
				FBQS1625+2646 ($z = 2.507$)				
1	3970.69[a]	0.19	1.27	0.07	2.01	18.0		
2	3993.43[a]	0.05	4.40	0.05	13.80	57.3		
3	4006.58[a]	0.15	1.59	0.07	6.84	21.7		
4	4025.38[a]	0.28	0.92	0.07	1.77	12.3		
5	4033.82[a]	0.40	0.66	0.07	4.81	8.9		
6	4058.62[a]	0.34	0.90	0.08	1.64	10.4		
7	4073.38[a]	0.12	2.07	0.07	5.64	27.7		
8	4083.31[a]	0.28	0.89	0.07	8.62	12.3		
9	4099.49[a]	0.20	1.17	0.06	7.83	17.2		
10	4106.39[a]	0.29	0.79	0.06	7.42	11.9		
11	4133.34[a]	0.06	3.36	0.05	5.35	50.5	Ly-a 1216[c]	2.4001
12	4144.83[a]	0.10	2.08	0.06	5.50	32.7		
13	4168.88[a]	0.37	0.62	0.06	1.78	9.7		
14	4185.11[a]	0.21	0.86	0.05	4.93	13.3		
15	4188.69[a]	0.04	4.34	0.04	7.22	66.2	Ly-a 1216	2.4456
16	4203.58[a]	0.11	1.71	0.05	7.68	29.6		
17	4212.26[a]	0.09	2.05	0.05	7.38	36.9		
18	4222.76[a]	0.05	3.02	0.04	6.92	58.0		
19	4254.37[a]	0.17	0.84	0.04	6.46	20.2	Si IV 1393	2.0525
20	4268.54[a]	0.50	0.27	0.04	4.69	7.1		
21	4273.07[a]	0.13	0.97	0.03	7.53	26.3		
22	4280.94[a]	0.09	1.32	0.03	8.09	37.0	Si IV 1402	2.0518
23	4289.25[a]	0.07	1.82	0.04	6.03	44.7	Ly-a 1216[c]	2.5283
25	4426.40	0.60	0.32	0.05	6.51	6.0	Fe II 2344	0.8882
26	4458.67	0.32	0.59	0.05	7.46	11.3	C IV 1548	1.8799
27	4465.61	0.39	0.48	0.05	7.12	9.1	C IV 1550	1.8796
28	4498.85	0.32	0.66	0.06	7.27	11.3	Fe II 2382	0.8881
30	4725.14	0.05	3.38	0.05	7.44	53.1	C IV 1548	2.0520
31	4733.12	0.08	2.53	0.05	7.52	40.0	C IV 1550	2.0521
32	4781.30	0.75	0.29	0.06	1.90	4.9	Fe II 2344	1.0396
34	4859.52	0.35	0.57	0.05	5.90	10.2	Fe II 2382	1.0394
35	4894.42	0.37	0.51	0.05	4.88	9.7	Mg II 2796	0.7503
37	4909.84	0.49	0.38	0.05	5.34	7.4	Fe II 2600	0.8883
							Mg II 2803	0.7513
38	5024.32	0.65	0.31	0.05	6.52	5.6	C IV 1548	2.2453
39	5030.81	1.06	0.19	0.06	7.05	3.4	C IV 1550	2.2441
41	5267.18	0.24	0.94	0.06	6.01	14.4	C IV 1548	2.4021

Table 4—Continued

N	λ	σ_λ	W_{obs}	σ_W	fwhm	SL	ID	z
42	5277.53	0.11	2.17	0.06	7.72	30.1	C IV 1550	2.4032
							Fe II 2586	1.0403
							Mg II 2796	0.8873
43	5292.39	0.18	1.21	0.06	6.95	18.6	Mg II 2803	0.8878
44	5303.47	0.40	0.59	0.06	6.27	9.0	Fe II 2600	1.0397
45	5332.14	0.73	0.33	0.07	6.97	4.9	C IV 1548	2.4441
46	5340.49	1.14	0.22	0.07	7.87	3.2	C IV 1550	2.4438
47	5386.23	0.63	0.40	0.07	10.57	5.7	Mg I 2852	0.8879
49	5463.33	0.69	0.54	0.10	6.16	5.2	C IV 1548[c]	2.5288
51	5591.67[b]	0.89	1.24	0.14	13.55	8.4		
54	5701.22	0.57	1.68	0.12	9.46	12.9	Mg II 2796	1.0388
55	5716.05	0.70	1.35	0.12	11.53	10.7	Mg II 2803	1.0389
57	5810.36	2.12	0.45	0.12	50.50	3.6	Mg I 2852	1.0366
58	5969.20	1.47	0.80	0.15	10.74	5.2	Mg II 2796[c]	1.1346
59	5977.66	1.57	0.75	0.15	9.87	4.9	Mg II 2803[c]	1.1322
61	6275.50[b]	1.17	0.79	0.12	17.78	6.5		
65	6711.78	0.72	1.05	0.10	15.86	10.4		
66	6728.49	0.65	1.15	0.10	17.37	11.5		
67	6778.26	1.48	0.60	0.11	15.61	5.2	Mg II 2796[c]	1.4240
68	6793.16	1.46	0.63	0.12	14.13	5.2	Mg II 2803[c]	1.4231
69	6847.34	1.48	0.72	0.14	17.64	5.2	Mg I 2852[c]	1.4001
70	6936.44	0.83	1.47	0.16	16.15	8.9	Mg II 2796[c]	1.4805
71	6953.81	1.14	1.00	0.15	19.11	6.6	Mg II 2803[c]	1.4804
72	6994.25[d]	1.09	1.00	0.14	13.06	6.9		
74	7173.03[d]	0.53	2.00	0.14	17.68	13.8		
75	7189.93[d]	0.50	2.13	0.14	16.09	14.5		
76	7202.77[d]	0.65	1.63	0.14	14.25	11.3		
78	7236.73[d]	1.28	0.92	0.15	14.19	5.9		
79	7253.15[d]	0.76	1.53	0.15	16.69	9.8		
80	7264.43[d]	1.48	0.75	0.14	13.00	5.1		
81	7284.87[d]	1.22	1.00	0.16	17.50	6.2		
83	7502.32[b]	1.17	0.96	0.14	15.05	6.5		
90	7897.62	0.99	1.47	0.19	12.74	7.5		
93	8142.20[d]	1.23	1.32	0.21	22.71	6.1		
94	8160.45[d]	0.67	2.42	0.21	19.03	10.7		
				FBQS1634+3203 ($z = 2.336$)				
1	3982.03[a]	0.09	2.14	0.05	7.40	36.4		
2	3999.30[a]	0.15	1.16	0.05	6.45	23.3		
3	4010.93[a]	0.61	0.29	0.05	6.81	5.9	Fe II 1608[c]	1.4937
4	4025.39[a]	0.13	1.26	0.04	5.50	25.9	O I 1302[c]	2.0913

Table 4—Continued

N	λ	σ_λ	W_{obs}	σ_W	fwhm	SL	ID	z
5	4034.03[a]	0.81	0.20	0.04	3.30	4.5	Si II 1304[c]	2.0927
6	4042.25[a]	0.15	1.00	0.04	6.41	23.3	Si III 1207	2.3504
7	4073.91[a]	0.03	4.69	0.03	7.00	97.5	Ly-a 1216	2.3512
							Ni II 1317	2.0928
9	4126.61	0.12	1.36	0.04	6.76	28.6	C II 1334	2.0922
10	4150.29	0.49	0.40	0.05	6.14	7.3	N V 1238	2.3502
11	4165.10	0.19	0.91	0.05	6.87	18.8	N V 1242	2.3514
							Al II 1670	1.4929
13	4238.83	0.27	0.72	0.05	6.16	13.1	Ni II 1317[c]	2.2181
14	4309.62	0.58	0.40	0.06	7.05	6.2	Si IV 1393	2.0921
15	4337.38	0.98	0.23	0.06	4.31	3.7	Si IV 1402	2.0920
16	4541.59	0.50	0.49	0.07	7.18	7.2	Si IV 1393	2.2585
17	4573.54	0.87	0.28	0.06	1.69	4.2	Si IV 1402	2.2604
19	4623.85	0.28	0.81	0.06	7.08	12.6	Al III 1854	1.4930
20	4644.95	0.47	0.47	0.06	8.41	7.7	Al III 1862	1.4935
21	4669.89	0.17	1.24	0.06	7.58	20.2	Si IV 1393	2.3506
22	4699.35	0.27	0.77	0.06	6.91	13.0	Si IV 1402	2.3500
23	4721.03	0.23	1.11	0.07	4.05	15.2	Si II 1526	2.0923
24	4787.38	0.61	0.39	0.06	2.04	5.9	C IV 1548	2.0922
25	4835.74	0.49	0.49	0.07	7.73	7.3	Mg II 2796	0.7293
26	4849.34	0.63	0.38	0.06	6.83	5.8	Mg II 2803	0.7297
28	4973.62	0.21	1.03	0.06	1.69	16.6	Fe II 1608	2.0922
29	5044.31	0.10	1.94	0.05	7.19	33.1	C IV 1548	2.2582
30	5052.83	0.17	1.14	0.05	7.43	20.1	C IV 1550	2.2583
31	5166.20	0.13	1.20	0.04	6.35	26.6	Al II 1670	2.0921
32	5187.13	0.04	3.20	0.04	6.68	66.5	C IV 1548	2.3504
33	5195.57	0.07	2.60	0.05	7.42	44.9	C IV 1550	2.3503
35	5284.86	1.05	0.24	0.07	1.78	3.4	Ni II 1709	2.0913
38	5599.39[e]	1.21	1.38	0.24	11.64	5.5		
42	5921.00	0.52	2.60	0.20	18.48	12.0	Fe II 2374	1.4936
43	5936.39	0.41	3.35	0.20	17.82	15.0		
44	5948.44	0.77	1.77	0.20	12.89	8.3	Fe II 2382	1.4964
45	5964.75	1.11	1.24	0.20	13.95	6.0		
49	6386.62[b]	0.94	1.00	0.13	14.57	7.2	Mg II 2796[c]	1.2839
50	6406.18[b]	1.62	0.58	0.13	40.70	4.2	Mg II 2803[c]	1.2850
52	6483.58	0.84	1.30	0.16	13.83	7.9	Fe II 2600	1.4935
54	6846.52	1.24	0.95	0.17	18.77	5.5		
55	6875.94	0.95	1.41	0.19	13.91	6.9		
56	6974.60	0.41	2.91	0.17	9.45	14.9	Mg II 2796	1.4942
57	6989.07	0.43	2.79	0.17	11.18	14.6	Mg II 2803	1.4930
59	7254.28	1.37	1.50	0.30	4.14	4.8	Fe II 2344	2.0945
60	7349.46	1.93	0.79	0.22	14.75	3.5	Fe II 2374	2.0952

Table 4—Continued

N	λ	σ_λ	W_{obs}	σ_W	fwhm	SL	ID	z
61	7369.27	1.02	1.53	0.22	16.65	6.5	Fe II 2382	2.0927
62	7672.12	1.75	0.96	0.24	19.75	3.8	Fe I 2484	2.0886
64	7767.43	1.21	1.29	0.23	9.16	5.5		
66	7807.47	1.08	1.48	0.23	33.56	6.1		
67	7833.37	1.06	1.51	0.23	19.43	6.2		
71	8004.01	1.45	1.36	0.28	2.98	4.5	Fe II 2586	2.0944
72	8036.83	0.95	2.08	0.29	13.46	6.8	Fe II 2600	2.0909
				FBQS1645+2244 ($z = 2.723$)				
1	3968.48[a]	0.26	1.06	0.08	1.82	13.3		
2	3983.82[a]	0.08	3.13	0.07	10.21	39.3		
3	4001.15[a]	0.13	2.11	0.07	7.60	26.3		
4	4034.56[a]	0.06	3.98	0.07	11.14	47.9		
5	4051.00[a]	0.51	0.61	0.08	4.45	7.0		
7	4074.47[a]	0.23	1.41	0.09	6.21	16.9		
8	4083.06[a]	0.48	0.66	0.09	5.72	8.0		
9	4100.94[a]	0.09	2.91	0.07	6.68	35.3		
10	4107.14[a]	0.20	1.37	0.07	6.74	16.4		
11	4132.70[a]	0.05	4.44	0.06	6.61	55.4	Ly-a 1216	2.3995
							Si IV 1393[c]	1.9652
12	4143.70[a]	0.10	2.62	0.07	7.53	31.5		
13	4161.17[a]	0.47	0.58	0.07	7.77	7.1	Si IV 1402[c]	1.9664
14	4167.50[a]	0.24	1.13	0.07	7.34	14.5		
15	4183.37[a]	0.16	1.61	0.07	6.39	22.2		
16	4197.74[a]	0.60	0.42	0.07	2.39	6.0		
17	4210.53[a]	0.09	2.44	0.06	21.36	34.9	N V 1238[c]	2.3988
18	4226.34[a]	0.48	0.50	0.07	3.83	7.5	N V 1242[c]	2.4007
19	4240.98[a]	0.12	1.92	0.06	6.87	28.7		
20	4251.56[a]	0.25	0.95	0.06	7.00	14.3		
21	4257.29[a]	0.11	1.95	0.06	7.62	29.5		
22	4267.10[a]	0.19	1.22	0.06	7.94	18.7		
23	4290.38[a]	0.11	1.96	0.06	8.98	29.4		
25	4320.98[a]	0.16	1.33	0.06	6.43	21.9		
26	4329.71[a]	0.34	0.65	0.06	6.64	10.8		
27	4344.67[a]	0.06	3.45	0.06	7.22	54.5	Ly-a 1216	2.5739
28	4352.57[a]	0.16	1.58	0.07	8.12	24.3		
29	4368.78[a]	0.09	2.07	0.05	6.09	34.7		
30	4374.37[a]	0.18	0.99	0.05	4.45	17.5		
31	4390.72[a]	0.72	0.26	0.05	4.88	5.0		
32	4396.75[a]	0.18	0.98	0.05	6.29	19.2		
33	4403.72[a]	0.09	1.77	0.04	8.58	34.6		

Table 4—Continued

N	λ	σ_λ	W_{obs}	σ_W	fwhm	SL	ID	z
34	4411.02[a]	0.04	3.48	0.04	8.01	67.9		
35	4417.03[a]	0.14	1.28	0.05	6.89	25.0		
36	4426.07[a]	0.21	0.89	0.05	9.35	17.4		
37	4432.64[a]	0.29	0.62	0.05	5.55	12.2		
38	4456.29[a]	0.18	0.81	0.04	7.53	19.3		
39	4469.22[a]	0.03	4.38	0.03	7.80	108.5		
40	4477.59[a]	0.03	3.35	0.03	8.95	85.5		
41	4484.75[a]	0.03	3.85	0.03	8.32	101.3		
42	4492.96[a]	0.03	3.77	0.03	8.49	102.9		
43	4503.42[a]	0.07	1.74	0.03	11.03	50.2		
44	4510.15[a]	0.27	0.43	0.03	5.58	12.8		
45	4515.85[a]	0.03	3.33	0.03	6.79	103.1		
46	4535.62	0.07	1.63	0.03	5.24	52.0	C II 1334	2.3987
47	4543.36	0.26	0.45	0.03	6.06	13.6		
49	4590.11	0.14	1.04	0.04	6.79	24.6	C IV 1548	1.9648
50	4598.22	0.24	0.62	0.04	6.50	14.7	C IV 1550	1.9651
52	4737.25	0.14	1.40	0.05	2.44	25.5	Si IV 1393	2.3989
53	4767.98	0.16	1.19	0.05	1.62	21.7	Si IV 1402	2.3990
54	4980.52	0.55	0.35	0.05	6.75	6.6	Si IV 1393	2.5735
55	5012.16	1.23	0.16	0.05	6.08	3.0	Si IV 1402	2.5730
58	5188.92	0.78	0.25	0.05	7.33	4.7	Si II 1526	2.3988
59	5262.59	0.08	2.44	0.06	6.15	39.0	C IV 1548	2.3992
60	5271.42	0.11	1.98	0.06	6.53	30.9	C IV 1550	2.3992
62	5533.02	0.73	0.67	0.13	10.45	4.9	C IV 1548	2.5738
63	5542.28	1.07	0.44	0.13	8.81	3.4	C IV 1550	2.5739
66	6277.27[b]	1.01	1.08	0.16	23.55	6.7		
69	6475.33[b]	1.14	0.87	0.14	16.44	6.1		
71	6690.11[b]	1.27	0.73	0.13	18.26	5.4		
72	6709.24[b]	0.96	0.98	0.14	12.13	7.2		
75	6815.83[b]	1.19	0.82	0.14	14.08	5.7		
76	6845.84[b]	0.79	1.24	0.14	19.66	8.1		
79	6984.39	1.34	0.72	0.14	14.19	5.2		
81	7260.15	1.04	1.19	0.18	42.14	6.4		
85	7381.72	1.19	1.13	0.19	3.06	5.7		
90	7773.15	1.34	1.11	0.21	18.08	5.1		
91	7834.53	1.01	1.57	0.23	4.55	6.5		
92	7898.71	1.34	1.31	0.25	3.09	5.1		
FBQS1651+4002 ($z = 2.339$)								
1	3979.73[a]	0.21	1.18	0.06	6.99	17.4		
2	3992.88[a]	0.72	0.38	0.07	1.77	5.3		
3	4005.93[a]	0.19	1.30	0.06	6.79	18.9		

Table 4—Continued

N	λ	σ_λ	W_{obs}	σ_W	fwhm	SL	ID	z
4	4014.12[a]	0.06	4.27	0.07	7.39	47.1		
5	4028.72[a]	0.12	1.56	0.05	6.36	30.0	Si II 1526[c]	1.6388
6	4043.71[a]	0.18	0.71	0.03	2.62	21.2		
7	4084.21	0.05	2.75	0.03	6.46	67.1	C IV 1548	1.6380
8	4090.81	0.07	2.14	0.04	4.92	49.2	C IV 1550	1.6379
10	4192.08	0.06	3.25	0.05	5.85	51.7	Mg II 2796	0.4991
11	4201.71	0.07	2.89	0.05	5.00	46.4	Mg II 2803	0.4987
12	4276.47	0.29	0.85	0.06	6.55	12.9	Mg I 2852	0.4990
13	4324.67	0.26	0.93	0.06	5.60	14.3		
14	4333.79	0.09	2.42	0.06	6.19	36.7	C IV 1548	1.7992
15	4341.16	0.13	1.67	0.06	7.04	26.3	C IV 1550	1.7994
16	4413.00	0.19	1.29	0.06	8.08	18.8	Si II 1526	1.8905
19	4476.17	0.05	4.27	0.05	7.80	57.7	C IV 1548	1.8912
20	4483.71	0.07	3.19	0.06	7.83	44.1	C IV 1550	1.8913
21	4632.21	0.55	0.45	0.06	6.45	6.9	C IV 1548	1.9920
22	4639.43	1.05	0.23	0.06	5.58	3.6	C IV 1550	1.9917
23	4789.27	0.52	0.53	0.07	7.59	7.3	C I 1657	1.8905
24	4829.97	0.25	1.29	0.08	6.83	14.6	Al II 1670	1.8908
25	4893.64	0.97	0.25	0.06	3.99	3.9	Al III 1854	1.6385
27	4939.50	1.06	0.37	0.10	7.19	3.6	C IV 1548	2.1905
28	4947.50	1.05	0.24	0.06	9.85	3.6	C IV 1550	2.1903
32	5233.88	0.77	0.28	0.06	10.19	5.0		
33	5361.31	0.81	0.41	0.09	7.37	4.7	Al III 1854[c]	1.8906
42	6343.87[b]	1.01	1.15	0.15	17.16	7.6		
46	6876.99	1.54	1.10	0.21	13.45	5.0		
47	6889.91	1.06	1.49	0.20	10.16	7.1	Fe II 2382[c]	1.8916
50	7259.04	0.92	1.85	0.21	17.10	8.3		
51	7298.15	1.32	1.32	0.22	25.18	5.9		
54	7380.80	1.10	1.60	0.22	12.02	6.9	Mg II 2796	1.6394
55	7393.36	1.39	1.29	0.23	7.72	5.5	Mg II 2803	1.6372
57	7513.32	2.38	0.76	0.23	4.08	3.3	Fe II 2600[c]	1.8895
59	7769.93	1.41	1.34	0.24	26.41	5.4		
60	7807.93	1.39	1.40	0.24	8.97	5.5		
61	7832.29	0.93	2.12	0.25	18.17	8.1		
62	7896.85	1.20	1.74	0.26	3.75	6.3		
63	7937.67	1.52	1.43	0.27	14.66	5.1		
67	8083.10	0.44	5.47	0.30	16.52	15.2	Mg II 2796	1.8906
68	8104.98	0.65	3.97	0.32	16.87	10.9	Mg II 2803	1.8910
				FBQS2216-0057 ($z = 2.392$)				
1	3974.58[a]	0.09	2.66	0.07	6.04	29.1		
2	3983.84[a]	0.25	1.10	0.08	5.29	12.4	C IV 1548[c]	1.5732
3	3991.42[a]	0.07	3.42	0.07	6.51	35.4	C IV 1550[c]	1.5738

Table 4—Continued

N	λ	σ_λ	W_{obs}	σ_W	fwhm	SL	ID	z
4	4002.29[a]	0.41	0.66	0.08	1.46	8.0	Fe II 2382[c]	0.6797
5	4014.65[a]	0.24	1.06	0.07	4.32	13.2		
6	4034.28[a]	0.05	4.01	0.06	7.14	49.2		
7	4046.60[a]	0.20	1.13	0.07	10.17	15.6		
8	4053.01[a]	0.07	2.66	0.05	6.90	37.4		
9	4065.66[a]	0.06	2.88	0.05	3.00	41.0		
10	4088.03[a]	0.08	1.62	0.04	7.69	36.2		
11	4094.03[a]	0.02	5.28	0.03	6.28	111.2		
12	4107.89[a]	0.08	1.33	0.03	8.02	38.3		
13	4124.63[a]	0.03	2.79	0.02	6.30	93.1	Ly-a 1216	2.3929
14	4138.79	0.34	0.29	0.03	1.45	9.7	Fe II 1608	1.5732
16	4164.63	0.59	0.23	0.04	7.42	5.7		
17	4298.42	0.17	1.05	0.05	6.56	18.6	Mg II 2796[c]	0.5372
							Al II 1670	1.5727
18	4312.19	0.44	0.51	0.07	7.70	7.5	Mg II 2803[c]	0.5381
19	4344.18	0.84	0.25	0.06	6.32	4.0	Fe II 2586	0.6795
20	4366.61	0.35	0.61	0.06	7.02	9.3	Fe II 2600	0.6794
21	4389.91	0.86	0.25	0.06	5.57	3.9	Mg I 2852 [c]	0.5387
22	4652.00	0.70	0.30	0.06	7.76	4.8	Si II 1808	1.5730
23	4695.48	0.16	1.30	0.06	6.38	19.4	Mg II 2796	0.6791
24	4707.46	0.20	1.08	0.07	6.38	15.4	Mg II 2803	0.6791
25	4771.20	0.70	0.26	0.05	1.62	4.8	Al III 1854	1.5725
27	4790.74	0.28	0.67	0.05	6.65	11.6	Mg I 2852	0.6792
							Al III 1862	1.5718
29	4903.73	0.53	0.38	0.06	5.22	6.3	C IV 1548[c]	2.1674
30	4910.07	0.43	0.46	0.06	6.06	7.7	C IV 1550[c]	2.1662
36	5252.60	0.45	0.29	0.04	5.88	7.4	C IV 1548	2.3927
37	5261.47	0.87	0.15	0.04	1.72	3.9	C IV 1550	2.3928
39	5702.51[b]	1.30	0.96	0.18	18.43	5.0		
40	5899.91	0.86	1.47	0.19	13.88	7.5		
42	6030.73	0.71	1.63	0.17	12.87	8.9	Fe II 2344	1.5726
43	6109.27	0.88	1.22	0.16	14.20	7.3	Fe II 2374	1.5729
44	6128.12	0.47	2.26	0.16	11.85	13.1	Fe II 2382	1.5719
45	6653.76	0.78	1.26	0.15	9.45	8.2	Fe II 2586	1.5723
46	6688.21	0.48	2.03	0.15	2.85	12.9	Fe II 2600	1.5722
48	6987.59	1.09	0.97	0.16	13.13	6.0		
50	7193.29	0.24	4.86	0.17	10.47	22.8	Mg II 2796	1.5724
51	7209.92	0.35	3.40	0.17	4.45	17.3	Mg II 2803	1.5717
				FBQS2233-0838 ($z = 2.339$)				
1	3993.06[a]	0.23	1.33	0.08	6.09	15.0		
2	4007.16[a]	0.10	2.62	0.07	6.61	33.5		
3	4013.17[a]	0.14	1.74	0.07	8.00	23.9		

Table 4—Continued

N	λ	σ_λ	W_{obs}	σ_W	fwhm	SL	ID	z
4	4025.68[a]	0.67	0.34	0.06	3.69	5.4		
5	4038.51[a]	0.08	2.31	0.05	6.80	43.8	Ly-a 1216[c]	2.3220
6	4049.61[a]	0.16	1.11	0.05	7.20	23.9		
7	4059.25[a]	0.08	1.75	0.04	5.43	42.3	Ly-a 1216	2.3391
8	4070.81[a]	0.09	1.56	0.04	3.81	36.6		
9	4097.25	0.07	2.96	0.05	6.67	49.6	C IV 1548	1.6465
10	4103.43	0.09	2.50	0.06	6.18	40.5	C IV 1550	1.6461
							Fe II 2586	0.5864
11	4123.93	0.16	1.31	0.06	6.66	22.2	Fe II 2600	0.5860
12	4137.00	0.30	0.73	0.06	1.76	12.2	N V 1238	2.3395
13	4150.35	0.46	0.49	0.06	2.09	7.8	N V 1242	2.3395
15	4200.00	0.51	0.52	0.07	7.71	7.1	Al II 1670	1.5138
16	4261.68	0.46	0.63	0.08	6.37	7.9	C IV 1548[c]	1.7527
17	4269.16	0.99	0.29	0.08	7.64	3.7	C IV 1550[c]	1.7529
18	4305.34	0.44	0.63	0.08	5.96	7.9	C IV 1548	1.7809
19	4313.29	0.62	0.46	0.08	6.74	5.8	C IV 1550	1.7814
20	4434.96	0.16	1.85	0.08	6.80	22.1	Mg II 2796	0.5860
21	4444.65	0.14	2.04	0.08	7.56	24.8	Mg II 2803	0.5854
22	4524.55	0.59	0.53	0.08	7.47	6.2	Mg I 2852	0.5859
23	4664.23	0.51	0.54	0.07	7.91	7.3		
24	4670.60	0.77	0.34	0.07	8.09	4.7	Al III 1854	1.5182
25	4680.93	0.72	0.36	0.07	7.42	5.1	Al III 1862	1.5129
26	4904.80	1.04	0.27	0.07	8.83	3.5	Al III 1854	1.6445
27	4931.60	1.23	0.22	0.07	7.03	3.0	Al III 1862	1.6474
29	5144.02[b]	0.61	0.32	0.05	7.54	6.0	C IV 1548[c]	2.3226
30	5151.44[b]	0.77	0.25	0.05	16.70	4.8	C IV 1550[c]	2.3218
31	5170.63	0.25	0.67	0.04	5.70	14.5	C IV 1548	2.3398
32	5180.59	0.43	0.41	0.05	1.51	8.6	C IV 1550	2.3406
33	5193.12	0.72	0.28	0.06	1.69	5.0		
38	5781.25[b]	1.97	0.98	0.24	10.75	4.1	Mg II 2796[c]	1.0674
39	5788.57[b]	2.10	0.92	0.24	31.28	3.8	Mg II 2803[c]	1.0647
40	5906.62[b]	1.85	1.11	0.26	19.44	4.2	Mg II 2796[c]	1.1123
41	5927.34[b]	2.51	0.74	0.23	8.47	3.2	Mg II 2803[c]	1.1142
42	5993.36	1.35	1.32	0.22	8.96	5.8	Fe II 2382	1.5153
47	6540.64	2.33	0.68	0.20	3.52	3.4	Fe II 2600	1.5155
48	6844.35	1.48	1.12	0.21	8.64	5.1		
52	7029.31	0.85	1.91	0.20	14.96	8.9	Mg II 2796	1.5137
53	7048.55	0.85	2.02	0.21	14.61	9.4	Mg II 2803	1.5142
54	7173.77	1.89	0.98	0.23	9.64	4.3	Mg I 2852	1.5145
56	7197.97	1.49	1.37	0.26	14.68	5.9		
58	7295.47	1.46	1.54	0.28	15.33	5.3		
68	8164.00	0.94	2.87	0.34	15.25	8.3		

Table 4—Continued

N	λ	σ_λ	W_{obs}	σ_W	fwhm	SL	ID	z

[a]Line in Lyman α forest

[b]Possibly a continuum fitting artifact

[c]Questionable identification

[d]Possibly a telluric residual

[e]Possible night sky artifact

Table 5. Absorption Line Samples.

Sample	Notes
S1	All data from Vanden Berk et al. (2001) and new data presented herein
S2	New data plus Vanden Berk et al. (2001) data with $2.2 \leq z_{em} \leq 2.8$
S3	New data presented herein
C4	Only C IV systems with both lines stronger than 0.15Å greater than 5σ
M2	Only M II systems with both lines stronger than 0.30Å greater than 5σ
L	Systems found in quasars with $\log L_{20} \geq 33.70\,\mathrm{ergs/s/cm^2/Hz}$
Q	Systems found in quasars with $\log L_{20} \leq 32.80\,\mathrm{ergs/s/cm^2/Hz}$
S	Systems found in quasars with $\alpha_6^{20} \leq -0.4$
F	Systems found in quasars with $\alpha_6^{20} > -0.4$

REFERENCES

Anderson, S. F., Weymann, R. J., Foltz, C. B., & Chaffee, F. H., Jr. 1987, AJ, 94, 278

Bahcall, J. N. & Spitzer, L., J. 1969, ApJ, 156, L63

Bahcall, J. N., et al. 1993, ApJS, 87, 1

Barlow, T. A. & Sargent, W. L. W. 1997, AJ, 113, 136

Burbidge, E. M., Lynds, C. R., & Burbidge, G. R. 1966, ApJ, 144, 447

Crotts, A. P. S. 1989, ApJ, 336, 550

Filippenko, A. V. 1982, PASP, 94, 715

Foltz, C. B., Chaffee, F. H., Jr., Weymann, R. J., & Anderson, S. F. 1988, in Proceedings of the QSO Absorption Line Meeting, ed. J. C. Blades, D. A. Turnshek, & C. A. Norman (Cambridge: Cambridge University Press), 53

Foltz, C. B., Weymann, R. J., Peterson, B. M., Sun, L., Malkan, M. A., & Chaffee, F. H., Jr. 1986, ApJ, 307, 504

Gregg, M. D., Becker, R. H., White, R. L., Helfand, D. J., McMahon, R. G., & Hook, I. M. 1996, AJ, 112, 407

Hamann, F., Barlow, T., Cohen, R. D., Junkkarinen, V., & Burbidge, E. M. 1997, in ASP Conf. Ser. 128: Mass Ejection from Active Galactic Nuclei, ed. N. Arav, I. Shlosman, & R. J. Weymann (San Francisco: ASP), 19

Horne, K. 1986, PASP, 98, 609

Jannuzi, B. T., et al. 1996, ApJ, 470, L11

—. 1998, ApJS, 118, 1

Moore, C. E. 1971, Atomic Energy Levels (Washington, D.C.: United States Department of Commerce, National Bureau of Standards)

Morton, D. C., York, D. G., & Jenkins, E. B. 1988, ApJS, 68, 449

Orr, M. J. L. & Browne, I. W. A. 1982, MNRAS, 200, 1067

Padovani, P. & Urry, C. M. 1992, ApJ, 387, 449

Quashnock, J. M., Vanden Berk, D. E., & York, D. G. 1996, ApJ, 472, L69

Richards, G. T., Laurent-Muehleisen, S., Becker, R., & York, D. G. 2000, ApJ, submitted

Richards, G. T., York, D. G., Yanny, B., Kollgaard, R. I., Laurent-Muehleisen, S. A., & Vanden Berk, D. E. 1999, ApJ, 513, 576

Rowan-Robinson, M. 1977, ApJ, 213, 635

Sargent, W. L. W., Steidel, C. C., & Boksenberg, A. 1988, ApJS, 68, 539

Schneider, D. P., et al. 1993, ApJS, 87, 45

Steidel, C. C. 1990, ApJS, 72, 1

Steidel, C. C., Dickinson, M., Meyer, D. M., Adelberger, K. L., & Sembach, K. R. 1997, ApJ, 480, 568

Stocke, J. T., Morris, S. L., Weymann, R. J., & Foltz, C. B. 1992, ApJ, 396, 487

Stockton, A. N. & Lynds, C. R. 1966, ApJ, 144, 451

Turnshek, D. A. 1988, in Proceedings of the QSO Absorption Line Meeting, ed. J. C. Blades, D. A. Turnshek, & C. A. Norman (Cambridge: Cambridge University Press), 17

Tytler, D. & Fan, X. M. 1992, ApJS, 79, 1

Vanden Berk, D. E. 1997, PhD thesis, University of Chicago

Vanden Berk, D. E., Quashnock, J. M., York, D. G., & Yanny, B. 1996, ApJ, 469, 78

Vanden Berk, D. E., et al. 1999, ApJS, 122, 355

—. 2001, in preparation

Weymann, R. 1997, in ASP Conf. Ser. 128: Mass Ejection from Active Galactic Nuclei, ed. N. Arav, I. Shlosman, & R. J. Weymann (San Francisco: ASP), 3

Weymann, R. J., Morris, S. L., Foltz, C. B., & Hewett, P. C. 1991, ApJ, 373, 23

York, D. G., Dopita, M., Green, R., & Bechtold, J. 1986, ApJ, 311, 610

York, D. G., Yanny, B., Crotts, A., Carilli, C., Garrison, E., & Matheson, L. 1991, MNRAS, 250, 24

York, D. G., et al. 1999, BAAS, 195, 52.07

Young, P., Sargent, W. L. W., & Boksenberg, A. 1982, ApJS, 48, 455